Mineralogy and Petrology

The Gold Flat Tuff, Nevada: insights into the evolution of peralkaline silicic magmas

--Manuscript Draft--

Manuscript Number:	
Full Title:	The Gold Flat Tuff, Nevada: insights into the evolution of peralkaline silicic magmas
Article Type:	Standard Article
Keywords:	Gold Flat Tuff; Nevada; peralkaline rhyolites; magma mixing; fluorite and chevkinite-(Ce) phenocrysts
Corresponding Author:	Ray Macdonald Uniwersytet Warszawski Warszawa, POLAND
Corresponding Author Secondary Information:	
Corresponding Author's Institution:	Uniwersytet Warszawski
Corresponding Author's Secondary Institution:	
First Author:	Ray Macdonald
First Author Secondary Information:	
Order of Authors:	Ray Macdonald
	Bogusław Bagiński
	Harvey E. Belkin
	John C. White
	Donald C. Noble
Order of Authors Secondary Information:	
Funding Information:	
Abstract:	The Gold Flat Tuff is the youngest (9.15 Ma) ash-flow sheet erupted from the Black Mountain Volcanic Centre, southwest Nevada, USA. This paper explores some aspects of the very complex nature of the tuff's plumbing system. The main body of the deposit is a mixed magma product, comprising pantelleritic and comenditic melts derived from independently evolving reservoirs, and antecrysts and enclaves derived from a range of basic to intermediate sources. Metre-scale cognate xenoliths point to the presence of alkali feldspar accumulation zones. The pantellerite contains phenocrysts of fluorite and chevkinite-(Ce). The inferred intermediate magma component contains perrierite-(Ce) phenocrysts. The pantellerite has unusually high contents of F (≤2.2 wt%), F+Cl (≤2.9 wt%) and ZrO_2 (≤1.04 wt%). The high halogen contents may have influenced the evolution of the strongly peralkaline magma. The crystallization conditions are poorly constrained but those for the pantelleritic magma may have been close to water-saturation (>4 wt% melt water) at temperatures ~740 °C and fO_2 around FMQ.
Suggested Reviewers:	Bruno Scaillet bscaille@cnrs-orleans.fr expert in peralkaline petrology
	Silvio Rotolo Universidad de Palermo silvio.rotolo@unipa.it expert on petrology of peralkaline rocks

The Gold Flat Tuff, Nevada : insights into the evolution of peralkaline silicic magmas

Ray Macdonald[1,2] Bogusław Bagiński[1] Harvey E. Belkin[3] John C. White[4] Donald C. Noble[5]

[1] Institute of Mineralogy, Geochemistry and Petrology, University of Warsaw, 02-089 Warszawa, Poland

[2] Environment Centre, Lancaster University, Lancaster LA1 4YQ, UK

[3] 11142 Forest Edge Drive, Reston, VA 20190-4026, USA

[4]. Department of Geosciences, Eastern Kentucky University, Richmond, KY 40475, USA

[5] PO Box 8077, Reno, NV 89507, USA

Abstract The Gold Flat Tuff is the youngest (9.15 Ma) ash-flow sheet erupted from the Black Mountain Volcanic Centre, southwest Nevada, USA. This paper explores some aspects of the very complex nature of the tuff's plumbing system. The main body of the deposit is a mixed magma product, comprising pantelleritic and comenditic melts derived from independently evolving reservoirs, and antecrysts and enclaves derived from a range of basic to intermediate sources. Metre-scale cognate xenoliths point to the presence of alkali feldspar accumulation zones. The pantellerite contains phenocrysts of fluorite and chevkinite-(Ce). The inferred intermediate magma component contains perrierite-(Ce) phenocrysts. The pantellerite has unusually high contents of F (≤2.2 wt%), F+Cl (≤2.9 wt%) and ZrO_2 (≤1.04 wt%). The high halogen contents may have influenced the evolution of the strongly peralkaline magma. The crystallization conditions are poorly constrained but those for the pantelleritic magma may have been close to water-saturation (>4 wt% melt water) at temperatures ~740 °C and fO_2 around FMQ.

Keywords Gold Flat Tuff Nevada peralkaline rhyolites magma mixing fluorite and chevkinite-(Ce) phenocrysts

Introduction

The Gold Flat Tuff member of the Silent Canyon Tuff, Black Mountain volcanic centre, SW Nevada, is a remarkable example of pantelleritic magmatism. It is thought to consist of at least 12 individual ash flows in a maximum total thickness of 30 m (Noble 1965; Minor et al. 1998). It has been reported to contain 15 phenocryst phases (Noble 1965; Minor et al. 1998). Concentrations of F, F+Cl and Zr are the highest recorded in a pantellerite (Noble 1965). Despite these unusual features, the tuff has not yet been studied in any detail, partly because it was mapped in only a reconnaissance manner (Christiansen and Noble 1968; Noble and Christiansen 1968, 1974). However, enough material is available to allow the use of new whole-rock, glass and phenocryst compositional data to (i) point out the complexity of the deposit and its magmatic system; (ii) clarify the true phenocryst assemblages in the tuff; and (iii) assess how the Gold Flat Tuff provides new information on the evolution of peralkaline silicic systems.

Geological Setting

SW Nevada volcanic field

The multicaldera silicic SW Nevada volcanic field (SWNVF) erupted, over the period 16-7 Ma, more than 20 major ash-flow sheets with the formation of at least eight collapse calderas (Byers et al. 1989; Sawyer et al. 1994). Associated with the ash-flow tuffs are lava flows and

minor pyroclastic rocks which erupted from a large number of smaller vents. The youngest major centre in the SWNVF is the Black Mountain Volcanic Centre (BMVC) (Fig. 1) which, according to Vogel et al. (1989, p.6041), "is one of the youngest, best preserved and exposed, and petrologically most interesting complexes in the western United States". The centre is a set of nested collapse structures and constructional volcanoes some 14 km across. Eruptive units of the centre, which are termed the Thirsty Canyon Tuff, comprise ash-flow sheets, lavas and unwelded tuffs erupted from the Black Mountain caldera between 9.43 and 9.15 Ma (Fleck et al. 1996) (Table 1). The ash-flow sheets total about 300 km^3 in volume (Sawyer et al. 1994).

The oldest unit, the Comendite of Ribbon Cliff, is a group of comenditic and trachytic lava flows and domes exposed marginally to the Black Mountain caldera. The oldest ash-flow sheet, the Rocket Wash Tuff, is a compositionally unzoned comendite, probably erupted from the caldera at 9.42 Ma. The overlying Pahute Mesa Tuff is a compositionally zoned, welded ash-flow sheet erupted from the caldera. It is probably one of the major units associated with caldera collapse (Sawyer et al. 1994). The Trail Ridge Tuff is a welded comenditic ash-flow sheet and may also have been one of the major units associated with caldera collapse.

Following caldera collapse, trachytic lavas of Pillar Spring partly filled the caldera. The youngest ash-flow sheet (9.15 Ma), the peralkaline Gold Flat Tuff, also accumulated within the caldera. The sheet overflowed the caldera to the north and south, being strongly channelled by the topographic rim of the Black Mountain caldera. It is uncertain whether its eruption was associated with any further caldera collapse (Minor et al. 1998).

Three features of the Black Mountain centre are important in our understanding of its evolution and to contextualise the role of the Gold Flat Tuff in that evolution: (i) Successive ash-flow sheets had smaller volumes (Table 1); (ii) Successive sheets had increasingly

peralkaline compositions (Noble et al. 1984; Weiss et al. 1989); and (iii) the complex probably evolved over a period of around 0.3 Ma (Noble et al. 1984; Weiss et al. 1989; Sawyer et al. 1994; Minor et al. 1998). It is also important to appreciate the role of basaltic and intermediate compositions in the history of the centre. For example, Miocene basalts were erupted prior to, during, and following the peralkaline volcanism of the centre and basaltic dykes are scattered throughout the area (Minor et al. 1998). Vogel et al. (1989) pointed to the presence of a mafic component in mixed magmas in, *inter alia*, the Rocket Wash and Gold Flat Tuffs. The Black Mountain centre was certainly basalt-driven, in the sense that basaltic magmas were parental to more evolved types and also supplied the thermal energy that drove the system.

Gold Flat Tuff

The Gold Flat Tuff is the only strongly peralkaline (pantelleritic) rhyolite in the SW Nevada field. Despite its importance, many aspects of the tuff are poorly known. Noble (1965) reported that the tuff is a compound cooling unit, made up of at least a dozen individual ash flows (see Noble 1974, fig. 6). As an indication of lithological variation in the unit, Noble et al. (1964, p. D27) referred to "a distinctive ash flow characterized by very abundant phenocrysts and by numerous cognate xenoliths as much as several feet in diameter and composed dominantly of phenocrysts" locally forming the top of the member. They also referred to the presence in the tuff of complexly twinned euhedral phenocrysts of alkali feldspar up to 3 cm long.

The deposit also contains other magmatic components: Vogel et al. (1983) published an analysis with SiO_2 65.29 wt%, reported to be from near the top of the sheet. As noted above,

Vogel et al. (1989) referred to mafic components in mixed magma rocks in the sheet. However, no clear statement of the vertical and lateral variations in composition and textures in the tuff has been published. A further major constraint on documenting the tuff is that it is almost always vapour phase altered and devitrified, such that Vogel et al. (1989) felt unable to include it in their magmatic evolutionary scheme of the Black Mountain complex.

Samples and analytical methods

Sample GF1 comes from a partially welded tuff, probably of fall origin, at the base of the sheet in Oasis Valley, around N37°05.583′ W116°39.919′. Sample Ttg-hg#1 is from a glassy, welded layer immediately above the basal fall and is probably from the earliest erupted ash-flow of the Gold Flat Tuff (N37°20′20″ W116°39′40″). It is similar to the material from which Noble (1965) separated pantelleritic glass. GF4 is a completely devitrified welded tuff from close to the top of the sheet, close to GF1. We have also studied in detail a cluster of intergrown feldspar crystals (sample FC) which may represent the cognate xenoliths mentioned above. Trachybasalts TM2 and TM3 were collected from small outcrops in Oasis Valley where they occur in geographical association with the Gold Flat Tuff. They most probably belong to the Basalt of Thirsty Mountain, which is Pliocene (4.63 Ma: Minor et al. 1998) and thus ~4.5 Ma younger than the Golf Flat Tuff. They are used here as proxies for possible magmas of intermediate composition in the Gold Flat plumbing system.

Major-, minor-, and trace-element compositions (Table 2) were determined by Activation Laboratories, Ancaster, Ontario, Canada. All samples were crushed and powdered with mild steel before analysis. Inductively coupled plasma-mass spectrometry (ICP-MS) and inductively coupled plasma-optical emission spectrometry (ICP-OES) were done using a

lithium metaborate–tetraborate fusion procedure before sample dissolution. Analytical techniques are as follows: ICP-MS (Ag, Bi, Ce, Co, Cs, Dy, Er, Eu, Ga, Gd, Ge, Hf, Ho, In, La, Lu, Mo, Nb, Nd, Pb, Pr, Rb, Sm, Sn, Ta, Tb, Th, Tl, Tm, U, W, Y, and Yb); ICP-OES (major oxides, Ba, Be, Cd, Cu, Ni, S, Sr, V, Zn, and Zr), loss on ignition (LOI) at 1000 °C, infrared spectrometry (CO_2), ion selective electrode (F), titration (FeO), instrumental neutron activation analysis (As, Au, Br, Cl, Cr, Ir, Sb, Sc, and Se), prompt gamma neutron activation analysis (B), and cold-vapour atomic absorption spectrometry (Hg). Quality control at Activation Laboratories is assessed by comparison with USGS, CANMET, and other appropriate in-house standards. Estimated uncertainty determined by duplicate, blank, and standard values is $\leq \pm 5\%$ if the analyte is $\geq 10 \times$ the detection limit and $\pm 20\%$ at the detection limit.

Mineral compositions were determined by electron microprobe analysis (EPMA) using a Cameca SX-100 microprobe equipped with four wavelength dispersive spectrometers. The analytical conditions were: accelerating voltage 15 kV and probe current 20-40 nA, with counting times of 20 s on peak and 10 s on each of two background positions. For feldspar, a beam spot diameter of 5 μm was used, to reduce Na loss. The standards, crystals and X-ray lines used and generalised detection limits are given in the Appendix. The 'PAP' $\varphi(\rho Z)$ program (Pouchou and Pichoir 1991) was used for corrections. Apatite was analysed using the technique outlined in Macdonald et al. (2008). Estimates of analytical precision (1σ; wt%) for all phases except glass are: Si 0.07, Ti 0.03, Al 0.02, Cr 0.02, Ni 0.03, Fe 0.09, Mn 0.03, Mg 0.04, Ca 0.08, Na 0.01, K 0.01.

For glass analyses, 15 kV and 6-10 nA and a dispersed spot of ~10-20 μm were used. Certain problems can arise with analysis of glass. As well as compositional variations related to incomplete mixing of melts, melts may have been compositionally variable because of (i)

proximity to different phenocrysts and (ii) contamination by microlites. In our experience, for example, contamination by feldspar and FeTi-oxide microlites can cause some scatter in Fe and Al abundances. We have attempted to mitigate these problems by analyzing clear pools of matrix glass as far as possible from phenocryst phases. For glass analyses, estimates of analytical precision (1σ; wt %) values are Si 0.40, Ti 0.03, Al 0.14, Fe 0.29, Mn 0.12, Mg 0.02, Ca 0.03, Na 0.17, K 0.11, P 0.03, Cl 0.03, F 0.08. Representative glass analyses are given in Table 3; the full phenocryst and glass data set is given in Supplementary Tables 1-5.

Also available for the study were six previously unpublished major element analyses of the Gold Flat Tuff, compiled by DCN (Supplementary Table 5b). Although lacking precise stratigraphic location, these analyses have been useful in establishing the compositional range in the tuff.

Petrography

The phenocryst assemblage in the Gold Flat Tuff was reported by Noble (1965) to be alkali feldspar, quartz, sodic plagioclase, olivine, clinopyroxene, barkevikite, and FeTi-oxides, with trace amounts of biotite, zircon, apatite and chevkinite. Minor et al. (1998, p.9) listed, in addition, hornblende and arfvedsonite and "rare primary fluorite and aenigmatite". It is highly unlikely that all these phases represent an equilibrium assemblage; more probably they point to magma mixing, a process recognized in BMVC rocks by Vogel et al. (1987, 1989). In the following sections, an attempt will be made to establish the (quasi-) equilibrium phenocryst assemblages in the various magmatic components.

The phenocryst phases in the trachybasalts are plagioclase, zoned from $An_{61}Ab_{36}Or_3$ to $An_{41}Ab_{53}Or_6$, and clusters of olivine ($Fo_{76.5\text{-}78.5}$) mantled by orthopyroxene ($En_{62\text{-}57}$). The

matrix consists of plagioclase laths (An $_{61\text{-}52}$), olivine, altered pyroxene and magnetite (X_{usp} 51-56), with streaks and patches of calcite and interstitial patches of devitrified glass.

Figure 2 shows a thin section of Gold Flat Tuff sample Ttg-hg#1, from the welded layer immediately above the basal fall. The dominant component is glass of at least three types. First, a dark olive green type forms relatively wide fiamme (≤2 mm) showing perlitic texture. This is almost certainly the material from which Noble (1965) separated glass. The second type forms very dark fiamme (1-3 mm) dotted with microcrystals, commonly intermingled with type 1 glass. Third is a poorly phyric or aphyric pale glass, occurring as wisps and ovoidal patches (≤1 mm) and less abundant than types 1 and 2. Sample GF4 is completely devitrified but appears to have been composed of the same glass types but with a higher proportion of type 3. The glass component of sample GF1, the basal fall unit, is also completely devitrified and its original nature must be deduced from phenocryst compositions (see below).

In the darker glass (and its devitrified equivalent) phenocrysts form ~35% modally. The most abundant in both GF1 and Ttg-hg#1 is alkali feldspar, subhedral to euhedral, sometimes occurring in clusters. The feldspars vary from partially resorbed plates up to 2 mm across to anhedral chips and needles which may be fragments of larger crystals (Fig. 2). Ttg-hg#1 contains several crystals of feldspar which, on analysis (below), proved to be much more calcic than the phenocrysts. Two are shown in Fig. 3. Both are highly resorbed and the larger crystal (Fig. 3a) developed an unusual reaction rim involving an incompletely resolved assemblage of albite, ilmenite and baddeleyite. These feldspar crystals are inferred to be antecrysts. Quartz phenocrysts are large (≤2.5 mm; Fig. 2), partially resorbed plates but also occur as small anhedral grains. The most abundant mafic phase is olivine, forming rounded crystals up to 830 μm across, often occurring in aggregates (Figs 4a and b). Amphibole occurs

as green-brown euhedral plates up to 625 μm across, prisms, mantles on clinopyroxene, and small anhedra which may be fragments of larger crystals Fig. 4c. Clinopyroxene is relatively uncommon, forming prisms up to 1 mm long, slightly resorbed plates, and inclusions in amphibole and olivine phenocrysts. Some crystals show zonation to greener rims.

Ilmenite is mainly associated with olivine, amphibole, zircon and a chevkinite-group mineral (Figs. 4a, c and d), especially in Ttg-hg#1. It often occurs as euhedral phenocrysts up to 150 μm across, anhedral plates but also as prisms. In the olivine phenocryst shown in Fig. 4a, it forms a stellate set of inclusions. Occasionally, it is mantled by brown mica. Magnetite is more common in GF1, forming anhedral microphenocrysts but also occurring as inclusions in amphibole.

Fluorite occurs in Ttg-hg#1 as discrete, euhedral, rectangular phenocrysts up to 210 x 155 μm in size, in clusters with fayalite, chevkinite and ilmenite (Fig. 4b), and partly enclosed in amphibole phenocrysts (Fig. 4c). This is only the third report of fluorite phenocrysts in a peralkaline rhyolite. Marshall et al. (1998) recorded it in comendites of the Olkaria complex, Kenya Rift Valley, where it forms hexagonal crystals up to 0.4 mm across. It has also been found as occasional phenocrysts in peralkaline rhyolites of the Yunshan caldera complex, China (Yan et al. 2018). In the Olkaria case, the fluorite crystallized in melts with F contents ranging from 0.2-1 wt% and Peralkalinity Indices (P.I.; mol. $(Na_2O+K_2O)/Al_2O_3$) from 1.11 to 1.31, indicating that its crystallization was not critically dependent on either parameter.

Chevkinite-group minerals occur in both samples, as fragmented, sometimes partially resorbed, phenocrysts up to 68 x 41 μm in size, and in a cluster with olivine and fluorite phenocrysts (Fig. 4b). As far as we know, Gold Flat is the only known occurrence of chevkinite phenocrysts in a pantelleritic extrusive rock. Fluorapatite is almost invariably

found associated with, and included in, the mafic phenocrysts. It forms euhedral cross-sections and prisms. The largest crystal, an inclusion in feldspar, is 73 x 23 μm in size and is oscillatory zoned. Like fluorapatite, zircon is mainly associated with the mafic phenocrysts, forming plates and prisms, the longest being 156 μm long. It is restricted to GF1; its absence from Ttg-hg#1 points to a high solubility of Zr in the strongly peralkaline melt.

The presence of aenigmatite phenocrysts noted by Minor et al. (1998) has not been confirmed in this study. It may be present in other parts of the tuff than sampled here or possibly it has been mistaken for chevkinite. In the pantellerite, biotite is of relatively late crystallization, replacing ilmenite, and is not of phenocryst status as suggested by Noble (1965).

Figure 5a shows a 2x2 cm aggregate of intergrown, euhedral, alkali feldspar crystals, the largest being 1 cm long. It is here termed a feldspar megacluster (FC). The feldspars are dusty due to inclusions of FeTi-oxides and mica. The main mafic phases form clusters along feldspar grain boundaries or at triple junctions. More rarely they are included in feldspar. They comprise olivine and clinopyroxene, the pyroxene sometimes mantling the olivine, ilmenite, mica and rare zircon (Fig. 5b). Tiny inclusions of baddeleyite occur in olivine and clinopyroxene. An important petrogenetic implication of the cluster is that crystallization of the mafic phases clearly post-dated significant amounts of feldspar crystallization.

It was recognized by Noble (1965) and Minor et al. (1998) that lithic fragments form 5-20% of the tuff, including porphyritic and non-porphyritic igneous rocks of various compositions. In addition, a common feature in the dark glass in Ttg-hg#1 and in GF1 is the presence of small (<2 cm), black, aphyric or sparsely phyric inclusions (Fig.6). They normally have sharp contacts with the host matrix, sometimes with crenulated margins, and vary in shape from blocky to rounded. Some show quench textures, e.g. the slender curved

plagioclases in Fig. 6b. They have certain similarities to the benmoreite-trachyte globules described in peralkaline ignimbrite 'TL' from Gran Canaria by Sumner and Wolff (2003). Like those authors, we interpret the Gold Flat enclaves as having been intruded into the tuff as melt and refer to them below as enclaves.

Mineral compositions

All analysed feldspar phenocrysts in Ttg-hg#1 occur in the pantelleritic glass (types 1 and 2). The total compositional range is $An_{39}Ab_{59}Or_2$ to $An_0Ab_{54}Or_{46}$, i.e. from andesine to sanidine. The degree of compositional variation is variable: some crystals are effectively homogeneous but many are zoned from more calcic cores to potassic rims. Profiles across three crystals exemplify the variations. In Fig. 7a, an andesine core is mantled by anorthoclase showing a slight increase in K/Na ratio towards the rim. The second profile (Fig. 7b) shows a fairly regular decrease in An content within the anorthoclase field. A more complex zonation is shown in Fig. 7c, where a central area showing rapid changes in An content is mantled by a homogeneous An-poor zone. The three feldspars follow slightly different trends on an An-Ab-Or plot (Fig. 8), indicating that they evolved along slightly different liquid-lines-of descent.

By analogy with studies of zoning in plagioclase, Troll and Schmincke (2002) considered that ranges of the order 3-4 mol% in peralkaline rhyolites of Gran Canaria lie within the compositional range of local disequilibrium and/or small P-T changes during crystal growth. On that basis, the Gold Flat feldspar phenocrysts are clearly recording both a higher-temperature phase of evolution and repeated changes in melt composition as they grew.

Feldspars in the feldspar cluster range from An_{25-2}, i.e. from oligoclase to sanidine, the same range as in the zoned phenocryst TTG 26, apart from the calcic core (Fig. 8). The

inferred antecryst shown in Fig. 3a is zoned, core to rim, from $An_{47}Ab_{49}Or_4$ to $An_{27}Ab_{70}Or_3$. The heavily resorbed crystal in Fig. 3b is oligoclase (An_{23-26}). Microphenocrysts in GF1 are as calcic as An_{79}. The antecrysts thus crystallized from magmas both less and more evolved than that which produced the most calcic cores in the phenocrysts.

Olivine

Three groups of olivine may be distinguished (Supplementary Table 2a). The first forms phenocrysts in both Ttg-hg#1 and GF1 and is in the range $Fo_{1.9-7.9}$, the more magnesian compositions tending to occur in crystal cores. The second ($Fo_{53.2-54.5}$) is found as partially resorbed phenocrysts only in GF1 and the third ($Fo_{26.2-38.3}$) is associated with clinopyroxene in the feldspar clusters. The tephroite content in all analyses is ≤5.2. Calcium is negatively correlated with Fo to Fo~10 (CaO ~0.4 wt%) and then decreases with further Fo increase to CaO <0.2 wt%.

Pyroxene

Clinopyroxene phenocrysts in Ttg-hg#1 are hedenbergite, ranging in composition from $Ca_{43.6}Mg_{18.6}Fe_{37.9}$ to $Ca_{41.3}Mg_{8.7}Fe_{47.3}$ (Fig. 9; Supplementary Table 2b). Zoning up to 6% Mg is common, with cores being more magnesian. Sodium values are low, ≤0.13 apfu (1.69 wt% Na_2O). Similar phenocrysts occur in GF1 but the sample also contains more magnesian microphenocrysts, up to $Ca_{41.9}Mg_{44.1}Fe_{14.1}$. In the feldspar clusters, the pyroxenes range from $Ca_{43.5}Mg_{34.6}Fe_{22.0}$ to $Ca_{44.1}Mg_{27.8}Fe_{28.1}$ (Fig. 9).

Of considerable interest is the presence in GF1 of an orthopyroxene microphenocryst with core and rim compositions of $Ca_{3.7}Mg_{65.7}Fe_{30.6}$ and $Ca_{3.4}Mg_{67.0}Fe_{29.6}$, respectively (Supplementary Table 2b). Orthopyroxene has been recorded in trachytes and peralkaline rhyolites by, *inter alios*, Freundt-Malecha et al. (2001), Sumner and Wolff (2003) and Rooney et al. (2012). Vogel et al. (1987) reported that orthopyroxene is rather common in tuffs of the BMVC. It is present as mantles on olivine phenocrysts in the trachybasalts of this study. It can be inferred that the orthopyroxene in GF1 was a relict from a higher-temperature magma, perhaps of intermediate composition.

Amphiboles

In the IMA classification scheme (Locock 2014), amphibole phenocrysts in Ttg-hg#1 are, with one exception, ferrorichterite, with $Mg/(Mg+Fe^{2+})$ ratios in the range 0.02-0.20 (Supplementary Table 2c). The exception is a small euhedral plate of arfvedsonite. An amphibole inclusion in an olivine phenocryst is slightly more magnesian, with a ratio of 0.30. Phenocrysts in GF1 are more magnesian (0.52-0.65) and more variable. They are mainly magnesio-hastingsite to hastingsite, but edenite and pargasite also occur. An amphibole inclusion in feldspar is ferro-ferri-katophorite and a small crystal fragment is magnesio-ferri-hornblende. The amphibole data for GF1 suggest crystallization from a range of intermediate magmas.

Ilmenite, magnetite, fluorapatite and mica

Ilmenite phenocrysts in Ttg-hg#1 are in the compositional range X_{ilm} 94.4-98.1, with 0.18-0.84 wt% Nb_2O_5 and 0.13-0.29 wt% V_2O_3 (Supplementary Table 3a). The ilmenite forming a

stellate cluster in an olivine phenocryst in GF1 (Fig. 4a) is X_{ilm} 91; the rock also contains a microphenocryst with X_{ilm} 77.6. The increase in X_{ilm} with increasing host-rock peralkalinity has been recorded in pantellerites from Pantelleria by Mahood and Stimac (1990) and White et al. (2005). Magnetite forming phenocrysts and inclusions in both samples is in a wide range X_{usp} 68-2. The compositions of fluorapatite are reported in Supplementary Table 3b. There are two main varieties: (i) one, occurring in GF1, has significant amounts of Cl (≤0.7 wt%) and SO_3 (≤0.62 wt%) and low britholite contents (1.1 – 2.9%, judging from the REE+Si contents); and (ii) one with slightly higher britholite component (2.1 – 4.9%), recorded only in Ttg-hg#1. These values may be compared with 15% britholite component reported in comendites of the Olkaria volcanic complex, Kenya (Macdonald et al. 2008), ~10% in pantellerites of the Nemrut volcano, Turkey (Macdonald et al. 2015) and ~5% in pantellerites from Pantelleria (Liszewska et al., in revision).

Although not a phenocryst phase, it may be noted that the mica in Ttg-hg#1, mainly associated with ilmenite, is in the range $Mg/(Mg+Fe^{2+})$ 0.25-0.30 whereas that in the feldspar cluster (FC) is more magnesian, 0.49-0.70, the differences reflecting the different melt compositions (pantelleritic vs trachytic) (Supplementary Table 3c).

Fluorite, chevkinite-group minerals and zircon

Fluorite analyses are given in Supplementary Table 4a. The most important substituting element is Y; most values are ≤0.24 wt% but two point analyses show 1.74 and 1.02 wt%. The latter analyses also have detectable Ce (0.63, 1.76 wt%). In comparison, fluorite phenocrysts in comendites of the Greater Olkaria Volcanic Complex contain Y in the range 0.26-0.58 wt% and Ce in the range 0.06-0.15 wt% (Marshall et al. 1998).

In the Macdonald et al. (2009) classification scheme, the chevkinite-group minerals in Ttg-hg#1 are chevkinite-(Ce), those in GF1 are both chevkinite-(Ce) and perrierite-(Ce) (Supplementary Table 4b). Macdonald and Belkin (2002) used the relationships between ($CaO+SrO+MgO+Al_2O_3$), $\Sigma(La_2O_3-Sm_2O_3)$ and FeO* to show that, in igneous parageneses, chevkinite tends to occur in more evolved, alkaline rocks whereas perrierite mainly forms in intermediate to mafic rocks and calcic granites. The Gold Flat CGM are consistent with having formed in two or more magmas, one pantelleritic, the other(s) of perhaps intermediate composition.

Zircon is close to stoichiometric: (Si + Zr) contents range from 1.94-1.99 apfu (Supplementary Table 4c). The most significant other component is Fe (≤3.04 wt% FeO*), although FeO* values above 2.5 wt% may have resulted from beam contamination by the host magnetites. The actinides are notable in only one point analysis (ThO_2 0.83 wt%; UO_2 0.30 wt%) and only two analyses show significant Y_2O_3 (0.59, 0.31 wt%).

Phenocrysts and host magma compositions

The glass and mineral compositional data allow us to distinguish three main magma types: one was pantelleritic, with the phenocryst assemblage alkali feldspar + quartz + fayalite + hedenbergite + ilmenite + fluorite + chevkinite-(Ce) + fluorapatite. The second was comenditic, with scarce phenocrysts of anorthoclase. A third component (or components) contained andesine-oligoclase + diopside/augite + forsteritic olivine + calcic amphibole + perrierite-(Ce) + fluorapatite + ilmenite + zircon. This assemblage would have formed in a more intermediate magma, e.g. trachyandesite or benmoreite. If the full range of phenocrysts, antecrysts and phenocrysts in enclaves in the pantelleritic component of Ttg-hg#1 and in GF1

can be taken as derived from the same plumbing system (Figs. 8 and 9), that system contained magmas ranging in composition from basalt to pantellerite. It may be further inferred that the system did not contain any significant compositional (Daly) gaps. However, with an absence of melt compositions less evolved than trachyte, it is impossible to identify precisely the liquid-lines-of-descent that generated the rhyolites. However, certain points relevant to the evolution of the complex and to peralkaline silicic magmatism in general can be made (see below).

Geochemistry

The trachybasalts are hy ± ol ± qz - normative, with SiO_2 50-51 wt% and Mg-number 0.35-0.46 (Mg/(Mg+Fe), calculated with all Fe as Fe^{2+}). The relatively low Na_2O/K_2O ratio of 1.3 is consistent with the observation that the SW Nevada suites containing peralkaline components are unusually potassic (Hedge and Noble 1971; Noble and Christiansen 1974). Sample GF1 from the basal fall deposit has a bulk trachytic composition but it is clear from the mineral compositions that it is a mixed magma rock. The bulk composition of Ttg-hg#1 is pantelleritic but, as noted above, it is also a mixed magma rock. Sample Ttg-1-1 is a comendite, but lacking petrographic and mineralogical information, it is unclear whether or not it is a mixed magma rock.

In the classification scheme of Macdonald (1974), the rhyolites form a trend from the comendite to pantellerite fields (Fig. 10). However, at least two rocks (Ttg-hg#1 and GF4) are mixed magma products and can best be described in terms of the glass components. The compositions of the two main components in Ttg-hg#1 are pantellerite (darker; Gl1 and Gl2, Fig. 2) and comendite (lighter; Gl3), the latter just entering the pantellerite field (Fig. 10). The

same components, although devitrified, are recognizable in GF1. On this plot, there is a suggestion that they form two separate lineages, which is confirmed on SiO_2-Al_2O_3 and SiO_2-FeO* plots (Fig. 11). The components thus evolved along different liquid-lines-of-descent in compositionally zoned, independent reservoirs before mingling prior to, or during, eruption. We observe no evidence of chill-textures, thus we assume that the separate reservoirs had broadly similar temperatures and heat capacities during melt mingling. While there are many examples in the literature of comenditic magma evolving to pantellerite (e.g. Barberi et al. 1975; Bohrson and Reid 1997; Peccerillo et al. 2003; Mungall and Martin 1995; Marshall et al. 2009; Giordano et al. 2014; Macdonald et al. 2015), this is, so far we know, the first record of the two independently evolving, peralkaline magma types being erupted as a mixed magma. On the FeO*-Al_2O_3 plot (Fig. 10), the pantelleritic glasses form a trend roughly parallel to the glasses synthesized by Di Carlo et al. (2010) in their high P-T experimental study of a pantellerite from Pantelleria, strongly suggesting that prior to mingling they were part of a compositionally zoned system.

It is clear from Fig. 11 that increases in Fe and decreases in Al, invariable compositional trends in evolving peralkaline rhyolites, are accompanied by decreasing SiO_2 contents. This can be ascribed to quartz fractionation, perhaps promoted by the early appearance of quartz phenocrysts as a result of the high F contents (Macdonald et al. 2011).

SiO_2 varies in the pantelleritic glass from 70.7 to 73.5 wt%, FeO* from 5 to 7 wt% and P.I. from 1.41 to 1.83. Abundances of MgO and CaO are very low, ≤0.03 wt% and ≤0.24 wt%, respectively. The range in compositions is shown in small differences in intensity on back-scattered intensity (BSE) images (e.g. Fig. 3b). Notable features, as appreciated by Noble (1965) and Noble et al. (1979), include the exceptionally high ZrO_2 (≤1.04 wt%), LREE (La-Sm: ≤1517 ppm), F (≤2.23 wt%) and Cl (≤0.94 wt%) contents (Table 2; Supplementary Table

5a). Although comendites from the Olkaria complex, Kenya, have F contents >1 wt% (Macdonald et al. 1987; Marshall et al. 2009), and Scaillet and Macdonald (2006) synthesized glass with F = 2.51 wt% in their experimental study of an Eburru pantellerite, we know of no other peralkaline rhyolite with such an elevated halogen content (F+Cl ≤2.9 wt%).

In the comenditic glass the ranges are SiO_2 73.2-75 wt%, FeO* 3.5-4.5 wt% and P.I. 1.20-1.51. In keeping with the less peralkaline composition, it has lower contents of ZrO_2 (0.32-0.56 wt%, F (0.35-0.91 wt%) and Cl (0.24-0.47 wt%) than the pantellerite glass. A melt inclusion in clinopyroxene in the feldspar cluster FC has trachytic composition (Table 3), the first confirmation of trachytic *melt* in the Gold Flat system. Its position in Fig. 10 is consistent with it being parental to the more peralkaline whole-rocks. Such trachytic melts may have been the source of some of the ternary feldspars and they may represent yet another melt component in the mixed magma rocks.

Chondrite-normalized REE patterns of the trachybasalts are strongly LREE-enriched ($[La/Yb]_{CN}$ 22, 24]) and do not have Eu anomalies (Fig. 12). The basal fall unit, GF1, is less LREE-enriched ($[La/Yb]_{CN}$ 13) and has a significant negative Eu anomaly (Eu/Eu* 0.45). These features suggest that GF1 is a mix of a trachyte/rhyolite magma and a magma more mafic than the trachybasalts. The most peralkaline rocks (Ttg-hg#1, GF4) show sharply decreasing values from La to Sm, strong negative Eu anomalies (Eu/Eu* 0.04, 0.05), and flat patterns from Gd to Yb, features found by Noble et al. (1979) for glass separated from the same unit as Ttg-hg#1. The pattern for comendite Ttg-1-1 is similar to those of the pantellerites.

Conditions of formation of Gold Flat Tuff

Determining meaningful estimates of the formation conditions of the tuff is complicated by the strong compositional and thermal effects of magma mixing and by the usually unknown effects of the high halogen contents on the stability of the mineral phases. However, an attempt is made below to extract some quantitative evidence on crystallization parameters of the pantellerite. Some constraints may also be placed by comparison with studies of other pantellerites.

There are no robust constraints on the *pressure* at which the Gold Flat magmas last equilibrated. However, geological evidence (Mahood 1984), thermodynamic and geochemical modelling (White et al. 2009; Neave et al. 2012), and experimental studies (Scaillet and Macdonald 2001, 2003, 2006: Di Carlo et al. 2010; Romano et al. 2018) are strongly in favour of low pressures for pantellerite formation, ≤3 kbar.

Iron-titanium oxides, olivine-clinopyroxene and clinopyroxene-liquid equilibria are the most commonly used methods for estimating temperature and oxygen fugacities (fO_2) in magmas but are of limited use here, despite the abundance of data, because of the great compositional diversity and the difficulty of determining which pairs might be in equilibrium. We are confident in only a single result determined from an adjacent pair of oxides in sample Ttg-hg#, (ilmenite 2/7 and magnetite analysis 2/8, Supplementary Table 3a) which passes the Bacon and Hirschmann (1988) test for equilibrium. The pair provides an Andersen and Lindsley (1988) temperature and fO_2 of 734 °C and -17.3 (FMQ-1.3). The QUILF programme (Andersen et al. 1988) provides a slightly lower temperature (724 °C) but similar fO_2 (-17.5 (FMQ-1.2)). The addition of an analysis of the olivine (analysis 2/5; Supplementary Table 2a) associated with the oxide pair provides a silica activity relative to quartz saturation (a_{SiO2}[Qtz]) of 0.633 at P = 1000 bar. This relatively low $aSiO_2$ at this low temperature may also explain the absence of aenigmatite from the Gold Flat Tuff, despite the pantelleritic

composition of the host glass and the highly reducing conditions. Macdonald et al. (2011) found the antipathetic relationship between fayalite and aenigmatite to be a function of T, P and $a\mathrm{SiO_2}$, with aenigmatite crystallizing at the expense of fayalite at T<750 °C at $a\mathrm{SiO_2}$ close to quartz saturation at 150 MPa. Figure 13 shows the calculated stability field of aenigmatite, ilmenite and fayalite as functions of $a\mathrm{SiO_2}$ (quartz) and temperature. If the thermodynamic parameters used here are applicable to the Gold Flat Tuff, the absence of aenigmatite in favour of fayalite + ilmenite with quartz phenocrysts ($a\mathrm{SiO_2}$ quartz ~1) might suggest crystallization of the pantellerite in the range 715-740 °C.

Temperatures for peralkaline glass in equilibrium with alkali feldspar may also be estimated by comparison with the experimental data of Carmichael and MacKenzie (1963), who determined the alkali feldspar liquidus surface in the system Q-Ab-Or-Ac-Ns in comenditic (P.I. ~1.2-1.5) and pantelleritic (P.I. ~1.5-2.0) bulk compositions. This method has been used by White et al. (2005) and Liszewska et al. (in revision) in studies of Pantescan pantellerites, who both demonstrated that the results are similar to those determined by methods using mafic mineral equilibria. For the Gold Flat glasses (Supplementary Table 5a) the normative mineralogy was calculated with FeO/FeO* = 0.9, which corresponds to $f\mathrm{O_2}$ buffered at FMQ-1 between 700 and 900 °C (Sack et al. 1980). The results are plotted in Fig. 14 which plots the P.I. of the glasses against calculated temperature. Pantellerites have lower estimated temperatures of 740 ± 6.0 °C, consistent with the single result from two-oxide geothermometry. Comendites have higher estimated temperatures of 767 ± 6.0 °C and the sole sample of trachytic glass, in FC, has the highest temperature of 840 °C, although this may an underestimate due to its low P.I. (1.01). The compositions of six alkali feldspars (Supplementary Table 1a) are plotted with the alkali feldspar solvi at 750 °C and 875°C, calculated with SolvCalc (Wen and Nekvasil 1994) using the mixing model of Fuhrman and

Lindsley (1988) (Fig. 15). In this figure, two distinct and separate trends are also observed: one corresponding to compositions that crystallized at <750 °C, and another as high as 875 °C.

White et al. (2005, 2009) used thermodynamic modelling to suggest that the phenocryst assemblage in the most evolved pantellerites on Pantelleria, viz. alkali feldspar + clinopyroxene + aenigmatite, equilibrated at low temperatures (<700 °C), low oxygen fugacities (FMQ-1), and high melt water contents (>4 wt%). Broadly similar results were found experimentally by Di Carlo et al. (2010) for a pantelleritic pumice fall from Fastuca, Pantelleria. In contrast, they found that, at ≥150 MPa, amphibole crystallization required lower temperatures and higher melt water contents, up to 6.5 wt% at 680 °C. Di Carlo et al. (2010) also found that the crystallization of quartz seemed to record conditions no wetter than 3 wt% melt water, much lower than for amphibole. In the Gold Flat pantellerite, quartz and amphibole are present as phenocrysts. One possible explanation is that the high F contents gave crystallization conditions different to those in the experiments, promoting, for example, the early appearance of quartz by lowering the temperature of the quartz-feldspar cotectic, as suggested by Macdonald et al. (2011) for peralkaline rhyolites carrying near-liquidus quartz phenocrysts.

Biotite is a rare phenocryst in peralkaline silicic rocks and little is known about its stability relationships (Macdonald et al. 2011). Scaillet and Macdonald (2001) synthesized biotite in a comendite from the Olkaria complex, Kenya, showing that at 150 MPa and fO_2 ~FMQ, its crystallization indicated temperatures as low as 660 °C under near water-saturated conditions (melt water content ~6 wt%). In the Gold Flat pantellerite, biotite was of relatively late crystallization, consistent with the 660 °C temperature found experimentally by Scaillet and Macdonald (2001) and Di Carlo et al. (2010) for near-solidus conditions.

On the basis of these various approaches, it may cautiously be suggested that the phenocryst phases in the Gold Flat pantelleritic magma started crystallizing at a temperature of ~740 °C, close to or at water-saturation, at fO_2 below FMQ. It reached the solidus at ~650 °C.

Gold Flat plumbing system

Our lack of knowledge about lithological variations in the tuff with time places severe constraints on our ability to determine the sequence of eruptive events and the nature of the Gold Flat plumbing system. However, some points are worth making in order to inform future research.

The first-erupted material (GF1) is a mixed magma rock, the main components being pantellerite and trachyte-trachyandesite. The basal welded tuff (Ttg-hg#1) is composed of pantelleritic and comenditic glass, a complex suite of phenocrysts and antecrysts, and benmoreite-trachyte enclaves. Two welded tuffs from near the top of the unit, but not necessarily coeval, are pantellerite (GF4) and comendite (Ttg-1-1). The reservoir was not simply compositionally zoned – at least two independently evolving sources were tapped during the eruption. If the An-rich antecrysts represent basaltic magma in the system, where was the magma located? Furthermore, if the feldspar megaclusters and the phenocryst-rich cognate ejecta noted by Noble et al. (1964) formed in an accumulitic zone, where was it located? A possible analogue is on the island of Pantelleria, where eruption at 45.7 ± 1 ka of the Green Tuff ignimbrite, compositionally zoned from comenditic trachyte to pantellerite, was followed during caldera resurgence by eruption of a series of feldspar-rich trachytes from vents inside the caldera (Mahood and Hildreth 1986; Scaillet et al. 2013). In addition, Weaver

(1977) described from the peralkaline volcano Emuruangogolak, Kenya Rift, syenite blocks which are closely similar to the Gold Flat examples.

The mixed-lineage nature of the Gold Flat magma is perhaps consistent with melt lenses within a much larger system, the "complex magma reservoirs" of Cashman and Giordano (2014), Cooper (2017) and Sparks and Cashman (2017). A further analogue may be the basalt-trachyte caldera volcano Silali (Kenya Rift Valley), where Macdonald et al. (1995) proposed the existence of two distinct storage/homogenization systems and a network of partly interconnected magma reservoirs. On the basis of compositional variations in the initial fall deposits and earliest ignimbrite of the Huckleberry Ridge Tuff, Yellowstone, Swallow et al. (2018) proposed the evacuation of an exceptionally complex and heterogeneous magma system.

Finally, throughout its 300 ka history, the BMVC erupted rhyolites of comenditic affinity. What were the conditions that promoted evolution to pantellerite evolution? One possibility is the unusually high F+Cl contents. They would complex with, and enrich, certain trace elements, such as Zr and the LREE, and perhaps more importantly lower the magma viscosities and prolong the fractionation history, allowing a comenditic parent to evolve into the pantellerite field.

Acknowledgements We thank Lidia Jeżak and Petras Jokubauskas for help in the electron microprobe laboratory and Marcin Syczewski for help with the SEM work. Financial support from grant number NN307 634040 is much appreciated.

References

Andersen DJ, Lindsley DH (1988) Internally consistent solution models for Fe-Mg-Mn-Ti oxides: Fe-Ti oxides. Am Mineral 73: 714-726

Andersen DJ, Lindsley DH, Davidson PM (1993) A Pascal program to assess equilibria among Fe-Mg-Mn-Ti oxides, pyroxene, olivine, and quartz. Comp Geosci 19: 1333-1350

Bacon CR, Hirschmann MC (1988) Mg/Mn partitioning as a test for equilibrium between coexisting Fe-Ti oxides. Am Mineral 73: 57-61

Barberi F, Ferrara G, Santacroce R, Treuil M, Varet J (1975) A transitional basalt-pantellerite sequence of fractional crystallisation, the Boina Centre (Afar, Ethiopia). J Petrol 16: 22-56

Bohrson WA, Reid MR (1997) Genesis of silicic peralkaline volcanic rocks in an ocean island setting by crustal melting and open-system processes: Socorro Island, Mexico. J Petrol 38: 1137-1166

Byers FM Jr, Carr WJ, Orkild, PP (1989) Volcanic centers of southwestern Nevada: Evolution of understanding, 1960-1988. J Geophys Res 94: 5908-5924

Carmichael ISE, MacKenzie WS (1963) Feldspar-liquid equilibria in pantellerites: an experimental study. Am J Sci 261: 382-396

Cashman KV, Giordano G (2014) Calderas and magma reservoirs. J Volcanol Geophys Res 288: 28-45

Christiansen RL, Noble DC (1968) Geologic map of the Trail Ridge quadrangle, Nye County, Nevada. US Geol Surv Geologic Quadrangle Map GQ-774

Cooper KM (2017) What does a magma reservoir look like? The "crystal's-eye" view. Elements 13: 23-28

Di Carlo I, Rotolo SG, Scaillet B, Buccheri V, Pichavant M (2010) Phase equilibrium constraints on pre-eruptive conditions of recent felsic explosive volcanism at Pantelleria Island, Italy. J Petrol 51: 2245-2276

Fleck RJ, Turrin BD, Sawyer DA, Warren RG, Champion DE, Hudson MR, Minor SA (1996) Age and character of basaltic rocks of the Yucca Mountain region, southern Nevada. J Geophys Res: Solid Earth 101: 8205-8227

Freundt-Malecha B, Schmincke H-U, Freundt A (2001) Plutonic rocks of intermediate composition on Gran Canaria: The missing link of the bimodal volcanic suite. Contrib Mineral Petrol 141: 430-445

Fridrich CJ, Minor SA, Slate JL, Ryder PL (2007) Geologic map of Oasis Valley spring-discharge area and vicinity, Nye County, Nevada. U.S. Geol Surv Sci Invest. Map, 2957

Fuhrman ML, Lindsley DH (1988) Ternary-feldspar modeling and thermometry. Am Mineral 73: 201-215

Giordano F, D'Antonio M, Civetta L, Tonarini S, Orsi G, Ayalew D, Yirgu G, Dell'Erba F,

Di Vito MA, Isaia R (2014) Genesis and evolution of mafic and felsic magmas at Quaternary volcanoes within the Main Ethiopian Rift: Insights from Gedemsa and Fanta'Ale complexes. Lithos 188: 130-144

Hedge CE, Noble DC (1971) Upper Cenozoic basalts with high $^{87}Sr/^{86}Sr$ and Sr/Rb ratios, southern Great Basin, western United States. Bull Geol Soc Am 82: 3503-3510

Lepage LD (2003) ILMAT: an Excel worksheet for ilmenite-magnetite geothermometry and geobarometry. Comp Geosci 29: 67-678

Liszewska KM, White JC, Macdonald R, Bagiński B (in revision) Compositional and thermodynamic variability in a stratified magma chamber: Evidence from the Green Tuff ignimbrite (Pantelleria, Italy). J. Petrol.

Locock AJ (2014) An Excel spreadsheet to classify chemical analyses of amphiboles following the IMA 2012 recommendations. Comp Geosci 62: 1-11

Macdonald R (1974) Nomenclature and petrochemistry of the peralkaline oversaturated volcanic rocks. Bull Volcanol 38: 498-516

Macdonald R, Davies GR, Bliss CM, Leat PT, Bailey DK, Smith RL (1987) Geochemistry of high-silica peralkaline rhyolites, Naivasha, Kenya Rift Valley. J Petrol 28: 979-1008

Macdonald R, Belkin HE (2002) Compositional variation in minerals of the chevkinite group. Mineral Mag 66: 1075-1098

Macdonald R, Davies GR, Upton BGJ, Dunkley PN, Smith M, Leat PT (1995) Petrogenesis of Silali volcano, Gregory Rift, Kenya. J Geol Soc London 152: 703-720

Macdonald R, Bagiński B, Belkin HE, Dzierżanowski P, Jeżak L (2008) *REE* partitioning between apatite and melt in a peralkaline volcanic suite, Kenya Rift Valley. Mineral Mag 72: 1147-1161

Macdonald R, Belkin HE, Wall F, Bagiński B (2009) Compositional variation in the chevkinite group: new data from igneous and metamorphic rocks. Mineral Mag 73:777-796

Macdonald R, Bagiński B, Leat PT, White JC, Dzierżanowski P (2011) Mineral stability in peralkaline silicic rocks: Information from trachytes of the Menengai volcano, Kenya. Lithos 125: 553-568

Macdonald R, Sumita M, Schmincke H-U, Bagiński B, White JC, Ilnicki SS (2015) Peralkaline felsic magmatism at the Nemrut volcano, Turkey: impact of volcanism on the evolution of Lake Van (Anatolia) IV. Contrib Mineral Petrol 169: 34

Mahood GA (1984) Pyroclastic rocks and calderas associated with strongly peralkaline magmatism. J Geophy Res 89: 8540-8552

Mahood GA, Hildreth W (1986) Geology of the peralkaline volcano at Pantelleria, Strait of Sicily. Bull Volcanol 48: 143-172

Mahood GA, Stimac JA (1990) Trace-element partitioning in pantellerites and trachytes, Geochim Cosmochim Acta 54: 2257-2276

Marshall AS, Hinton RW, Macdonald R (1998) Phenocrystic fluorite in peralkaline rhyolites,

Olkaria, Kenya Rift Valley. Mineral Mag 62: 477-486

Marshall AS, Macdonald R, Rogers NW, Fitton JG, Tindle AG, Nejbert K, Hinton RW (2009) Extreme fractionation of peralkaline silicic magmas: the Greater Olkaria Volcanic Complex, Kenya Rift Valley. J Petrol 50: 323-359

Minor SA, Orkild PP, Sargent KA, Warren RG, Sawyer DA, Workman JB (1998) Digital geologic map of the Thirsty Canyon NW Quadrangle. US Geol Surv Open-File Report 98-623: 22 pp

Mungall JE, Martin RF (1995). Petrogenesis of basalt-comendite and basalt-pantellerite suites, Terceira, Azores, and some implications for the origin of ocean-island rhyolites. Contrib Mineral Petrol 119: 43-55

Neave DA, Fabbro G, Herd RA, Petrone CM, Edmonds M (2012) Melting, differentiation and degassing at the Pantelleria volcano, Italy. J Petrol 53: 637-663

Noble DC (1965) Gold Flat Member of the Thirsty Canyon Tuff – a pantellerite ash-flow sheet in southern Nevada. US Geol Surv Prof Paper 525-B: B85-B90

Noble DC (1974) Road log and field trip guide, Black Mountain volcanic center. In: Nevada Bureau of Mines and Geology Report 19: 22-26

Noble DC, Christiansen RL (1968) Geologic map of the southwest quarter of the Black Mountain quadrangle, Nye County, Nevada. US Geol Surv Miscellaneous Geol Investigations Map I-562

Noble DC, Christiansen RL (1974) Black Mountain volcanic center in Nevada. In: Nevada

Bureau of Mines and Geology Report 19: 27-34

Noble DC, Anderson RE, Ekren EB, O'Connor JT (1964) Thirsty Canyon Tuff of Nye and Esmeralda Counties, Nevada. US Geol Surv Prof Paper 475-D: D24-D27

Noble DC, Parker DF (1974) Peralkaline silicic volcanic rocks of the western United States. Bull Volcanol 38: 803-827

Noble DC, Vogel TA, Weiss SI, Erwin JW, McKee EH, Younker LW (1984) Stratigraphic relations and source areas of ash-flow sheets of the Black Mountain and Stonewall Mountain volcanic centers, Nevada. J Geophys Res 89: 8593-8602

Noble DC, Rigot WL, Bowman HR (1979) Rare-earth-element content of some highly differentiated ash-flow tuffs and lavas. Geol Soc Am Spec Paper 180: 77-85

Peccerillo A, Barberio MR, Yirgu G, Ayalew D, Barbieri M, Wu TW (2003) Relationships between mafic and peralkaline silicic magmatism in continental rift settings: a petrological, geochemical and isotopic study of the Gedemsa volcano, Central Ethiopian Rift. J Petrol 44: 2003-2032

Pouchou JL, Pichoir JF (1991) Quantitative analysis of homogeneous or stratified microvolumes applying the model 'PAP'. In: Heinrich KFJ, Newbury DE (eds) Electron probe quantification. Plenum Press, New York, pp 31-75

Ren M, Omenda PA, Anthony EA, White JC, Macdonald R, Bailey DK (2006) Application of

the QUILF thermobarometer to the peralkaline trachytes and pantellerites of the Eburru volcanic complex, East African Rift, Kenya. Lithos 91: 109-124

Romano P, Andujar J, Scaillet B, Romengo N, Di Carlo I, Rotolo SG (2018) Phase equilibria of Pantelleria trachytes (Italy): constraints on pre-eruptive conditions and on the metaluminous to peralkaline transition in silicic magmas. J Petrol 59: 559-588

Rooney TO, Hart WK, Hall CM, Ayalew D, Ghiorso MS, Hidalgo P, Yirgu G (2012) Peralkaline magma evolution and the tephra record in the Ethiopian Rift. Contrib Mineral Petrol 164: 407-426

Sack RO, Carmichael ISE, Rivers M, Ghiorso MS (1980) Ferric-ferrous equilibria in natural silicate liquids at 1 bar. Contrib Mineral Petrol 75: 369-376

Sawyer DA, Fleck RJ, Lanphere MA, Warren RG, Broxton DE, Hudson MR (1994) Episodic caldera volcanism in the Miocene southwestern Nevada volcanic field: Revised stratigraphic framework, $^{40}Ar/^{39}Ar$ geochronology, and implications for magmatism and extension. Geol Soc Am Bull 106: 1304-1318

Scaillet B, Macdonald R (2001) Phase relations of peralkaline silicic magmas and petrogenetic implications. J Petrol 42: 825-845

Scaillet B, Macdonald R (2003) Experimental constraints on the relationships between peralkaline rhyolites of the Kenya Rift Valley. J Petrol 44: 1867-1894

Scaillet B, Macdonald R (2004) Fluorite stability in silicic magmas. Contrib Mineral Petrol

147: 319-329

Scaillet B, Macdonald R (2006) Experimental constraints on pre-eruption conditions of pantelleritic magmas: evidence from the Eburru complex, Kenya Rift. Lithos 91: 95-108

Scaillet S, Vita-Scaillet G, Rotolo SG (2013). Millenial-scale phase relationships between ice-core and Mediterranean marine records: insights from high-precision $^{40}Ar/^{39}Ar$ dating of the Green Tuff of Pantelleria, Sicily Strait. Quat Sci Rev 78: 141-154

Slate JL, Berry ME, Rowley PD, Fridrich CJ, Morgan KS, Workman JB, Young OD, Dixon GL, Williams VS, McKee EH, Ponce DA (2000) Digital geologic map of the Nevada Test Site and vicinity, Nye, Lincoln, and Clark Counties, Nevada, and Inyo County, California. No. USGS/OFR-99-554. U.S. Geol Surv, Las Vegas, Nevada

Sparks RSJ, Cashman KV (2017) Dynamic magma systems: implications for forecasting volcanic activity. Elements 13: 35-40

Sumner JM, Wolff J (2003) Petrogenesis of mixed-magma, high-grade, peralkaline ignimbrite 'TL' (Gran Canaria): diverse styles of mixing in a replenished, zoned magma chamber. J Volcanol Geotherm Res 126: 109-126

Sun S-S, McDonough WF (1989) Chemical and isotopic systematics of oceanic basalts: implications for mantle composition and processes. In: Saunders AD, Norry MJ (eds), Magmatism in the ocean basins. Geol Soc Lond Spec Publ 42: 313-345

Swallow EJ, Wilson CJN, Myers ML, Wallace PJ, Collins KS, Smith EGC (2018) Evacuation

of multiple magma bodies and the onset of caldera collapse in a supereruption, captured in glass and mineral compositions. Contrib Mineral Petrol 173: 33

Troll VR, Schmincke H-U (2002) Magma mixing and crystal recycling recorded in ternary feldspar from compositionally zoned peralkaline ignimbrite 'A', Gran Canaria, Canary Islands. J Petrol 43: 243-270

Vogel TA, Noble DC, Younker LW (1983) Chemical evolution of a high-level magma system: the Black Mountain volcanic center, southern Nevada. Report, Lawrence Livermore National Laboratory, Livermore, California. 49 pp

Vogel TA, Ryerson FJ, Noble DC, Younker LW (1987) Limits to magma mixing based on chemistry and mineralogy of pumice fragments erupted from a chemically zoned magma body. J Geol 95: 659-670

Vogel TA, Noble DC, Younker LW (1989) Evolution of a chemically zoned magma body: Black Mountain volcanic center, southwestern Nevada. J Geophys Res 94: 6041-6058

Weaver SD (1977) The Quaternary caldera volcano Emuruangogolak, Kenya Rift, and the petrology of a bimodal ferrobasalt – pantelleritic trachyte association. Bull Volcanol 40: 1-22

Weiss SI, Noble DC, McKee EH (1989) Paleomagnetic and cooling constraints on the duration of the Pahute Mesa-Trail Ridge eruptive event and associated magmatic evolution,

Black Mountain volcanic center, southwestern Nevada. J Geophys Res 94: 6075-6084

Wen S, Nekvasil H (1994) SOLVCALC: An interactive graphics program package for calculating the ternary feldspar solvus and for two-feldspar geothermometry. Comp Geosci 20: 1025-1040

White JC, Ren M, Parker DF (2005). Variation in mineralogy, temperature, and oxygen fugacity in a suite of strongly peralkaline lavas and tuffs, Pantelleria, Italy. Can Mineral 43: 1331-1347

White JC, Parker DF, Ren M (2009). The origin of trachyte and pantellerite from Pantelleria, Italy: Insights from major element, trace element, and thermodynamic modelling. J Volcanol Geotherm Res 179: 33-55

Yan L, He Z, Beler C, Klemd R (2018) Geochemical constraints on the link between volcanism and plutonism at the Yunshan caldera complex, SE China. Contrib Mineral Petrol 173: doi.org/10.1007/s00410-017-1430-5

Figure captions

Fig. 1 Generalized geological map showing the distribution of the Gold Flat Member of the Thirsty Canyon Tuff, modified from Noble (1965). Faults in pre-Gold Flat rocks are not

shown nor are all the intermittent drainage systems. For more detailed maps, the reader should consult Fridrich et al. (2007) and Slate et al. (2000)

Fig. 2 Part of thin section of sample Ttg-hg#1 (plane polarised light), showing three main glass types. Gl1 – russet-brown perlitic fiamme; Gl2 – dark brown fiamme with microcrysts; Gl3 – aphyric to poorly phric colourless fiamme and patches. Representative quartz (Qtz), alkali feldspar (Afs), olivine (Ol) and amphibole (Am) phenocrysts marked

Fig. 3 BSE **a** Image of plagioclase (Pl) antecryst in perlitic glass (Gl), sample Ttg-hg#1. Compositions along the profile marked by an arrow are given in Supplementary Table 1c, columns B to F. The rim of the crystal has been extensively altered to a complex mix of albite, baddeleyite and ilmenite. **b** Highly resorbed plagioclase antecryst in Ttg-hg#1. Compositions are given in Supplementary Table 1c, columns G and H. The light patch at upper right comprises secondary micaceous material

Fig. 4 BSE images. **a** Stellate cluster of ilmenite (Ilm) inclusions in olivine (Ol) phenocryst, sample GF1A. The bright grains are magnetite (Mag); the grey grain is titanite (Ttn). The grey fragments are mainly variably altered glass. **b** Cluster of olivine, fluorite (Fl) and CGM (Chv) phenocrysts in glass type 1 (Gl1) in Ttg-hg#1. **c** Fluorite crystals partly enclosed in amphibole (Am) phenocryst, in perlitic glass Gl1, sample Ttg-hg#1. The bright prismatic phase is ilmenite. Both amphibole and ilmenite contain melt inclusions (MI). **d** Ilmenite phenocryst with associated zircon (Zrn), fluorapatite (Ap) and CGM. Sample GF1A

Fig. 5 a Cluster of alkali feldspars (Afs), sample FC. The dusty appearance of the feldspars is due to inclusions of FeTi-oxides and biotite. The positions of six core to rim compositional profiles across crystals (Supplementary Table 1b) are shown by solid lines. Mafic phases tended to form along boundaries between feldspars. The position of Fig. 5b is marked. Plane polarized light. **b** BSE image of arc-shaped group of mafic phases from central part of Fig. 5a. Clinopyroxene (Cpx) has generally overgrown olivine. Ilmenite (Ilm) and baddeleyite (Bdl) grains are associated with both olivine (Ol) and pyroxene. The prismatic crystal in bottom right is biotite (Bt) and fluorapatite (Ap) forms tiny prisms. The red arrow points to a melt inclusion of trachytic composition (Table 2)

Fig. 6 a BSE image of enclave with elongate, curved feldspars typical of quench texture. The area in the box is shown in **b**. Xen is a quartz-feldspar-bearing xenolith. Sample Ttg-hg#1. **c** BSE image of enclave in GF1A showing quench texture. The phenocrysts are alkali feldspar, clinopyroxene and FeTi-oxides. The area in the box is shown in **d.**

Fig. 7 Core to rim compositional profiles (expressed as mol% An) across three alkali feldspar phenocrysts in Ttg-hg#1. Data from Supplementary Table 1a, TTG 21, 23, and 26

Fig. 8 An-Ab-Or plot for Gold Flat Tuff feldspars. Data for the three feldspars used in Fig. 7 are representative of the whole range of phenocrysts. Note that they evolved along slightly different trends; also note the calcic cores in TTG-26. Also shown are the compositions of

various antecrysts, with light solid lines marking the zonation in two examples, and data for crystal II in the feldspar cluster. Data from Supplementary Tables 1a, b and c

Fig. 9 Pyroxene compositions plotted in the Di-Hd-En-Fs quadrilateral. Data from Supplementary Table 2b

Fig. 10 Whole rocks (and separated glass) and glasses plotted in the classification scheme for peralkaline silicic extrusive rocks of Macdonald (1974). The dashed line is the trend of experimental glasses in a Pantescan pantellerite synthesised over a range of P and T by Di Carlo et al. (2010). , CT, comenditic trachyte; PT, pantelleritic trachyte; C, comendite; P, pantellerite. Data from Table 2 and Supplementary Table 5

Fig. 11 a SiO_2-FeO* and **b** SiO_2-Al_2O_3 plots to show that the pantelleritic and comenditic melts (glasses) in Ttg-hg#1 evolved along slightly different trends. Note the generally negative correlations between Al_2O_3 and decreasing SiO_2 and the positive correlations between FeO* and decreasing SiO_2. The arrows suggest evolution with quartz fractionation. Data from Supplementary Table 5a

Fig. 12 Chondrite-normalized REE patterns for trachybasalts (TM2, TM3), mixed magma rock from basal fall unit (GF1), and comendite (Ttg-1-1) and pantellerite (Ttg-hg#1) from welded tuff. Data from Table 2. Normalizing factors from Sun and McDonough (1989)

Fig. 13 Silica activity plotted against temperature for subsuites of rocks from Pantelleria and Eburru (White et al. 2005, 2009; Ren et al. 2006; Liszewska et al., in revision); subsuites are based on simplified phenocryst assemblages (White et al. 2005) and are shown by different symbols. Modified from Macdonald et al. (2011), with curves calculated at 1500, 1000 and 500 bars, with X_{ilm} = 0.95 and X_{Fa} = 1.0. The absence of aenigmatite in favour of fayalite + ilmenite with quartz phenocrysts ($a$$SiO_2$ quartz ~1) in the Gold Flat Tuff might suggest that the phenocrysts crystallized at temperatures ≥740 °C in a melt with relatively low silica activity

Fig. 14 Peralkalinity Index (P.I.: mol (Na_2O+K_2O)/Al_2O_3)) plotted against calculated temperatures for pantelleritic and comenditic glasses in sample Ttg-hg#1 and trachytic glass in FC. Data from Supplementary Table 5

Fig. 15 Compositions of selected alkali feldspar phenocrysts plotted in the ternary feldspar diagram, along with the solvi for 875 °C and 750 °C (Wen and Nekvasil 1994). The feldspars crystallized over a range of temperatures, representing zonation in the pre-eruptive reservoir. Data from Supplementary Table 1a

Figure 1

Click here to access/download;Line Figure;Fig. 1.tif

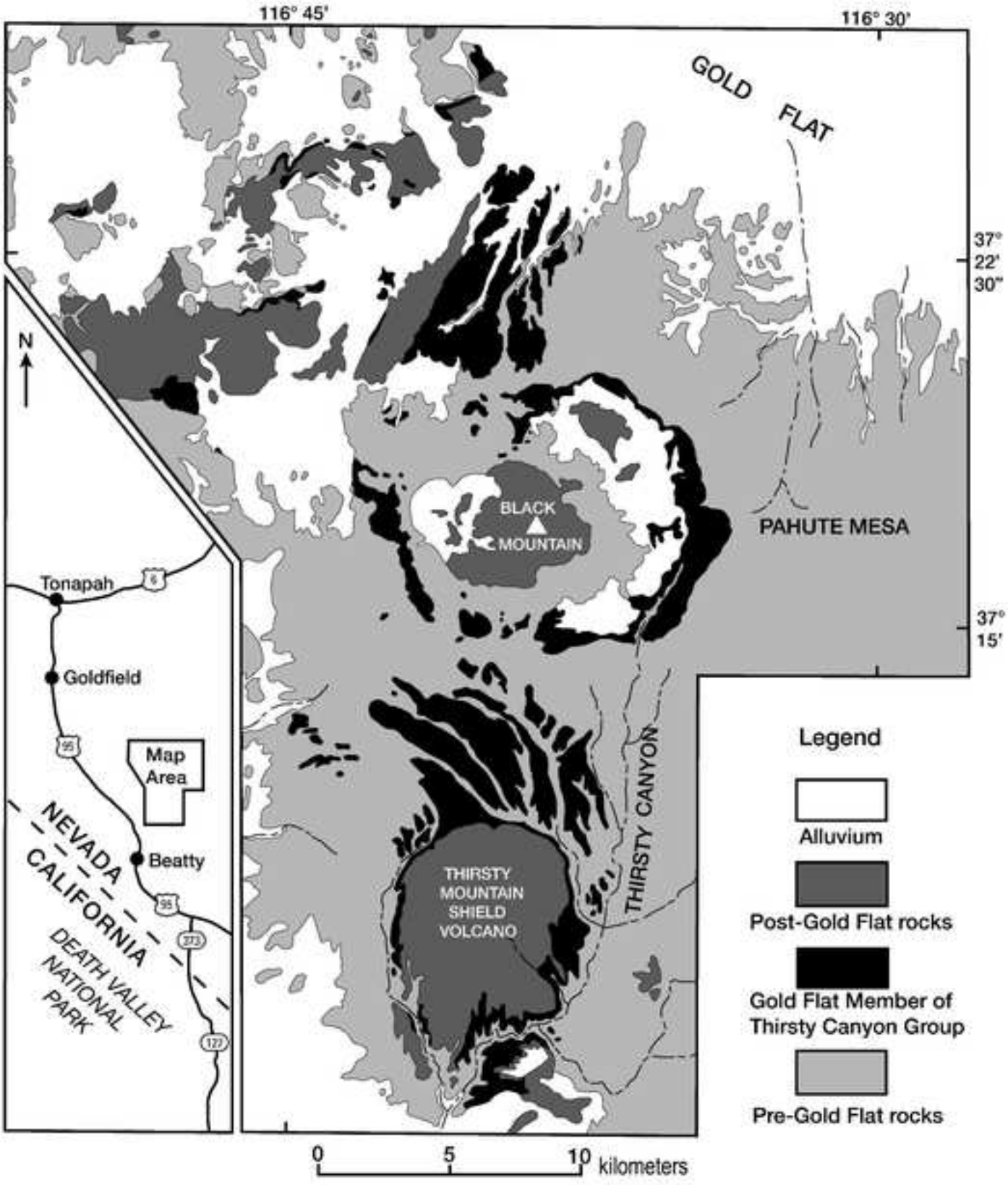

Figure 2

Click here to access/download;Colour Figure;Fig. 2.tif

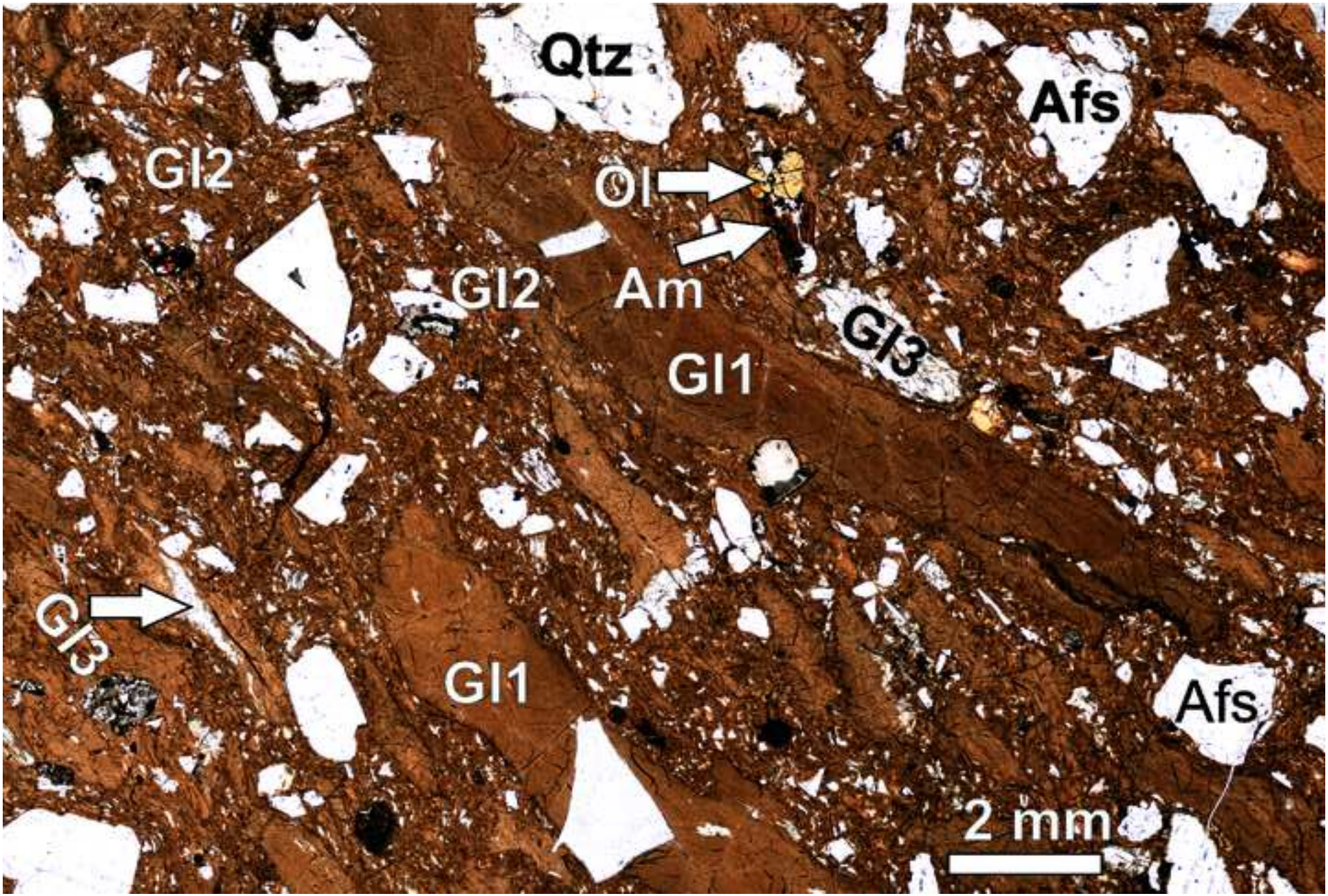

Figure 3

Click here to access/download;Line Figure;Fig. 3.tif

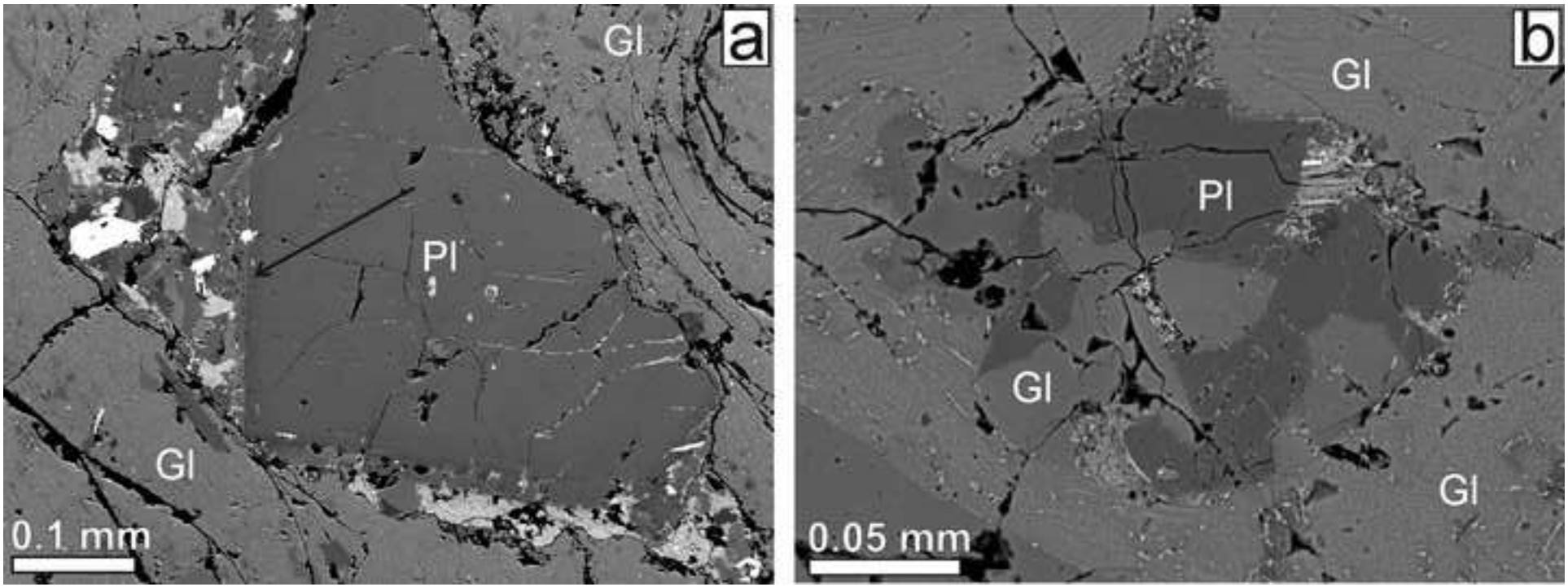

Figure 4

Click here to access/download;Line Figure;Fig.4.tif

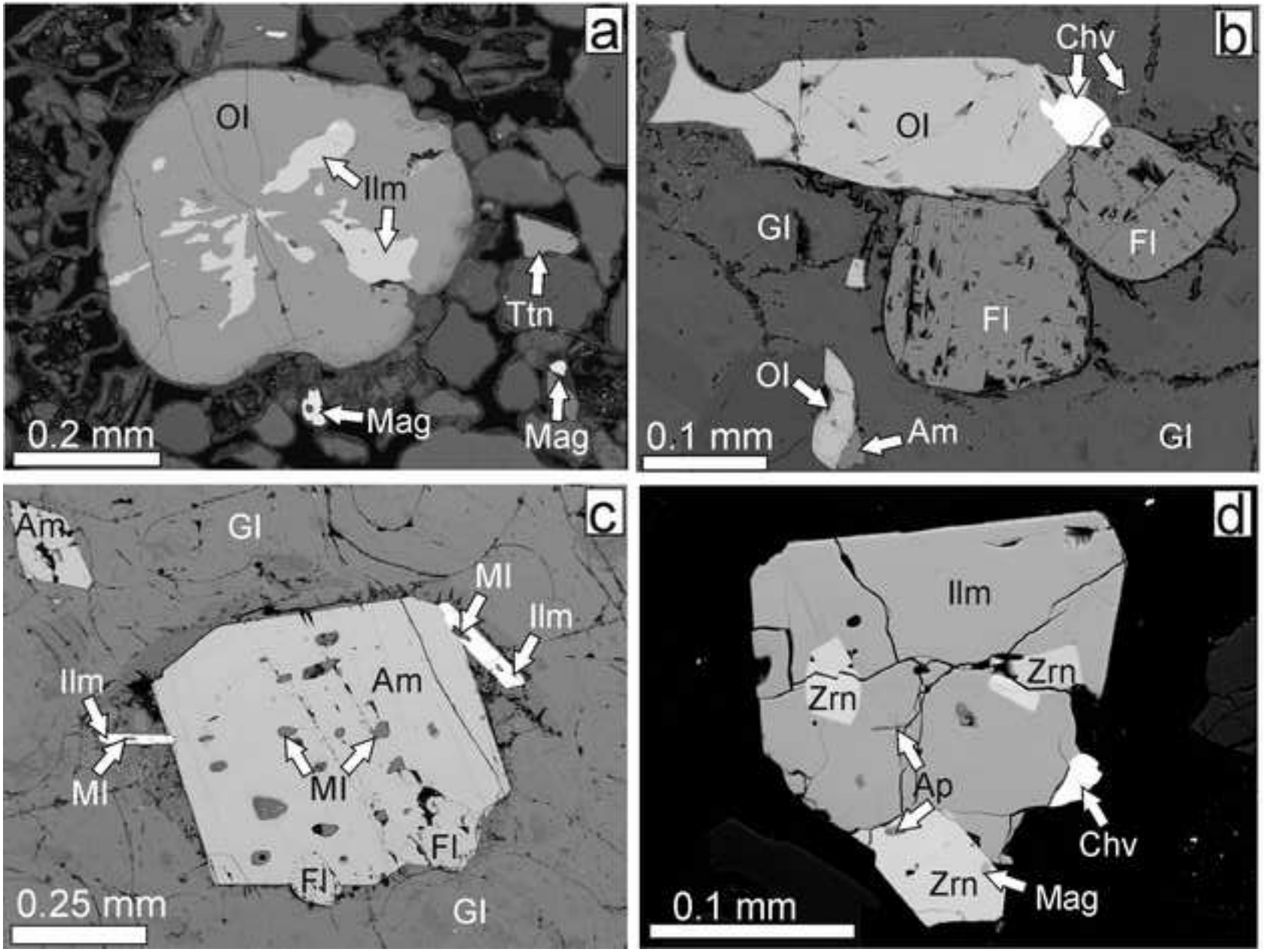

Figure 5

Click here to access/download;Colour Figure;Fig.5.tif

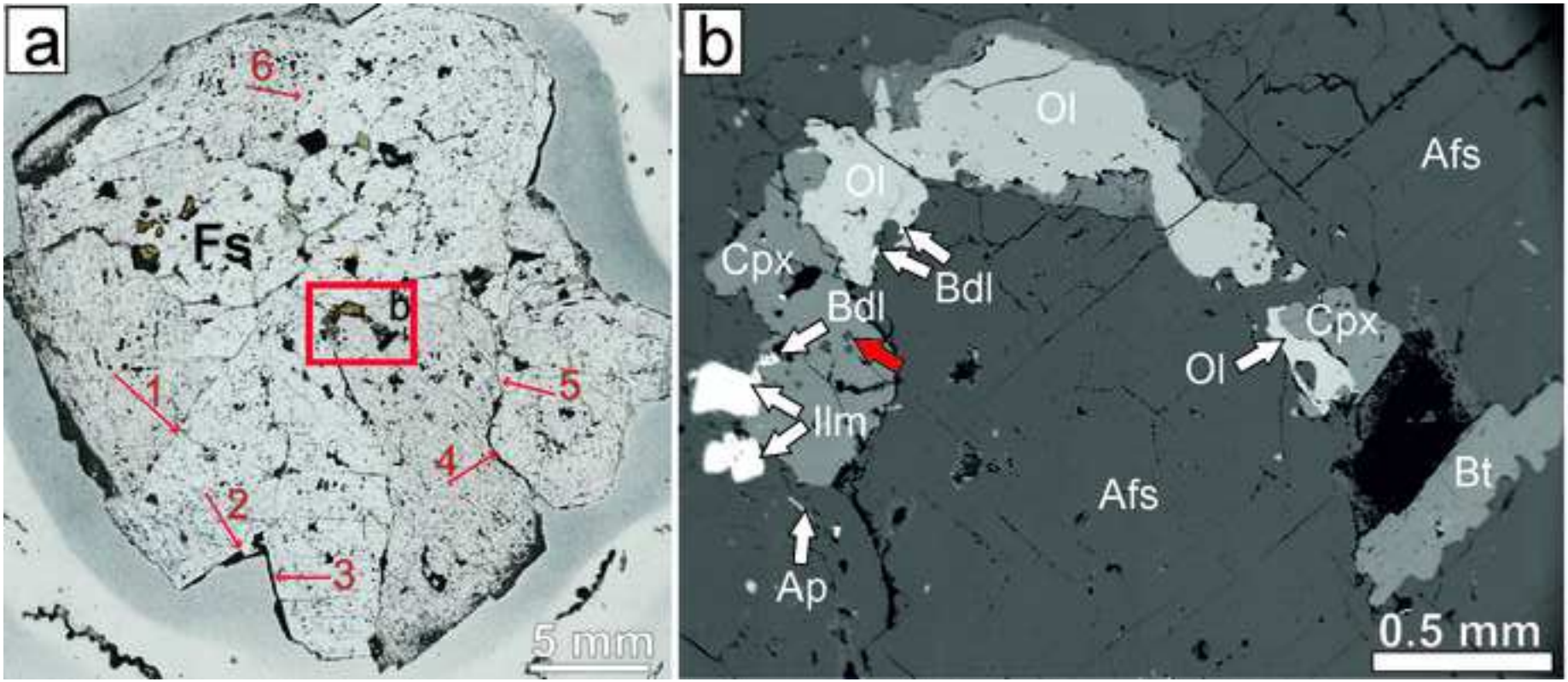

Figure 6

Click here to access/download;Line Figure;Fig.6.tif

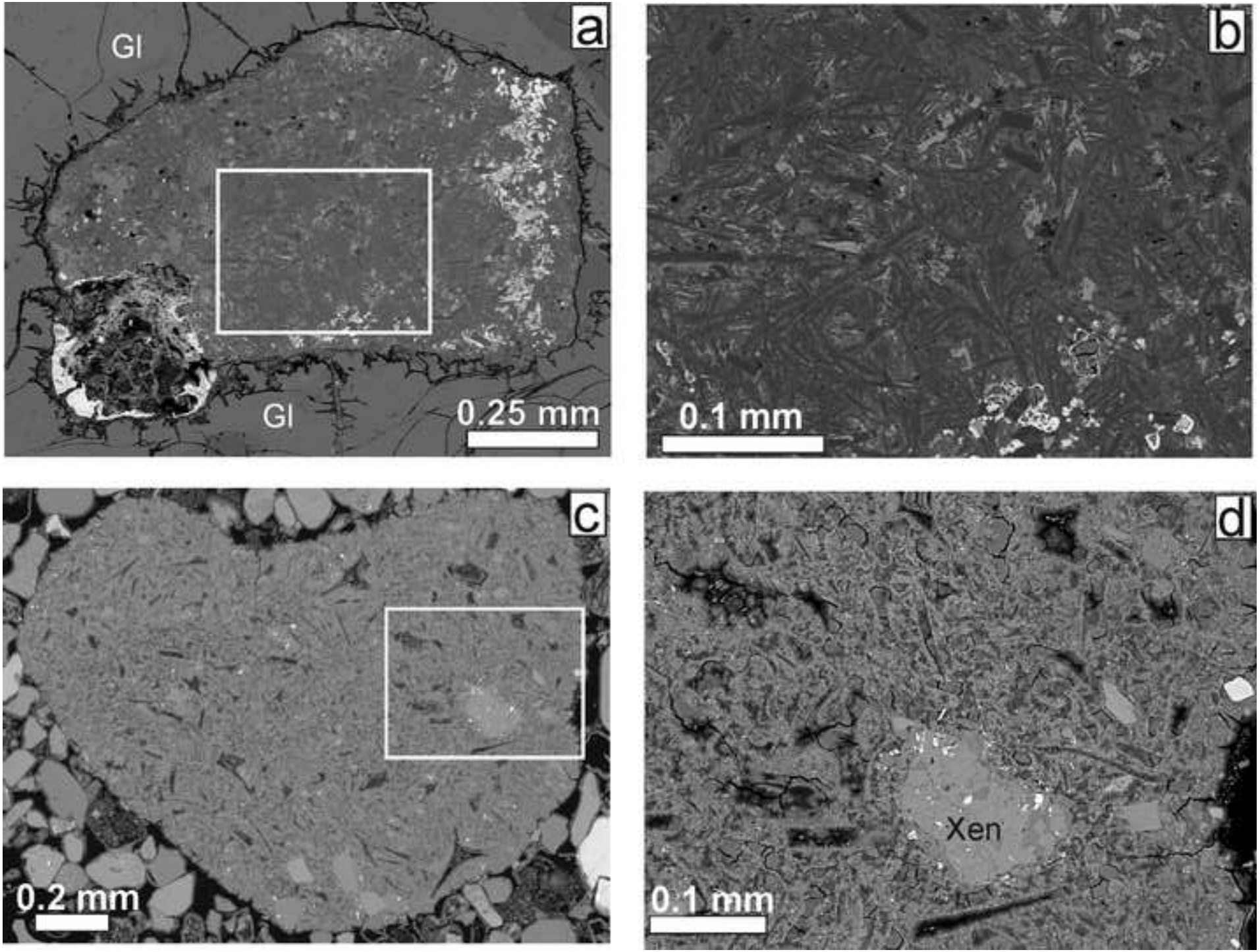

Figure 7

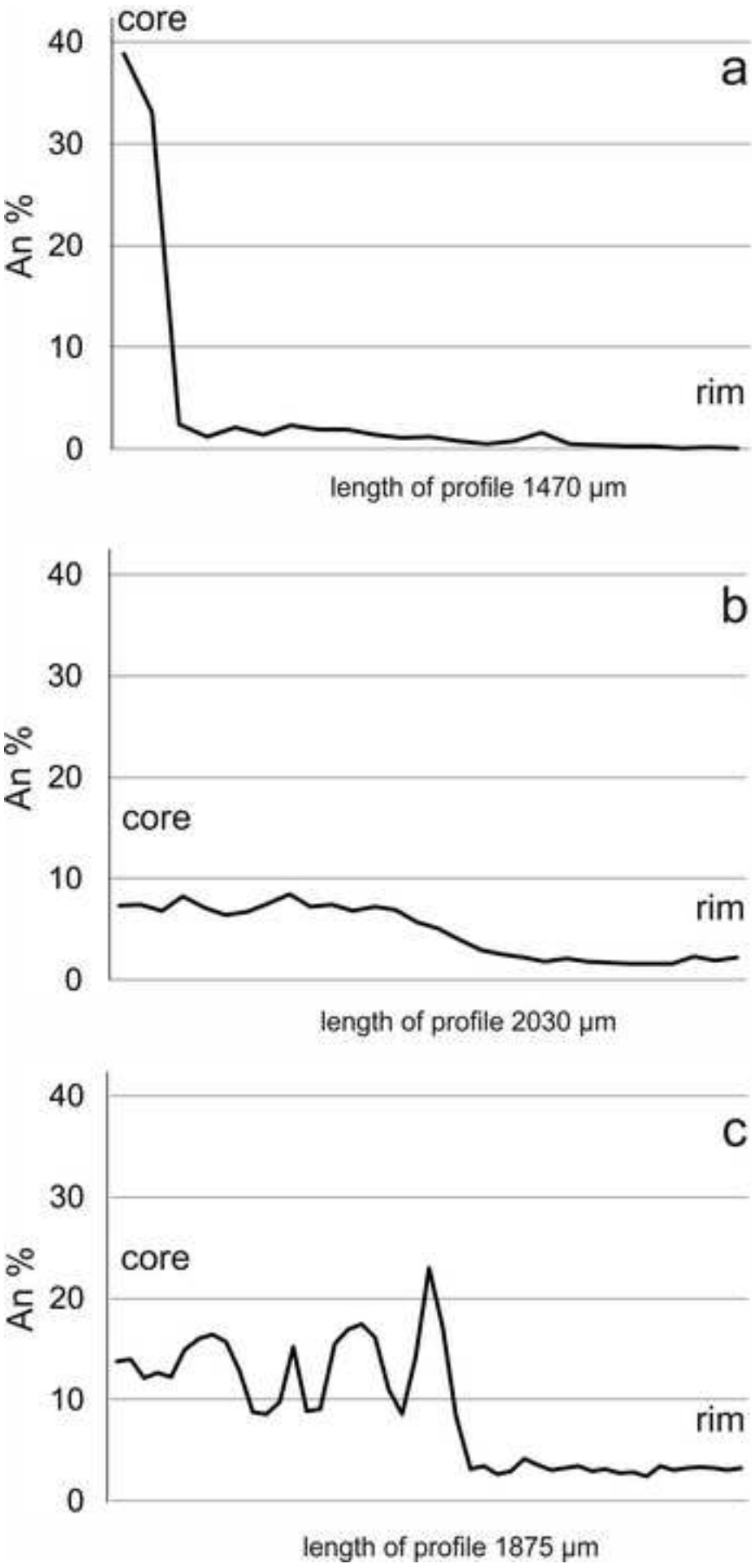

Figure 8

Click here to access/download;Colour Figure;Fig.8.tif

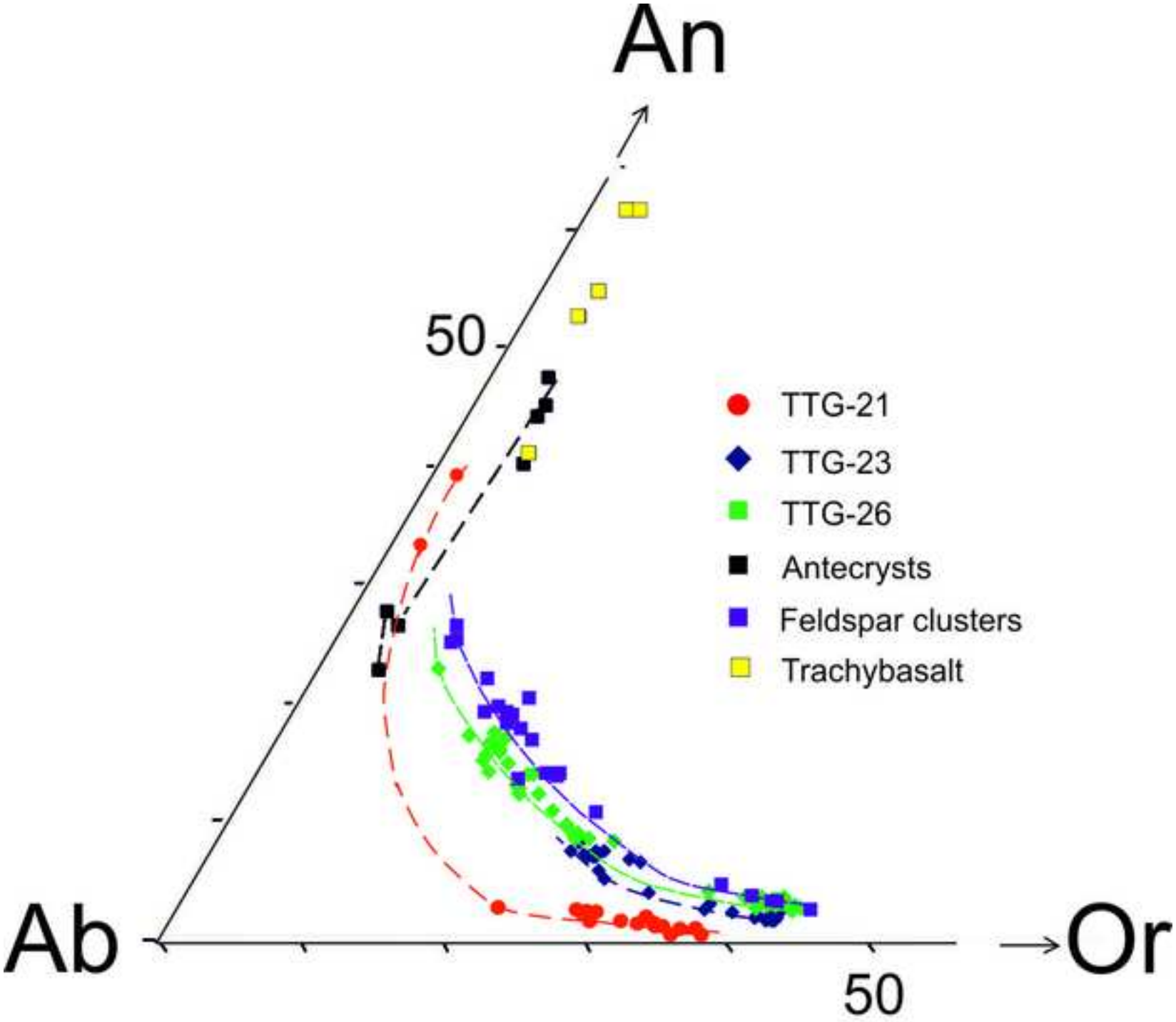

Figure 9

Click here to access/download;Line Figure;Fig.9.tif

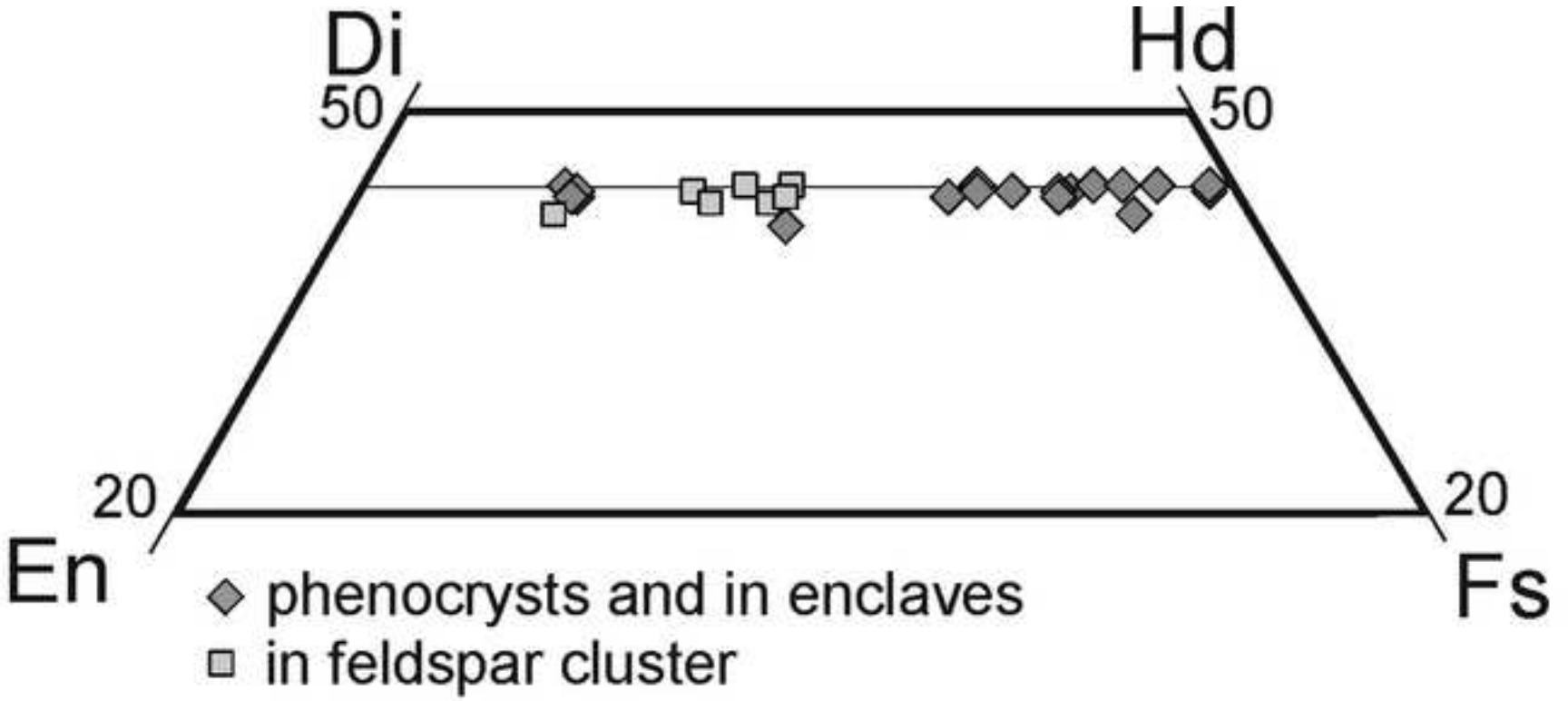

Figure 10

Click here to access/download;Line Figure;Fig.10.tif

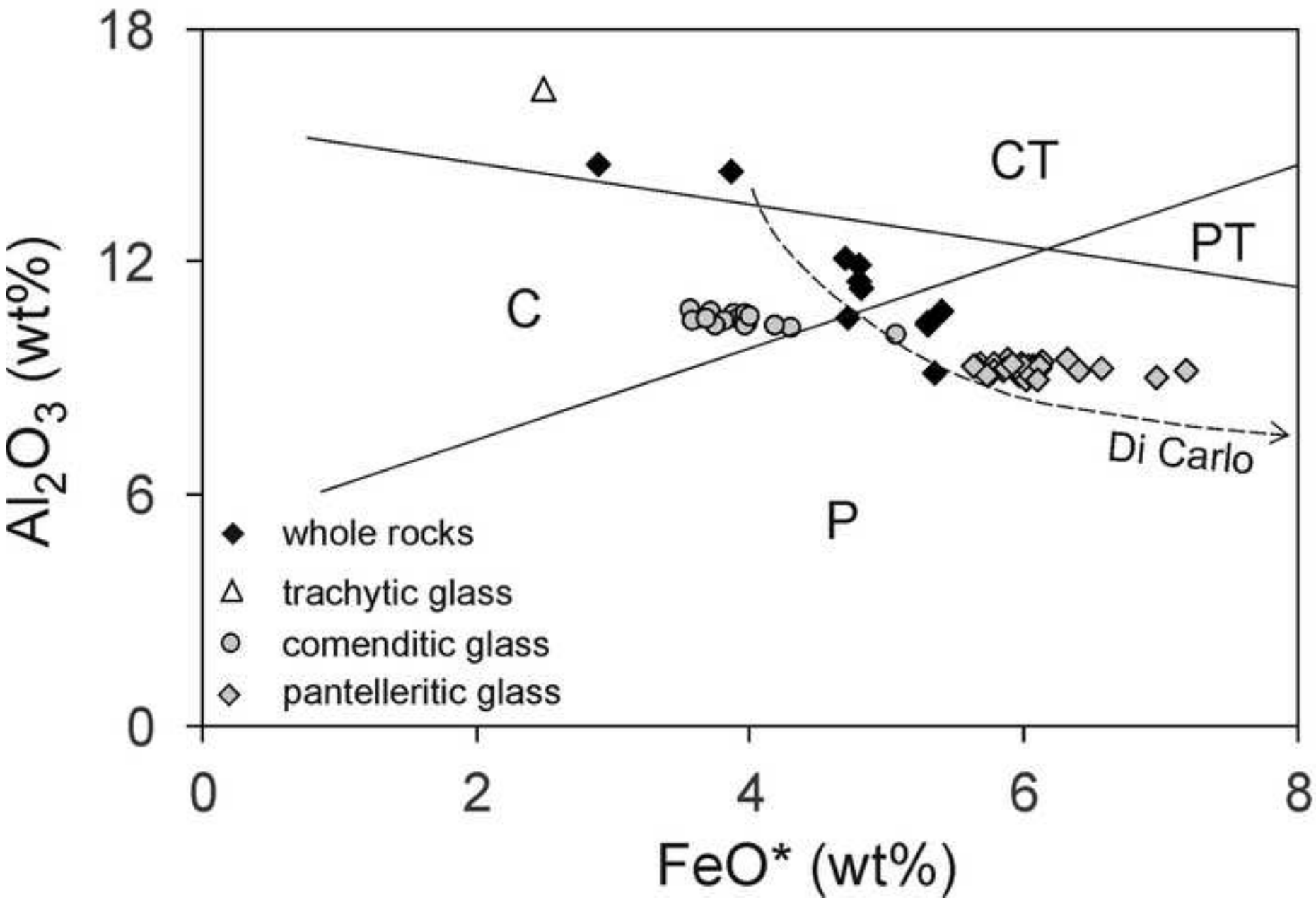

Figure 11

Click here to access/download;Line Figure;Fig.11.tif

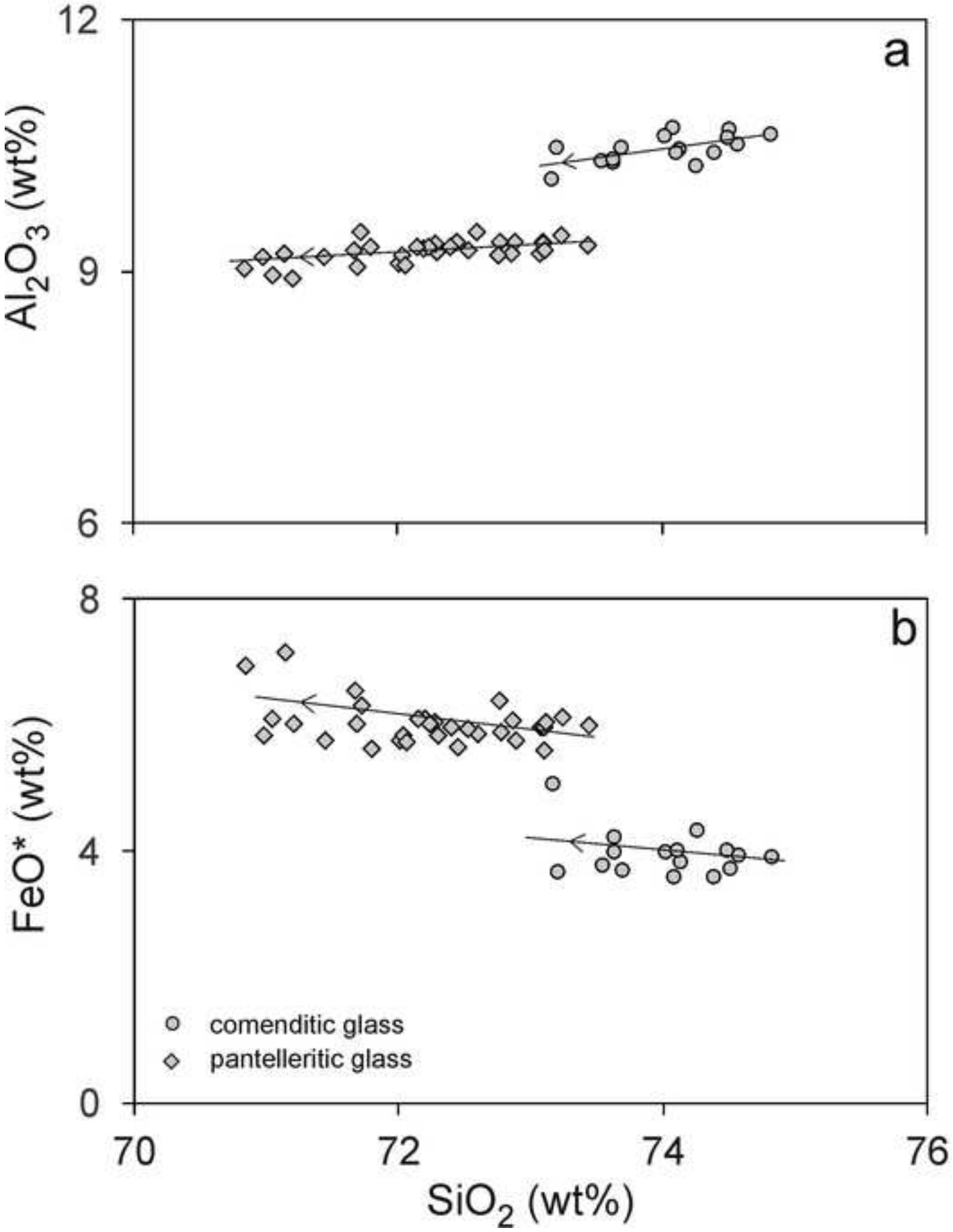

Figure 12

Click here to access/download;Line Figure;Fig.12.tif

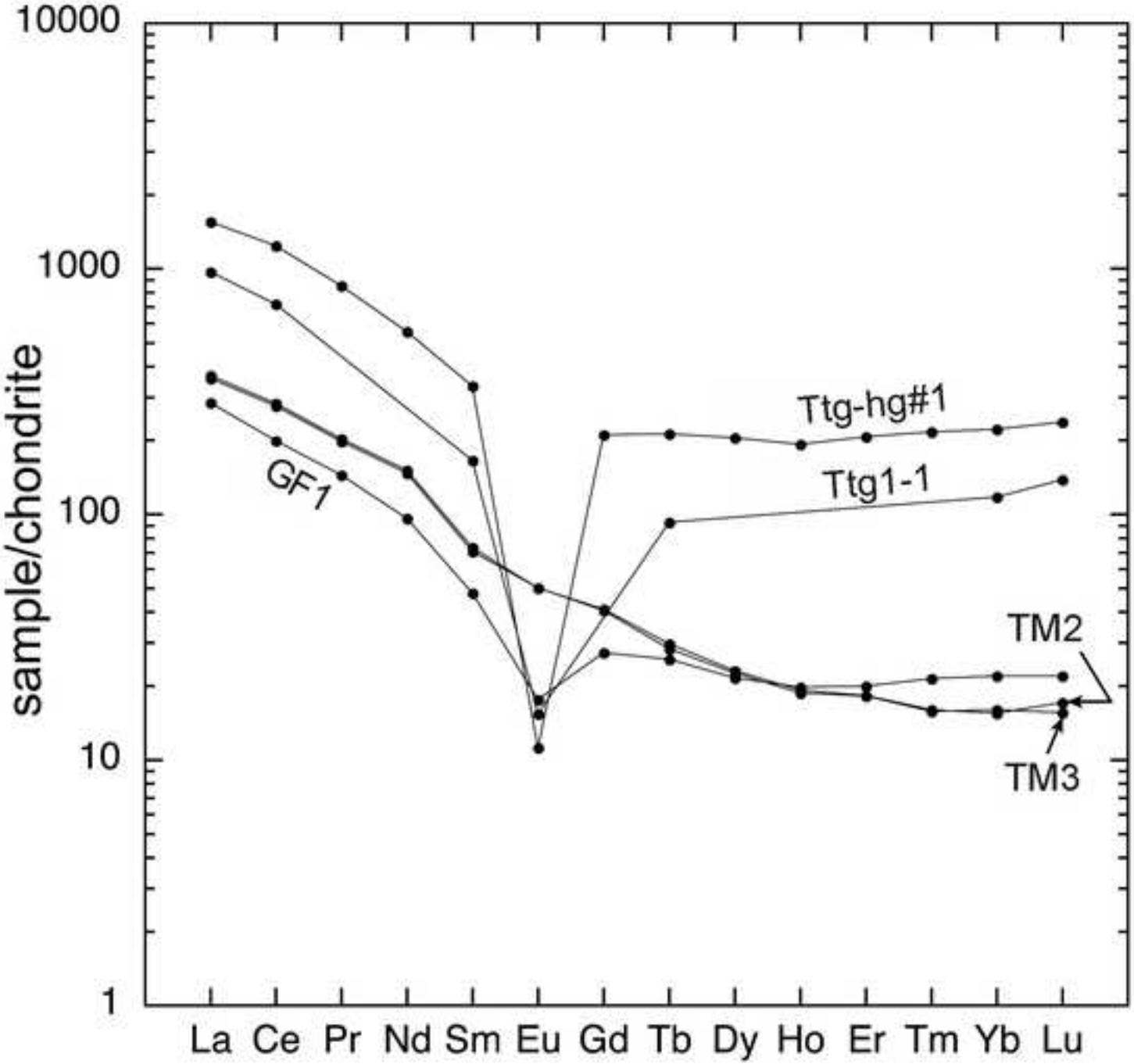

Figure 13

Click here to access/download;Line Figure;Fig.13.tif

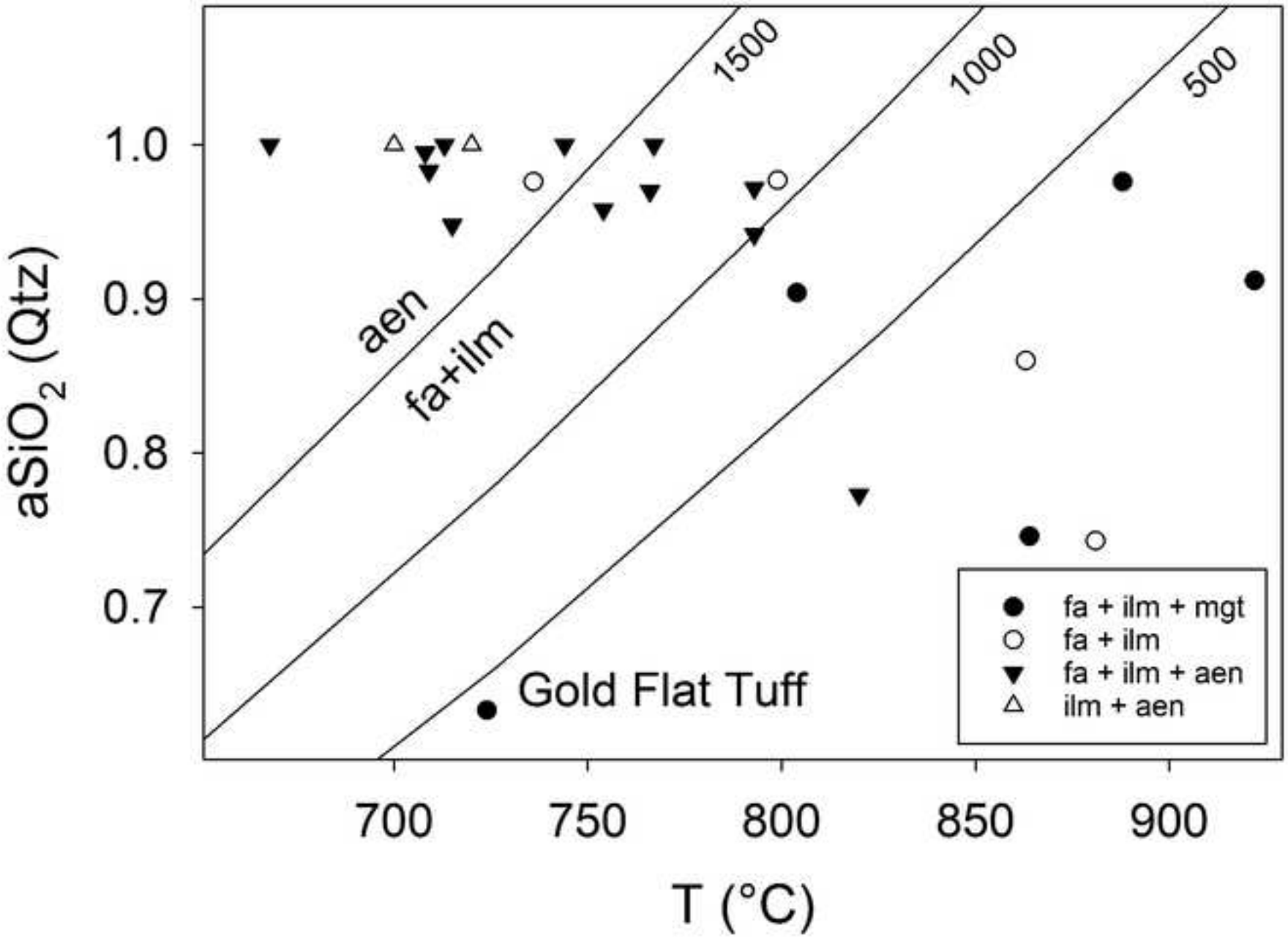

Figure 14

Click here to access/download;Line Figure;Fig.14.tif

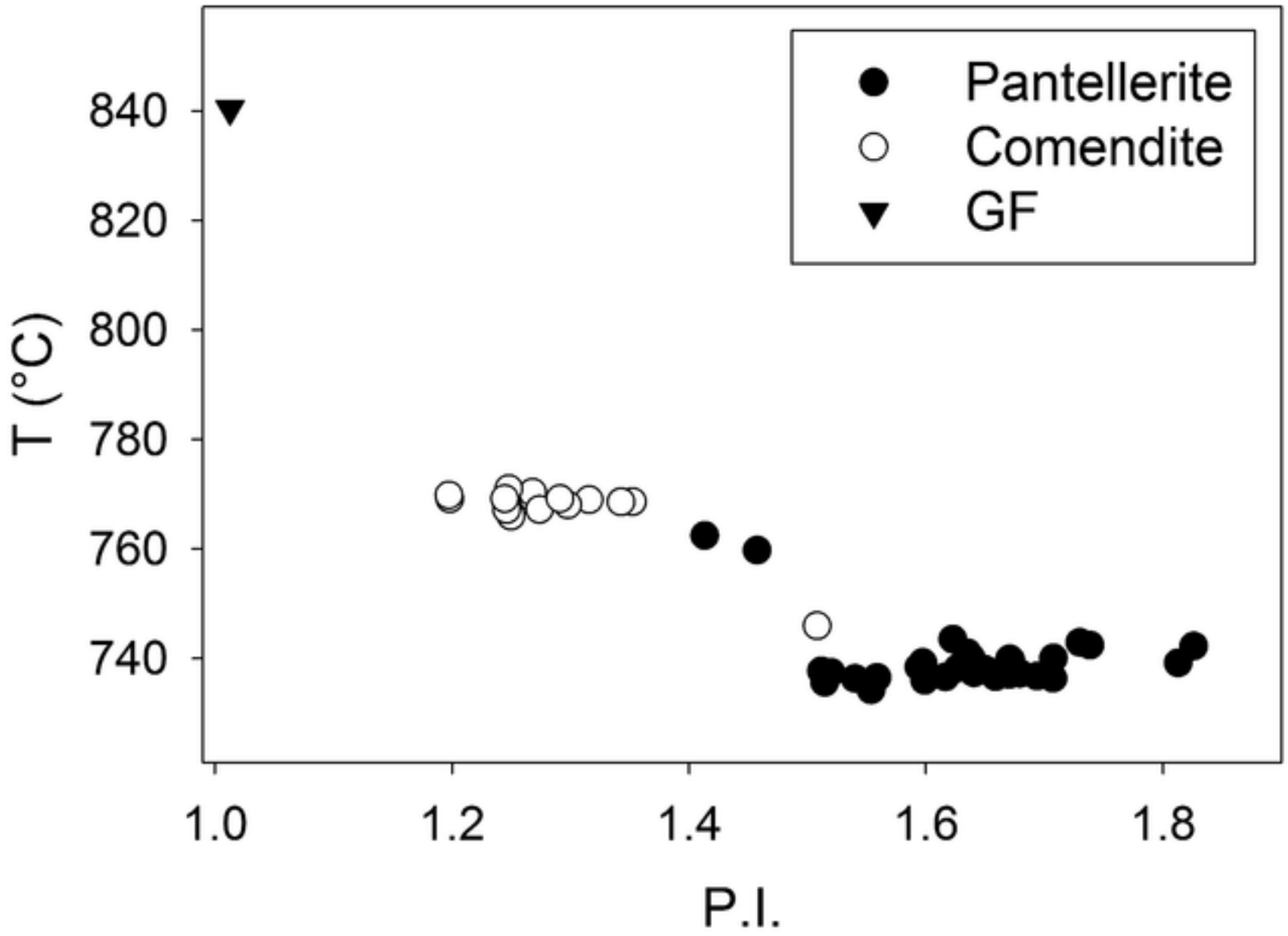

Figure 15

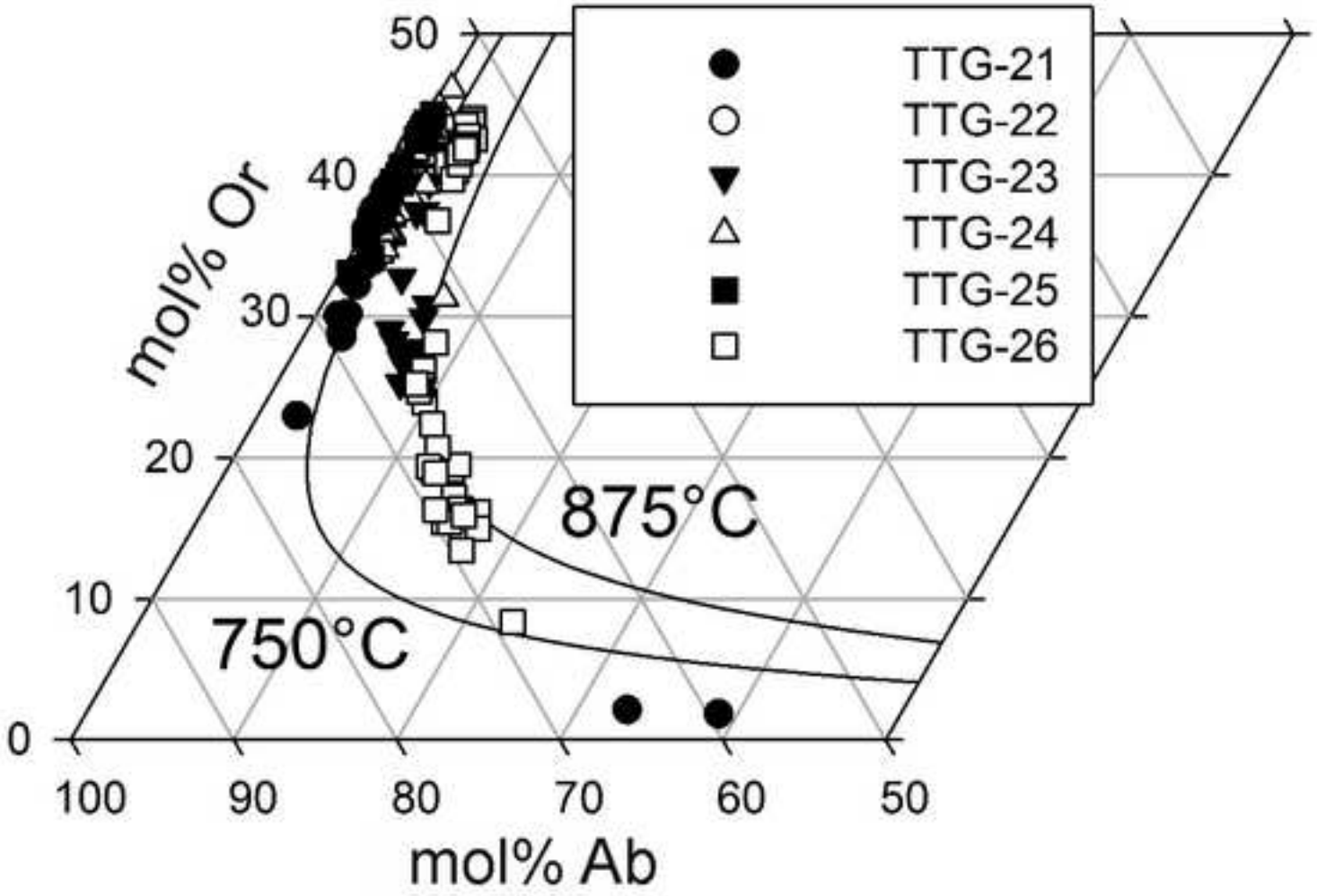

Table 1 Volcanic stratigraphy of Thirsty Canyon Group

Unit	Main deposits	Age (Ma)	MET (m)	Volume (km^3)	SiO_2 (anh.%)
Gold Flat Tuff	ash flow tuff	9.15	30	20	66.9-71.5
Pillar Spring	lavas	-	125	-	64.4-70.0
Trail Ridge Tuff	ash flow tuff	-	80	25	66.7-73.6
Pahute Mesa Tuff	ash-flow tuff	-	35	50-75	65.7-74.6
Rocket Wash Tuff	ash-flow tuff	9.42	20	50-75	67.8-73.4
Ribbon Cliff	lavas and domes	-	100	-	55.6-70.8

MET, maximum exposed thickness (estimated). Compiled from data in Vogel et al. (1989) and Minor et al. (1998)

Table 2 Chemical composition of rocks and separated glass

	1	2	3	4	5	6	7	8
Sample	TM2	TM3	GF1	Ttg-1-1	GF4	D100126	N-90-NG	Ttg-hg#1
wt%								
SiO_2	50.57	50.82	65.47	66.86	67.67	69.25	69.30	69.58
TiO_2	1.88	1.83	0.44	0.30	0.31	0.25	0.25	0.291
Al_2O_3	17.21	17.18	14.53	14.32	10.52	9.10	9.05	10.35
Fe_2O_3	3.57	6.42	2.10	-	4.45	3.70	3.73	3.00
FeO	5.50	2.60	1.00	-	0.70	2.01	2.60	2.60
FeO*	8.71	8.38	2.89	3.85	4.70	5.34	5.96	5.30
MnO	0.16	0.15	0.09	0.13	0.16	0.19	0.20	0.17
MgO	4.15	2.49	1.88	1.53	0.28	0.011	0.01	0.10
CaO	7.02	7.32	2.09	1.55	3.10	0.06	0.10	0.39
Na_2O	3.86	3.86	3.37	5.74	4.83	7.00	7.04	5.73
K_2O	2.91	2.91	3.34	5.14	4.16	4.29	4.37	4.22
P_2O_5	1.06	1.08	0.08	0.10	0.14	0.01	0.01	0.09
SO_3	0.03	0.03	0.04	-	0.02	0.08	-	0.05
Cl	0.02	0.04	0.03	-	0.05	0.78	0.77	0.55
F	0.07	0.07	0.08	-	0.16	1.30	1.35	0.71
LOI	0.97	1.67	5.18	-	1.30	-	-	2.26
H_2O+	-	-	-	-	-	0.14	0.13	-
H_2O-	-	-	-	-	-	0.01	0.02	-
CO_2	0.20	0.38	0.04	-	1.89	0.08	0.00	0.05
Sum	99.17	98.84	99.75	99.52	99.75	98.26	98.93	100.14
O ≡ F, Cl	0.04	0.04	0.04	-	0.08	0.77	0.78	0.45
Total	99.14	98.82	99.71	99.52	99.67	98.27*	98.15	99.71
ppm								
Ba	2250	2217	785	448	230	-	1.54	117
Sr	1030	1022	317	136	195	-	1.5	41
Rb	48	50	113	408	581	-	900	726
Cs	0.4	1.1	8.8	6.24	8.4	-	-	15.1
Zr	354	344	406	1976	3450	-	6500	4281
Hf	7.3	6.8	10.3	55.9	90.4	-	144	107
Ga	21	21	20	-	35	-	44	38
Co	22	22	4	-	3	-	0.24	2
Cr	65	65	32	-	<5	-	≤1	10
Ni	48	47	7	44	2	-	<2	2
Sc	15.1	14.4	5.1	-	2.5	-	7	1.6
V	155	153	49	-	15	-	<5	6
Cu	21	21	6	-	15	-	3	10
Zn	90	94	69	250	386	-	-	497
Pb	10	11	27	-	124	-	210	140
Sn	2	2	3	-	31	-	52	35
Y	31	32.1	28.1	175	227	-	500	326
Nb	31.6	33	34.9	219	313	-	680	349
Ta	1.58	1.65	2.39	12.8	19.6	-	-	22.4
Sb	1.3	<0.2	0.3	-	0.5	-	-	159

Th	5.25	5.38	23.7	75.3	140	-	223	159
U	0.62	1.4	3.33	-	23.8	-	45.9	34.7
La	84.5	87.1	67.4	230	320	-	439	367
Ce	169	173	122	438	676	-	796	759
Pr	18.8	19.3	13.7	-	69.9	-	-	80.8
Nd	68.7	70.5	44.9	-	228		-	259
Sm	10.8	11.2	7.31	25.4	43.7		64.8	50.9
Eu	2.91	2.9	1.02	0.89	0.701		0.59	0.65
Gd	8.32	8.44	5.61	-	35.9		-	43.2
Tb	1.06	1.11	0.96	3.47	6.45		10.9	7.94
Dy	5.74	5.86	5.48	-	41.5		-	52
Ho	1.06	1.09	1.12	-	8.24		-	10.9
Er	3.01	3.02	3.3	-	25.4		-	34.2
Tm	0.402	0.407	0.546	-	4.16		-	5.51
Yb	2.72	2.63	3.74	19.94	29.7		55	37.7
Lu	0.396	0.435	0.557	3.51	4.75		6.9	6.03
Ag	1.2	1.2	4.9	-	11.3	-	-	14.4
As	0.8	6.7	6.2	-	18.5	-	-	20.7
B	16	22	28	-	79	-	-	104
Be	2	3	4	-	41	-	-	48
Bi	<0.1	<0.1	0.2	-	0.4	-	-	0.3
Ge	1.5	1.6	2.6	-	2.9	-	-	3.3
Hg	-	-	18	-	-	-	-	
Tl	0.27	0.46	0.91	-	0.81	-	-	1.9
W	<0.5	0.8	3	-	7.4	-	-	9.9
Mo	4	<2	<2	-	-	-	-	<2
Sb	<0.2	0.3	0.5	-	1.3	-	-	2.1
Eu/Eu*	0.96	0.92	0.45	0.11	0.05	-	0.03	0.04

Explanation: analyses 1 and 2 from Basalt of Thirsty Mountain; analyses 3-8 from Gold Flat Tuff

Sources: Analyses, 1, 2, 3, 5, 8, 9 - this paper; 4, Vogel et al. 1989; 6, Noble 1965; 7, Noble and Parker 1974

*, total includes 0.78 wt% ZrO_2

LOI, loss on ignition

FeO*, all Fe as Fe^{2+}

Dash, not reported

Table 3 Representative EPMA analyses of glass

	Pantelleritic						Comenditic	
	1	2	3	4	5	6	7	8
wt%								
SiO_2	72.60	73.10	70.98	71.67	71.21	71.69	73.18	74.09
TiO_2	0.22	0.28	0.26	0.30	0.23	0.26	0.23	0.14
ZrO_2	0.89	0.91	0.83	0.92	0.77	0.84	0.63	0.32
Al_2O_3	9.47	9.35	9.17	9.24	8.92	9.06	10.07	10.70
FeO*	5.88	5.98	5.85	6.57	6.02	6.04	5.07	3.58
MnO	0.08	0.25	0.21	0.26	0.23	0.18	0.09	0.13
MgO	0.02	b.d.l.	b.d.l.	0.02	b.d.l.	b.d.l.	0.02	0.02
CaO	0.10	0.10	0.12	0.08	0.05	0.09	0.15	0.18
Na_2O	6.12	5.84	4.60	6.46	5.96	5.99	6.06	4.74
K_2O	5.00	5.18	4.98	5.02	5.01	4.95	4.82	5.13
SO_3	b.d.l.	0.03	0.03	b.d.l.	b.d.l.	b.d.l.	b.d.l.	0.04
F	1.62	0.96	1.08	2.23	1.23	0.92	0.91	0.65
Cl	0.80	0.72	0.82	0.67	0.79	0.77	0.24	0.47
Sum	102.80	102.70	98.93	103.44	100.42	100.79	101.47	100.19
O ≡ F, Cl	0.86	0.57	0.64	1.09	0.74	0.60	0.44	0.38
Total	101.94	102.13	98.29	102.35	99.68	100.19	101.03	99.81
PI	1.63	1.63	1.41	1.74	1.71	1.68	1.51	1.25
F + Cl	2.42	1.68	1.90	2.90	2.02	1.69	1.15	1.12

Explanation: analyses 1-9 from sample Ttg-hg#1; analysis 10 from FC

b.d.l., below detection limit

FeO*, all Fe as Fe^{2+}

PI, Peralkalinity Index (mol. $(Na_2O+K_2O)/Al_2O_3$)

	Trachytic
9	10
74.14	67.04
0.16	0.30
0.18	0.43
10.44	16.47
3.83	2.49
0.15	0.13
b.d.l.	0.04
0.19	0.45
4.50	6.05
5.18	6.21
b.d.l.	0.04
0.47	0.46
0.49	0.49
99.73	100.60
0.34	0.33
99.39	100.27
1.25	1.01
0.96	0.95

APPENDIX General EPMA analytical conditions				
Element	Line	Crystal	Standard	Approx. detection limit (wt%)
Al	Kα	TAP	orthoclase	0.01
Ba	Lα	LiF	barite	0.11
Ca	Kα	PET	$CaSiO_3$	0.01
Ce	Kα	PET	CeP_5O_{14}	0.05
Dy	Lß	LiF	REE1	0.31
Eu	Lß	LiF	REE2	0.26
Fe	Kα	LiF	hematite	0.03
Gd	Lß	LiF	GdP_5O_{14}	0.13
Hf	Mα	TAP	Hf-SPI	0.03
La	Lα	PET	LaB_6	0.05
Mg	Kα	TAP	diopside	0.01
Mn	Kα	LiF	rhodonite	0.04
Na	Kα	TAP	albite	0.01
Nb	Lα	PET	Nb metal	0.05
Nd	Lß	LiF	NdP_5O_{14}	0.12
P	Kα	PET	apatite Jap2	0.01
Pr	Lß	LiF	PrP_5O_{14}	0.12
Sc	Kα	PET	Sc metal	0.01
Si	Kα	TAP	$CaSiO_3$	0.01
Sm	Lß	LiF	SmP_5O_{14}	0.13
Sr	Lα	TAP	$SrTiO_3$	0.03
Ta	Mα	TAP	Ta metal	0.04
Tb	Lα	LiF	REE4	0.14
Th	Mα	PET	ThO_2 synthetic	0.09
Ti	Kα	PET	rutile	0.02
U	Mß	PET	vorlanite	0.08
Y	Lα	TAP	$Y_3Al_5O_{12}$	0.03
Yb	Lα	liF	REE3	0.14
Zr	Lα	PET	zircon ED2	0.05

REE1 to 4: glasses with REE (reference samples of Jarosewich and Boatner (1991) Rare-earth element reference samples for electron microprobe analysis. Geostandards Newsletter 15: 397-399

Supplementary Table 1a Compositions of feldspar phenocrysts

		wt%						
Table no.	Anal. no.	SiO_2	Al_2O_3	FeO*	MnO	CaO	SrO	Na_2O
1	1 / 1 .	58.06	26.69	0.07	b.d.l.	8.08	0.31	6.82
2	1 / 2 .	59.72	25.68	0.11	b.d.l.	6.87	0.22	7.43
4	1 / 4 .	67.21	19.79	0.16	b.d.l.	0.50	b.d.l.	8.67
6	1 / 6 .	67.25	19.24	0.17	b.d.l.	0.25	b.d.l.	7.63
7	1 / 7 .	66.13	19.15	0.53	b.d.l.	0.44	b.d.l.	7.79
8	1 / 8 .	67.33	19.29	0.13	b.d.l.	0.30	b.d.l.	7.90
9	1 / 9 .	67.44	19.33	0.20	b.d.l.	0.48	b.d.l.	7.84
10	1 / 10 .	67.29	19.65	0.07	b.d.l.	0.39	b.d.l.	7.78
11	1 / 11 .	66.83	19.40	0.22	b.d.l.	0.40	b.d.l.	7.81
12	1 / 12 .	66.64	19.10	0.30	b.d.l.	0.29	b.d.l.	7.51
13	1 / 13 .	67.05	19.29	0.09	b.d.l.	0.24	b.d.l.	7.40
14	1 / 14 .	67.31	19.15	0.24	b.d.l.	0.25	b.d.l.	7.56
15	1 / 15 .	67.20	18.88	0.19	b.d.l.	0.18	b.d.l.	7.33
16	1 / 16 .	67.26	19.16	0.25	b.d.l.	0.10	b.d.l.	7.00
17	1 / 17 .	67.37	19.12	0.25	b.d.l.	0.18	b.d.l.	7.24
18	1 / 18 .	66.20	19.09	0.48	0.13	0.31	b.d.l.	7.07
19	1 / 19 .	67.25	18.86	0.30	b.d.l.	0.10	b.d.l.	7.08
20	1 / 20 .	67.65	18.82	0.15	0.04	0.09	b.d.l.	7.07
21	1 / 21 .	67.70	18.87	0.23	0.05	0.07	b.d.l.	7.04
22	1 / 22 .	67.48	18.63	0.34	0.05	0.05	b.d.l.	7.17
23	1 / 23 .	67.69	18.28	0.35	b.d.l.	0.03	b.d.l.	6.68
24	1 / 24 .	68.02	18.67	0.30	b.d.l.	0.04	b.d.l.	7.13
25	1 / 25 .	67.54	18.56	0.41	b.d.l.	0.02	b.d.l.	6.98
26	2 / 1 .	67.43	18.30	1.05	b.d.l.	b.d.l.	b.d.l.	6.72
27	2 / 2 .	69.43	18.87	0.97	b.d.l.	0.06	b.d.l.	7.06
28	2 / 3 .	67.06	18.02	1.07	0.03	b.d.l.	b.d.l.	6.46
29	2 / 4 .	66.95	18.05	1.03	b.d.l.	0.02	b.d.l.	6.33
30	2 / 5 .	66.08	18.01	1.06	b.d.l.	0.02	b.d.l.	6.29
31	2 / 6 .	67.43	18.05	0.99	b.d.l.	b.d.l.	b.d.l.	6.38
32	2 / 7 .	67.07	18.14	0.89	b.d.l.	0.05	b.d.l.	6.60
33	2 / 8 .	67.20	18.03	1.01	b.d.l.	b.d.l.	b.d.l.	6.68
34	2 / 9 .	65.50	17.67	0.96	0.03	0.08	b.d.l.	6.45
35	2 / 10 .	67.63	18.23	1.07	b.d.l.	b.d.l.	b.d.l.	6.91
36	2 / 11 .	67.35	18.33	0.88	b.d.l.	b.d.l.	b.d.l.	6.53
37	2 / 12 .	67.34	17.98	0.94	0.06	b.d.l.	b.d.l.	6.59
38	2 / 13 .	67.12	18.14	1.10	b.d.l.	b.d.l.	b.d.l.	6.39
39	2 / 14 .	67.03	18.10	0.95	b.d.l.	b.d.l.	b.d.l.	6.40
40	2 / 15 .	66.92	17.94	1.06	b.d.l.	b.d.l.	b.d.l.	6.52
41	2 / 16 .	66.87	18.15	1.00	b.d.l.	b.d.l.	b.d.l.	6.54
42	2 / 17 .	67.19	18.03	0.98	b.d.l.	b.d.l.	b.d.l.	6.32
43	2 / 18 .	67.63	17.92	0.95	b.d.l.	0.04	b.d.l.	6.48
44	2 / 19 .	67.24	18.12	0.99	0.03	0.02	b.d.l.	6.56
45	2 / 20 .	67.55	18.22	1.00	b.d.l.	b.d.l.	b.d.l.	6.59
46	2 / 21 .	66.31	17.70	1.05	0.07	b.d.l.	b.d.l.	6.42
47	2 / 22 .	67.05	17.97	0.96	b.d.l.	b.d.l.	b.d.l.	6.47
48	2 / 23 .	66.71	18.32	0.98	b.d.l.	b.d.l.	b.d.l.	6.46

49	2 / 24 .	66.77	17.98	1.15	b.d.l.	b.d.l.	b.d.l.	6.64
50	2 / 25 .	67.20	18.03	0.94	0.03	b.d.l.	b.d.l.	6.50
51	3 / 1 .	65.29	20.58	0.18	0.03	1.51	b.d.l.	7.56
52	3 / 2 .	65.29	20.39	0.13	0.05	1.55	b.d.l.	7.54
53	3 / 3 .	65.52	20.42	0.29	0.08	1.40	b.d.l.	7.48
54	3 / 4 .	65.13	20.69	0.12	b.d.l.	1.69	b.d.l.	7.51
55	3 / 5 .	65.97	20.33	0.28	b.d.l.	1.47	b.d.l.	7.55
56	3 / 6 .	64.64	19.79	0.17	0.03	1.29	b.d.l.	6.96
57	3 / 7 .	65.23	20.14	0.08	b.d.l.	1.35	b.d.l.	7.08
58	3 / 8 .	65.51	20.58	0.03	0.04	1.56	b.d.l.	7.72
59	3 / 9 .	65.32	20.64	0.06	b.d.l.	1.74	b.d.l.	7.53
60	3 / 10 .	65.18	20.23	0.27	0.04	1.47	b.d.l.	7.37
61	3 / 11 .	65.83	20.40	0.23	b.d.l.	1.48	b.d.l.	7.19
62	3 / 12 .	65.27	20.20	0.11	0.08	1.41	b.d.l.	7.50
63	3 / 13 .	65.91	20.37	0.21	b.d.l.	1.50	b.d.l.	7.67
64	3 / 14 .	65.16	20.07	0.15	b.d.l.	1.40	b.d.l.	7.32
65	3 / 15 .	65.60	20.25	0.19	b.d.l.	1.18	b.d.l.	7.47
66	3 / 16 .	65.96	20.06	0.26	0.05	1.04	b.d.l.	7.51
67	3 / 17 .	66.30	19.64	0.26	b.d.l.	0.80	b.d.l.	7.07
68	3 / 18 .	66.16	19.11	0.25	0.04	0.62	b.d.l.	6.91
69	3 / 19 .	66.13	19.20	0.19	0.10	0.49	b.d.l.	6.63
70	3 / 20 .	67.34	19.43	0.18	b.d.l.	0.46	b.d.l.	6.61
71	3 / 21 .	66.59	19.01	0.16	b.d.l.	0.37	b.d.l.	6.42
72	3 / 22 .	65.92	19.16	0.14	b.d.l.	0.43	b.d.l.	6.37
73	3 / 23 .	66.52	19.17	0.23	0.04	0.35	b.d.l.	6.19
74	3 / 24 .	66.13	19.14	0.20	b.d.l.	0.35	b.d.l.	6.26
75	3 / 25 .	66.89	19.20	0.18	b.d.l.	0.34	b.d.l.	6.43
76	3 / 26 .	66.48	19.29	0.14	b.d.l.	0.34	b.d.l.	6.18
77	3 / 27 .	66.55	18.87	0.15	0.03	0.33	b.d.l.	6.34
78	3 / 28 .	66.65	19.28	0.17	b.d.l.	0.48	b.d.l.	6.39
79	3 / 29 .	66.80	19.13	0.25	b.d.l.	0.41	b.d.l.	6.23
80	3 / 30 .	66.31	19.42	0.20	b.d.l.	0.47	b.d.l.	6.21
81	4 / 1 .	66.98	19.45	0.13	b.d.l.	0.36	b.d.l.	6.55
82	4 / 2 .	66.42	19.38	0.18	b.d.l.	0.41	b.d.l.	6.62
83	4 / 3 .	66.77	19.34	0.12	0.03	0.45	b.d.l.	6.82
84	4 / 4 .	66.85	19.35	0.11	b.d.l.	0.30	b.d.l.	6.83
85	4 / 5 .	66.85	19.19	0.02	0.07	0.30	b.d.l.	6.54
86	4 / 6 .	66.79	19.42	0.13	b.d.l.	0.32	b.d.l.	6.90
87	4 / 7 .	66.92	19.18	0.26	b.d.l.	0.28	b.d.l.	6.24
88	4 / 8 .	66.73	19.37	0.41	b.d.l.	0.23	b.d.l.	6.58
89	4 / 9 .	67.04	19.21	0.17	b.d.l.	0.18	b.d.l.	6.44
90	4 / 10 .	67.16	19.14	0.29	0.03	0.21	b.d.l.	6.50
91	4 / 11 .	66.29	18.87	0.27	b.d.l.	0.18	b.d.l.	6.44
92	4 / 12 .	67.02	19.34	0.16	b.d.l.	0.30	b.d.l.	6.94
93	4 / 13 .	66.79	19.33	0.24	b.d.l.	0.35	b.d.l.	7.29
94	4 / 14 .	66.71	19.46	0.16	0.03	0.37	b.d.l.	7.02
95	4 / 15 .	66.86	19.20	0.19	b.d.l.	0.29	b.d.l.	7.28
96	4 / 16 .	66.67	19.40	0.11	b.d.l.	0.41	b.d.l.	7.29

97	4 / 17 .	66.94	19.29	0.19	0.03	0.35	b.d.l.	7.15
98	4 / 18 .	66.46	19.21	0.16	b.d.l.	0.35	b.d.l.	7.02
99	4 / 19 .	67.59	19.48	0.10	0.05	0.26	b.d.l.	7.20
100	4 / 20 .	67.17	19.51	0.16	b.d.l.	0.28	b.d.l.	7.13
101	4 / 21 .	66.21	19.09	0.15	b.d.l.	1.59	b.d.l.	7.46
102	4 / 22 .	67.37	19.13	0.09	b.d.l.	0.23	b.d.l.	7.00
103	4 / 23 .	67.44	19.07	0.24	b.d.l.	0.11	b.d.l.	6.47
104	4 / 24 .	66.71	19.13	0.34	b.d.l.	0.12	b.d.l.	6.56
105	4 / 25 .	67.07	19.14	0.25	b.d.l.	0.05	b.d.l.	6.59
106	4 / 26 .	66.57	18.44	0.64	b.d.l.	0.07	b.d.l.	5.88
107	4 / 27 .	66.73	18.88	0.28	b.d.l.	0.09	b.d.l.	6.44
108	4 / 28 .	66.81	18.79	0.21	0.03	0.09	b.d.l.	6.62
109	4 / 29 .	66.52	18.86	0.14	b.d.l.	0.05	b.d.l.	6.20
110	4 / 30 .	66.48	18.73	0.36	b.d.l.	0.09	b.d.l.	6.46
111	4 / 31 .	68.90	20.02	0.39	b.d.l.	0.27	b.d.l.	7.72
114	4 / 34 .	67.24	18.92	0.43	0.03	0.07	b.d.l.	6.56
115	4 / 35 .	67.50	18.90	0.37	b.d.l.	0.04	b.d.l.	6.51
116	5 / 1 .	67.59	18.61	0.62	b.d.l.	0.03	b.d.l.	6.92
117	5 / 2 .	67.61	18.50	0.47	b.d.l.	0.05	b.d.l.	7.10
118	5 / 3 .	70.42	19.78	0.47	0.05	0.13	b.d.l.	8.12
119	5 / 4 .	65.84	18.42	0.37	b.d.l.	0.07	b.d.l.	6.91
120	5 / 5 .	67.44	18.18	0.77	b.d.l.	0.05	b.d.l.	7.16
121	5 / 6 .	67.46	18.11	1.20	b.d.l.	b.d.l.	b.d.l.	7.12
122	5 / 7 .	67.36	18.19	0.99	b.d.l.	b.d.l.	b.d.l.	7.10
123	5 / 8 .	67.61	18.09	1.03	b.d.l.	0.03	b.d.l.	7.17
124	5 / 9 .	67.32	18.03	1.01	b.d.l.	b.d.l.	b.d.l.	7.14
125	5 / 10 .	67.33	18.33	1.06	b.d.l.	0.04	b.d.l.	7.06
126	5 / 11 .	66.16	17.88	1.22	0.04	0.09	b.d.l.	6.71
127	5 / 12 .	67.87	18.25	0.95	b.d.l.	b.d.l.	b.d.l.	6.97
128	5 / 13 .	67.76	18.13	0.99	0.03	b.d.l.	b.d.l.	7.00
129	5 / 14 .	67.63	18.06	0.88	0.03	0.02	b.d.l.	6.52
130	5 / 15 .	67.29	18.11	1.09	0.03	b.d.l.	b.d.l.	6.32
131	5 / 16 .	67.01	17.95	0.95	b.d.l.	0.02	b.d.l.	6.26
132	5 / 17 .	67.22	18.21	0.94	b.d.l.	b.d.l.	b.d.l.	6.30
133	5 / 18 .	67.46	18.14	0.92	b.d.l.	b.d.l.	b.d.l.	6.41
134	5 / 19 .	67.63	18.59	0.50	0.07	0.02	b.d.l.	6.47
135	5 / 20 .	68.71	19.08	0.41	b.d.l.	0.11	b.d.l.	7.08
136	5 / 21 .	67.38	18.50	0.58	b.d.l.	0.00	b.d.l.	6.89
137	5 / 22 .	67.47	18.61	0.57	b.d.l.	0.01	b.d.l.	6.96
138	5 / 23 .	67.43	18.46	0.56	b.d.l.	0.06	b.d.l.	7.06
139	5 / 24 .	67.36	18.22	1.08	b.d.l.	0.00	b.d.l.	7.21
140	5 / 25 .	67.35	18.00	0.98	b.d.l.	0.02	b.d.l.	6.95
141	5 / 26 .	67.81	18.09	0.90	b.d.l.	0.03	b.d.l.	6.96
142	5 / 27 .	67.37	17.92	1.06	b.d.l.	b.d.l.	b.d.l.	6.84
143	5 / 28 .	67.39	17.95	1.01	b.d.l.	b.d.l.	b.d.l.	6.91
144	5 / 29 .	67.53	17.96	1.03	0.05	0.06	b.d.l.	7.20
145	5 / 30 .	67.81	18.30	1.03	0.13	0.05	b.d.l.	7.37
146	5 / 31 .	67.46	18.23	0.89	b.d.l.	0.02	b.d.l.	7.00
147	5 / 32 .	69.62	18.82	0.94	0.10	b.d.l.	b.d.l.	7.16

148	5 / 33 .	67.33	17.95	0.91	b.d.l.	b.d.l.	b.d.l.	6.57
150	5 / 35 .	67.42	17.98	0.94	b.d.l.	0.04	b.d.l.	7.06
151	5 / 36 .	67.58	18.31	0.94	b.d.l.	0.04	b.d.l.	7.01
153	5 / 38 .	67.75	18.24	0.93	b.d.l.	0.02	b.d.l.	7.10
154	5 / 39 .	67.42	18.23	0.90	b.d.l.	0.02	b.d.l.	7.15
155	5 / 40 .	66.29	18.51	0.76	0.04	0.28	b.d.l.	7.02
157	5 / 42 .	67.96	18.81	0.40	b.d.l.	0.06	b.d.l.	7.04
158	5 / 43 .	67.99	18.75	0.47	0.03	0.03	b.d.l.	7.27
159	5 / 44 .	67.84	18.57	0.35	b.d.l.	b.d.l.	b.d.l.	7.23
160	5 / 45 .	67.46	18.49	0.45	0.05	b.d.l.	b.d.l.	6.98
161	5 / 46 .	67.88	18.37	0.49	b.d.l.	b.d.l.	b.d.l.	6.91
162	5 / 47 .	67.45	18.38	0.60	b.d.l.	0.03	b.d.l.	6.78
163	5 / 48 .	67.43	18.36	0.70	0.09	b.d.l.	b.d.l.	6.55
164	5 / 49 .	67.84	18.59	0.49	b.d.l.	b.d.l.	b.d.l.	6.31
165	5 / 50 .	67.22	18.40	0.60	b.d.l.	b.d.l.	b.d.l.	6.29
166	6 / 1 .	64.19	21.67	0.15	b.d.l.	2.85	0.08	7.64
167	6 / 2 .	63.69	21.72	0.31	b.d.l.	2.86	0.13	7.48
168	6 / 3 .	64.17	21.25	0.22	b.d.l.	2.48	0.07	7.55
169	6 / 4 .	64.41	21.73	0.14	0.04	2.60	0.06	7.77
170	6 / 5 .	64.44	21.83	0.26	b.d.l.	2.53	0.17	7.78
171	6 / 6 .	64.09	21.90	0.24	0.03	3.04	0.21	7.67
172	6 / 7 .	63.71	22.14	0.36	0.04	3.27	0.12	7.68
173	6 / 8 .	64.00	22.24	0.16	b.d.l.	3.34	0.10	7.71
174	6 / 9 .	63.54	21.76	0.23	b.d.l.	3.17	0.14	7.57
175	6 / 10 .	64.07	21.61	0.17	b.d.l.	2.60	b.d.l.	7.62
176	6 / 11 .	65.07	20.69	0.14	b.d.l.	1.80	b.d.l.	7.46
177	6 / 12 .	65.38	21.00	0.27	b.d.l.	1.76	0.06	7.46
178	6 / 13 .	65.39	20.95	0.22	0.07	2.00	b.d.l.	7.50
179	6 / 14 .	63.75	22.05	0.25	b.d.l.	3.14	b.d.l.	7.94
180	6 / 15 .	65.30	20.71	0.21	b.d.l.	1.86	b.d.l.	7.63
181	6 / 16 .	65.07	20.82	0.21	b.d.l.	1.88	b.d.l.	7.63
182	6 / 17 .	64.00	21.82	0.24	b.d.l.	3.22	b.d.l.	7.90
183	6 / 18 .	62.95	21.88	0.27	b.d.l.	3.38	0.03	7.37
184	6 / 19 .	63.31	22.25	0.25	b.d.l.	3.63	0.11	7.73
185	6 / 20 .	63.46	22.26	0.22	0.07	3.32	0.12	7.74
186	6 / 21 .	65.06	21.07	0.32	0.03	2.24	b.d.l.	7.55
187	6 / 22 .	64.84	20.83	0.21	b.d.l.	1.77	0.10	7.56
188	6 / 23 .	63.78	21.82	0.22	b.d.l.	2.91	0.10	7.83
189	6 / 24 .	62.49	23.12	0.24	b.d.l.	4.69	0.03	7.77
190	6 / 25 .	63.83	22.12	0.18	b.d.l.	3.52	0.11	7.81
191	6 / 26 .	65.57	20.45	0.19	b.d.l.	1.69	b.d.l.	7.17
192	6 / 27 .	66.51	19.52	0.15	b.d.l.	0.65	b.d.l.	6.46
193	6 / 28 .	65.90	19.41	0.30	b.d.l.	0.70	b.d.l.	6.35
194	6 / 29 .	66.46	19.46	0.14	0.07	0.55	b.d.l.	6.42
195	6 / 30 .	66.52	19.46	0.21	b.d.l.	0.61	b.d.l.	6.27
196	6 / 31 .	66.01	19.79	0.19	b.d.l.	0.86	b.d.l.	6.76
197	6 / 32 .	66.07	19.54	0.17	b.d.l.	0.72	b.d.l.	6.41
198	6 / 33 .	66.10	19.27	0.22	b.d.l.	0.61	b.d.l.	6.26
199	6 / 34 .	66.16	19.50	0.24	0.04	0.66	b.d.l.	6.24

200	6 / 35 .	66.09	19.46	0.21	0.09	0.70	b.d.l.	6.29
204	6 / 39 .	66.43	19.30	0.23	b.d.l.	0.60	b.d.l.	6.19
205	6 / 40 .	66.42	19.47	0.26	0.04	0.65	b.d.l.	6.29
206	6 / 41 .	66.13	19.21	0.10	0.03	0.55	b.d.l.	5.90
207	6 / 42 .	66.27	19.22	0.12	b.d.l.	0.58	b.d.l.	6.10
208	6 / 43 .	66.19	19.39	0.19	b.d.l.	0.49	b.d.l.	6.08
209	6 / 44 .	66.16	19.76	0.08	b.d.l.	0.70	b.d.l.	6.06
210	6 / 45 .	65.84	19.43	0.10	0.07	0.63	b.d.l.	6.19
211	6 / 46 .	66.29	19.51	0.15	0.06	0.68	b.d.l.	6.23
212	6 / 47 .	65.37	19.54	0.21	b.d.l.	0.70	b.d.l.	6.34
213	6 / 48 .	64.67	18.92	0.19	b.d.l.	0.66	b.d.l.	6.11
214	6 / 49 .	66.29	19.47	0.21	b.d.l.	0.63	b.d.l.	6.26
215	6 / 50 .	66.84	19.68	0.18	0.03	0.67	b.d.l.	6.27
215	9	67.34	18.92	0.26	-	0.12	bd	7.35
216	13	67.28	18.74	0.28	-	0.05	bd	7.22
217	17	67.48	17.99	1.02	-	0.04	bd	6.90
220	38	67.92	18.15	1.14	-	bd	bd	7.32
221	39	67.85	18.53	0.46	-	bd	bd	7.01

FeO*, all Fe as Fe^{2+}

b.d.l., below detection limit

Dash, not reported

K_2O	BaO	Total	Crystal	
0.31	0.07	100.41	TTG-21	Subhedral, rectangular, plate
0.38	0.17	100.57	TTG-21	1910 x 1470 µm; core to rim.
4.05	0.15	100.53	TTG-21	straddles dark and olive glasses
5.63	0.06	100.23	TTG-21	
4.98	0.06	99.07	TTG-21	
5.26	0.05	100.25	TTG-21	
4.91	0.07	100.26	TTG-21	
5.16	0.09	100.43	TTG-21	
5.28	0.08	100.02	TTG-21	
5.54	0.03	99.41	TTG-21	
6.08	0.08	100.24	TTG-21	
5.89	0.09	100.48	TTG-21	
6.17	0.03	99.97	TTG-21	
6.58	b.d.l.	100.35	TTG-21	
5.99	0.05	100.19	TTG-21	
5.65	b.d.l.	98.91	TTG-21	
6.31	b.d.l.	99.90	TTG-21	
6.48	b.d.l.	100.30	TTG-21	
6.40	b.d.l.	100.35	TTG-21	
6.36	0.09	100.17	TTG-21	
5.79	0.09	98.91	TTG-21	
6.33	b.d.l.	100.48	TTG-21	
6.64	0.05	100.20	TTG-21	
7.03	b.d.l.	100.53	TTG-22	Rectangular plate, one side
7.13	b.d.l.	103.52	TTG-22	slightly resorbed. 1955 x 1475 µm
7.38	b.d.l.	100.02	TTG-22	core to rim.
7.36	b.d.l.	99.75	TTG-22	Mainly in dark glass
7.25	b.d.l.	98.71	TTG-22	
7.35	b.d.l.	100.19	TTG-22	
7.05	b.d.l.	99.79	TTG-22	
6.99	b.d.l.	99.90	TTG-22	
6.62	b.d.l.	97.31	TTG-22	
6.47	0.08	100.38	TTG-22	
7.08	b.d.l.	100.16	TTG-22	
7.28	b.d.l.	100.18	TTG-22	
7.33	0.03	100.12	TTG-22	
7.57	b.d.l.	100.05	TTG-22	
7.29	b.d.l.	99.72	TTG-22	
7.28	b.d.l.	99.83	TTG-22	
7.14	b.d.l.	99.65	TTG-22	
7.31	b.d.l.	100.34	TTG-22	
7.17	b.d.l.	100.12	TTG-22	
7.19	b.d.l.	100.55	TTG-22	
7.25	b.d.l.	98.80	TTG-22	
7.18	b.d.l.	99.64	TTG-22	
7.25	b.d.l.	99.71	TTG-22	

7.34	b.d.l.	99.87	TTG-22	
7.32	0.03	100.05	TTG-22	
4.60	0.49	100.22	TTG-23	Slightly resorbed, subhedral
4.74	0.47	100.15	TTG-23	plate. Little bit fractured.
4.63	0.38	100.21	TTG-23	2030 x 1955 µm
4.38	0.41	99.92	TTG-23	core to rim
4.75	0.34	100.69	TTG-23	Mainy in dark glass
5.20	0.42	98.50	TTG-23	
5.07	0.34	99.29	TTG-23	
4.41	0.30	100.14	TTG-23	
4.39	0.35	100.02	TTG-23	
4.66	0.31	99.52	TTG-23	
4.67	0.31	100.11	TTG-23	
4.72	0.28	99.57	TTG-23	
4.66	0.34	100.65	TTG-23	
4.65	0.16	98.90	TTG-23	
4.85	0.18	99.71	TTG-23	
5.03	0.06	99.96	TTG-23	
5.56	0.11	99.74	TTG-23	
6.62	0.10	99.81	TTG-23	
6.26	0.07	99.06	TTG-23	
6.80	0.12	100.93	TTG-23	
7.07	b.d.l.	99.61	TTG-23	
7.04	0.08	99.12	TTG-23	
7.16	0.07	99.73	TTG-23	
7.37	0.04	99.49	TTG-23	
7.29	0.04	100.38	TTG-23	
7.22	0.04	99.68	TTG-23	
7.29	b.d.l.	99.55	TTG-23	
7.39	0.15	100.50	TTG-23	
7.22	0.06	100.09	TTG-23	
7.36	0.13	100.09	TTG-23	
7.14	0.08	100.69	TTG-24	slightly resorbed, elongated
6.75	0.12	99.87	TTG-24	plate. 1625 x 750 µm. Some
6.97	b.d.l.	100.48	TTG-24	fractures. Core to rim.
6.61	0.06	100.12	TTG-24	In dark glass
7.11	b.d.l.	100.07	TTG-24	
6.74	0.09	100.38	TTG-24	
7.53	0.09	100.50	TTG-24	
7.16	0.05	100.53	TTG-24	
7.33	b.d.l.	100.37	TTG-24	
7.53	b.d.l.	100.85	TTG-24	
7.54	b.d.l.	99.59	TTG-24	
6.43	0.12	100.30	TTG-24	
5.97	0.07	100.03	TTG-24	
6.07	0.09	99.91	TTG-24	
6.20	0.12	100.14	TTG-24	
6.08	0.06	100.01	TTG-24	

6.27	0.08	100.29	TTG-24	
6.13	0.06	99.38	TTG-24	
6.53	0.09	101.29	TTG-24	
6.24	0.11	100.61	TTG-24	
5.79	0.12	100.40	TTG-24	
6.42	0.07	100.31	TTG-24	
7.36	0.15	100.84	TTG-24	
7.27	0.12	100.25	TTG-24	
7.13	0.10	100.33	TTG-24	
7.68	b.d.l.	99.28	TTG-24	
7.52	b.d.l.	99.94	TTG-24	
7.42	0.06	100.02	TTG-24	
7.66	0.08	99.51	TTG-24	
7.35	0.06	99.51	TTG-24	
6.70	0.05	104.03	TTG-24	
7.15	0.07	100.46	TTG-24	
7.37	0.10	100.80	TTG-24	
6.69	b.d.l.	100.46	TTG-25	Subhedral plate associated
6.53	b.d.l.	100.26	TTG-25	with other fs phens. 1720 x
6.15	b.d.l.	105.12	TTG-25	1563 µm. Rim to rim
6.48	0.07	98.15	TTG-25	Mainly in dark glass
6.34	0.03	99.97	TTG-25	
6.31	b.d.l.	100.20	TTG-25	
6.46	b.d.l.	100.10	TTG-25	
6.11	0.11	100.15	TTG-25	
6.27	b.d.l.	99.76	TTG-25	
6.47	b.d.l.	100.29	TTG-25	
6.08	b.d.l.	98.16	TTG-25	
6.59	b.d.l.	100.63	TTG-25	
6.56	b.d.l.	100.46	TTG-25	
6.62	b.d.l.	99.76	TTG-25	
7.33	b.d.l.	100.17	TTG-25	
7.59	b.d.l.	99.77	TTG-25	
7.42	0.06	100.14	TTG-25	
7.34	b.d.l.	100.27	TTG-25	
7.29	b.d.l.	100.57	TTG-25	
7.06	b.d.l.	102.44	TTG-25	
6.85	0.08	100.27	TTG-25	
6.65	b.d.l.	100.26	TTG-25	
6.55	0.03	100.14	TTG-25	
6.50	0.03	100.39	TTG-25	
6.55	b.d.l.	99.85	TTG-25	
6.46	0.05	100.30	TTG-25	
6.61	b.d.l.	99.79	TTG-25	
6.67	b.d.l.	99.93	TTG-25	
6.40	b.d.l.	100.24	TTG-25	
6.25	b.d.l.	100.95	TTG-25	
6.41	0.03	100.03	TTG-25	
6.91	b.d.l.	103.55	TTG-25	

6.84	0.04	99.64	TTG-25	
6.52	b.d.l.	99.96	TTG-25	
6.55	b.d.l.	100.43	TTG-25	
6.31	0.03	100.38	TTG-25	
6.37	b.d.l.	100.09	TTG-25	
5.65	b.d.l.	98.54	TTG-25	
6.47	b.d.l.	100.72	TTG-25	
6.46	0.06	101.07	TTG-25	
6.40	b.d.l.	100.38	TTG-25	
6.62	b.d.l.	100.05	TTG-25	
6.63	b.d.l.	100.28	TTG-25	
6.61	b.d.l.	99.85	TTG-25	
7.36	b.d.l.	100.49	TTG-25	
7.34	b.d.l.	100.56	TTG-25	
7.45	b.d.l.	99.95	TTG-25	
3.31	0.34	100.22	TTG-26	Slightly elongated plate
3.33	0.34	99.87	TTG-26	Euhedral. 1875 x 1250 µm.
3.54	0.48	99.76	TTG-26	Mainly in dark glass
3.30	0.56	100.59	TTG-26	core to rim
3.34	0.48	100.82	TTG-26	
2.94	0.54	100.65	TTG-26	
2.76	0.49	100.58	TTG-26	
2.56	0.41	100.51	TTG-26	
2.77	0.44	99.62	TTG-26	
3.21	0.36	99.62	TTG-26	
4.35	0.37	99.89	TTG-26	
4.54	0.40	100.86	TTG-26	
4.12	0.34	100.59	TTG-26	
2.68	0.22	100.04	TTG-26	
4.41	0.23	100.36	TTG-26	
4.32	0.40	100.31	TTG-26	
2.67	0.31	100.15	TTG-26	
2.70	0.56	99.13	TTG-26	
2.60	0.54	100.42	TTG-26	
2.74	0.41	100.35	TTG-26	
3.84	0.40	100.50	TTG-26	
4.37	0.33	100.02	TTG-26	
2.79	0.34	99.78	TTG-26	
1.43	0.15	99.91	TTG-26	
2.30	0.20	100.06	TTG-26	
4.82	0.45	100.35	TTG-26	
7.10	0.29	100.68	TTG-26	
6.92	0.17	99.75	TTG-26	
7.07	0.23	100.41	TTG-26	
7.10	0.15	100.32	TTG-26	
6.40	0.26	100.27	TTG-26	
6.81	0.23	99.97	TTG-26	
7.25	0.22	99.92	TTG-26	
7.17	0.20	100.19	TTG-26	

6.98	0.23	100.05	TTG-26	
7.23	0.17	100.15	TTG-26	
7.20	0.17	100.51	TTG-26	
7.41	0.24	99.56	TTG-26	
7.55	0.19	100.03	TTG-26	
7.43	0.31	100.08	TTG-26	
7.26	0.35	100.37	TTG-26	
7.42	0.34	100.01	TTG-26	
7.30	0.31	100.52	TTG-26	
7.33	0.30	99.79	TTG-26	
7.15	0.39	98.09	TTG-26	
7.13	0.39	100.37	TTG-26	
7.28	0.26	101.21	TTG-26	
6.19	b.d.l.	100.18	Ttg - 1	part of platy phen: 242x161 µm
6.29	b.d.l.	99.86	Ttg-1	subh square phen: 645x645 µm
6.61	b.d.l.	100.04	Ttg-1	subh rectang phen: 806x258 µm
6.32	b.d.l.	100.85	GF1A-12	subhedral hexagonal phen.
6.35	b.d.l.	100.2	GF1A-12	core and rim; 889 x 889 µm

Formulae on basis of 8 oxygens

Na	K	Ca	Mn	Fe^{3+}	Sr	Ba	Al
0.591	0.018	0.387	0.001	0.003	0.008	0.001	1.405
0.641	0.021	0.327	0.001	0.004	0.006	0.003	1.345
0.742	0.228	0.024	0.001	0.006	0.000	0.003	1.030
0.658	0.320	0.012	0.000	0.006	0.000	0.001	1.008
0.679	0.286	0.021	0.000	0.02	0.000	0.001	1.016
0.68	0.298	0.014	0.000	0.005	0.000	0.001	1.009
0.674	0.278	0.023	0.001	0.007	0.000	0.001	1.010
0.668	0.291	0.019	0.000	0.003	0.000	0.002	1.025
0.675	0.300	0.019	0.000	0.008	0.000	0.001	1.019
0.653	0.317	0.014	0.000	0.011	0.000	0.001	1.009
0.639	0.346	0.011	0.000	0.003	0.000	0.001	1.013
0.651	0.334	0.012	0.001	0.009	0.000	0.002	1.003
0.634	0.351	0.008	0.000	0.007	0.000	0.001	0.994
0.605	0.373	0.005	0.000	0.009	0.000	0.000	1.005
0.624	0.34	0.008	0.000	0.009	0.000	0.001	1.002
0.618	0.325	0.015	0.005	0.018	0.000	0.000	1.014
0.613	0.359	0.005	0.000	0.011	0.000	0.000	0.993
0.61	0.368	0.004	0.001	0.005	0.000	0.000	0.987
0.607	0.363	0.003	0.002	0.008	0.000	0.000	0.989
0.62	0.362	0.003	0.002	0.013	0.000	0.002	0.98
0.581	0.332	0.001	0.001	0.013	0.000	0.002	0.967
0.613	0.358	0.002	0.000	0.011	0.000	0.000	0.976
0.604	0.378	0.001	0.000	0.015	0.000	0.001	0.976
0.582	0.401	0.000	0.000	0.039	0.000	0.000	0.963
0.594	0.395	0.003	0.000	0.035	0.000	0.000	0.964
0.564	0.423	0.000	0.001	0.040	0.000	0.000	0.955
0.553	0.423	0.001	0.000	0.039	0.000	0.000	0.959
0.556	0.421	0.001	0.000	0.040	0.000	0.000	0.967
0.554	0.42	0.000	0.000	0.037	0.000	0.000	0.954
0.575	0.404	0.002	0.000	0.033	0.000	0.000	0.961
0.582	0.400	0.000	0.000	0.038	0.000	0.000	0.955
0.576	0.389	0.004	0.001	0.037	0.000	0.000	0.959
0.598	0.368	0.000	0.000	0.04	0.000	0.001	0.959
0.567	0.404	0.000	0.000	0.033	0.000	0.000	0.967
0.573	0.417	0.000	0.002	0.035	0.000	0.000	0.950
0.557	0.420	0.000	0.000	0.041	0.000	0.001	0.960
0.558	0.434	0.000	0.001	0.036	0.000	0.000	0.959
0.57	0.419	0.000	0.000	0.040	0.000	0.000	0.953
0.571	0.418	0.000	0.000	0.038	0.000	0.000	0.963
0.551	0.410	0.000	0.000	0.037	0.000	0.000	0.956
0.563	0.417	0.002	0.000	0.036	0.000	0.000	0.945
0.570	0.410	0.001	0.001	0.037	0.000	0.000	0.958
0.571	0.410	0.000	0.000	0.037	0.000	0.000	0.959
0.567	0.421	0.000	0.003	0.040	0.000	0.000	0.950
0.565	0.413	0.000	0.000	0.036	0.000	0.000	0.954
0.564	0.417	0.000	0.000	0.037	0.000	0.000	0.973

0.580	0.422	0.000	0.000	0.043	0.000	0.000	0.955
0.566	0.420	0.000	0.001	0.035	0.000	0.001	0.955
0.655	0.262	0.072	0.001	0.007	0.000	0.009	1.083
0.653	0.270	0.074	0.002	0.005	0.000	0.008	1.075
0.647	0.263	0.067	0.003	0.011	0.000	0.007	1.074
0.650	0.250	0.081	0.000	0.004	0.000	0.007	1.09
0.650	0.269	0.070	0.000	0.01	0.000	0.006	1.064
0.613	0.301	0.063	0.001	0.006	0.000	0.007	1.060
0.617	0.291	0.065	0.000	0.003	0.000	0.006	1.068
0.667	0.251	0.075	0.001	0.001	0.000	0.005	1.081
0.651	0.25	0.083	0.000	0.002	0.000	0.006	1.086
0.641	0.267	0.071	0.001	0.010	0.000	0.005	1.070
0.621	0.265	0.071	0.000	0.009	0.000	0.005	1.071
0.652	0.27	0.068	0.003	0.004	0.000	0.005	1.068
0.66	0.264	0.072	0.000	0.008	0.000	0.006	1.066
0.639	0.267	0.067	0.000	0.006	0.000	0.003	1.066
0.648	0.277	0.056	0.000	0.007	0.000	0.003	1.068
0.650	0.286	0.050	0.002	0.010	0.000	0.001	1.055
0.613	0.317	0.038	0.000	0.01	0.000	0.002	1.035
0.603	0.379	0.03	0.002	0.01	0.000	0.002	1.012
0.579	0.360	0.024	0.004	0.007	0.000	0.001	1.020
0.568	0.385	0.022	0.000	0.007	0.000	0.002	1.015
0.559	0.405	0.018	0.000	0.006	0.000	0.000	1.007
0.558	0.406	0.021	0.000	0.005	0.000	0.001	1.021
0.539	0.41	0.017	0.001	0.009	0.000	0.001	1.015
0.548	0.424	0.017	0.000	0.008	0.000	0.001	1.017
0.557	0.415	0.016	0.000	0.007	0.000	0.001	1.010
0.538	0.413	0.016	0.000	0.005	0.000	0.001	1.021
0.553	0.419	0.016	0.001	0.006	0.000	0.000	1.001
0.553	0.421	0.023	0.000	0.006	0.000	0.003	1.015
0.54	0.412	0.019	0.000	0.009	0.000	0.001	1.009
0.54	0.421	0.022	0.000	0.008	0.000	0.002	1.026
0.565	0.406	0.017	0.000	0.005	0.000	0.001	1.020
0.575	0.386	0.020	0.000	0.007	0.000	0.002	1.024
0.590	0.396	0.021	0.001	0.004	0.000	0.000	1.017
0.591	0.377	0.014	0.000	0.004	0.000	0.001	1.018
0.567	0.406	0.014	0.003	0.001	0.000	0.000	1.012
0.596	0.383	0.015	0.001	0.005	0.000	0.002	1.021
0.54	0.429	0.013	0.001	0.010	0.000	0.002	1.009
0.569	0.408	0.011	0.000	0.015	0.000	0.001	1.019
0.558	0.417	0.009	0.000	0.006	0.000	0.000	1.010
0.561	0.428	0.01	0.001	0.011	0.000	0.000	1.004
0.563	0.434	0.008	0.000	0.010	0.000	0.000	1.003
0.599	0.366	0.014	0.000	0.006	0.000	0.002	1.015
0.631	0.340	0.017	0.000	0.009	0.000	0.001	1.017
0.608	0.346	0.018	0.001	0.006	0.000	0.002	1.024
0.630	0.353	0.014	0.000	0.007	0.000	0.002	1.010
0.631	0.346	0.019	0.000	0.004	0.000	0.001	1.021

0.618	0.356	0.017	0.001	0.007	0.000	0.001	1.013
0.611	0.351	0.017	0.000	0.006	0.000	0.001	1.017
0.617	0.368	0.012	0.002	0.004	0.000	0.002	1.014
0.614	0.354	0.013	0.000	0.006	0.000	0.002	1.021
0.647	0.330	0.076	0.001	0.006	0.000	0.002	1.005
0.604	0.364	0.011	0.001	0.003	0.000	0.001	1.003
0.558	0.417	0.005	0.000	0.009	0.000	0.003	0.999
0.569	0.415	0.006	0.000	0.013	0.000	0.002	1.010
0.571	0.406	0.002	0.001	0.009	0.000	0.002	1.007
0.515	0.443	0.003	0.000	0.024	0.000	0.000	0.982
0.561	0.431	0.004	0.000	0.01	0.000	0.000	0.999
0.576	0.425	0.004	0.001	0.008	0.000	0.001	0.994
0.541	0.440	0.002	0.000	0.005	0.000	0.001	1.002
0.565	0.423	0.004	0.000	0.013	0.000	0.001	0.995
0.645	0.368	0.012	0.000	0.014	0.000	0.001	1.017
0.567	0.407	0.003	0.001	0.016	0.000	0.001	0.995
0.561	0.419	0.002	0.000	0.014	0.000	0.002	0.991
0.598	0.380	0.001	0.000	0.023	0.000	0.000	0.977
0.613	0.372	0.003	0.001	0.017	0.000	0.000	0.972
0.669	0.333	0.006	0.002	0.017	0.000	0.000	0.991
0.610	0.377	0.004	0.000	0.014	0.000	0.001	0.990
0.621	0.362	0.002	0.000	0.029	0.000	0.000	0.959
0.618	0.360	0.001	0.000	0.045	0.000	0.000	0.954
0.616	0.369	0.000	0.000	0.037	0.000	0.000	0.959
0.621	0.349	0.002	0.000	0.039	0.000	0.002	0.953
0.621	0.359	0.001	0.000	0.038	0.000	0.000	0.953
0.612	0.369	0.002	0.000	0.039	0.000	0.000	0.966
0.593	0.353	0.004	0.002	0.046	0.000	0.000	0.961
0.602	0.374	0.001	0.000	0.035	0.000	0.000	0.957
0.605	0.373	0.001	0.001	0.037	0.000	0.000	0.953
0.567	0.378	0.001	0.001	0.033	0.000	0.000	0.954
0.550	0.420	0.000	0.001	0.041	0.000	0.000	0.958
0.547	0.436	0.001	0.000	0.036	0.000	0.000	0.954
0.548	0.425	0.000	0.001	0.035	0.000	0.001	0.963
0.557	0.419	0.000	0.000	0.034	0.000	0.000	0.957
0.559	0.414	0.001	0.003	0.019	0.000	0.000	0.976
0.600	0.394	0.005	0.000	0.015	0.000	0.000	0.983
0.597	0.390	0.000	0.000	0.022	0.000	0.001	0.974
0.602	0.378	0.000	0.000	0.021	0.000	0.000	0.979
0.611	0.373	0.003	0.000	0.021	0.000	0.001	0.972
0.625	0.370	0.000	0.001	0.040	0.000	0.001	0.959
0.605	0.375	0.001	0.000	0.037	0.000	0.000	0.952
0.602	0.368	0.002	0.000	0.034	0.000	0.001	0.951
0.595	0.378	0.000	0.001	0.040	0.000	0.000	0.948
0.601	0.382	0.000	0.000	0.038	0.000	0.000	0.949
0.625	0.365	0.003	0.002	0.039	0.000	0.000	0.947
0.635	0.354	0.002	0.005	0.038	0.000	0.000	0.958
0.607	0.366	0.001	0.000	0.033	0.000	0.000	0.961
0.601	0.382	0.000	0.004	0.034	0.000	0.000	0.960

0.573	0.392	0.000	0.001	0.034	0.000	0.001	0.951
0.613	0.373	0.002	0.000	0.035	0.000	0.000	0.950
0.606	0.373	0.002	0.000	0.035	0.000	0.000	0.963
0.614	0.359	0.001	0.000	0.035	0.000	0.001	0.958
0.620	0.364	0.001	0.000	0.034	0.000	0.000	0.961
0.616	0.326	0.013	0.001	0.029	0.000	0.000	0.988
0.605	0.366	0.003	0.000	0.015	0.000	0.000	0.982
0.624	0.365	0.002	0.001	0.017	0.000	0.001	0.978
0.623	0.363	0.000	0.000	0.013	0.000	0.000	0.973
0.605	0.377	0.000	0.002	0.017	0.000	0.000	0.974
0.597	0.377	0.000	0.000	0.018	0.000	0.000	0.965
0.588	0.377	0.001	0.000	0.023	0.000	0.000	0.97
0.567	0.420	0.000	0.003	0.026	0.000	0.000	0.967
0.544	0.417	0.000	0.000	0.018	0.000	0.000	0.975
0.547	0.426	0.001	0.000	0.022	0.000	0.000	0.973
0.660	0.188	0.136	0.000	0.006	0.002	0.006	1.138
0.650	0.190	0.137	0.000	0.012	0.003	0.006	1.146
0.656	0.202	0.119	0.001	0.008	0.002	0.008	1.122
0.669	0.187	0.124	0.001	0.005	0.001	0.01	1.138
0.669	0.189	0.120	0.000	0.01	0.004	0.008	1.141
0.661	0.167	0.145	0.001	0.009	0.005	0.009	1.147
0.662	0.157	0.156	0.001	0.013	0.003	0.008	1.161
0.663	0.145	0.159	0.000	0.006	0.003	0.007	1.162
0.658	0.158	0.152	0.000	0.009	0.004	0.008	1.149
0.661	0.183	0.125	0.000	0.006	0.001	0.006	1.139
0.646	0.248	0.086	0.000	0.005	0.000	0.006	1.09
0.641	0.257	0.084	0.001	0.01	0.002	0.007	1.098
0.646	0.233	0.095	0.002	0.008	0.000	0.006	1.096
0.686	0.152	0.150	0.000	0.009	0.000	0.004	1.158
0.659	0.251	0.089	0.001	0.008	0.000	0.004	1.087
0.659	0.245	0.090	0.000	0.008	0.000	0.007	1.094
0.682	0.152	0.153	0.000	0.009	0.000	0.005	1.145
0.644	0.155	0.163	0.000	0.010	0.001	0.010	1.162
0.668	0.148	0.173	0.000	0.009	0.003	0.010	1.169
0.669	0.156	0.159	0.003	0.008	0.003	0.007	1.169
0.651	0.218	0.107	0.001	0.012	0.000	0.007	1.104
0.655	0.249	0.085	0.000	0.008	0.003	0.006	1.098
0.679	0.159	0.139	0.000	0.008	0.002	0.006	1.149
0.671	0.081	0.224	0.000	0.009	0.001	0.003	1.214
0.674	0.130	0.168	0.000	0.007	0.003	0.003	1.159
0.62	0.274	0.081	0.000	0.007	0.000	0.008	1.074
0.559	0.404	0.031	0.000	0.006	0.000	0.005	1.027
0.554	0.397	0.034	0.001	0.011	0.000	0.003	1.03
0.557	0.403	0.026	0.003	0.005	0.000	0.004	1.026
0.543	0.405	0.029	0.000	0.008	0.000	0.003	1.026
0.587	0.365	0.041	0.001	0.007	0.000	0.005	1.043
0.558	0.390	0.035	0.000	0.007	0.000	0.004	1.034
0.546	0.416	0.030	0.000	0.008	0.000	0.004	1.021
0.542	0.410	0.032	0.001	0.009	0.000	0.003	1.031

0.547	0.400	0.034	0.003	0.008	0.000	0.004	1.03
0.538	0.413	0.029	0.000	0.009	0.000	0.003	1.019
0.545	0.410	0.031	0.002	0.01	0.000	0.003	1.026
0.516	0.426	0.026	0.001	0.004	0.000	0.004	1.021
0.531	0.433	0.028	0.000	0.005	0.000	0.003	1.018
0.529	0.426	0.024	0.000	0.007	0.000	0.005	1.027
0.526	0.414	0.034	0.000	0.003	0.000	0.006	1.043
0.540	0.426	0.030	0.002	0.004	0.000	0.006	1.031
0.541	0.417	0.032	0.002	0.006	0.000	0.005	1.029
0.555	0.422	0.034	0.000	0.008	0.000	0.005	1.040
0.544	0.418	0.032	0.000	0.007	0.000	0.007	1.024
0.544	0.407	0.030	0.000	0.008	0.000	0.007	1.028
0.540	0.412	0.032	0.001	0.007	0.000	0.005	1.030
0.634	0.351	0.006	-	0.015	0.000	0.000	0.992
0.625	0.358	0.002	-	0.016	0.000	0.000	0.985
0.596	0.375	0.002	-	0.059	0.000	0.000	0.944
0.626	0.356	0.000	-	0.066	0.000	0.000	0.944
0.603	0.360	0.000	-	0.027	0.000	0.000	0.970

Si	Σ cations	An	Ab	Or
2.594	5.01	38.9	59.3	1.8
2.655	5.00	33.1	64.8	2.1
2.968	5.00	2.4	74.6	22.9
2.99	5.00	1.2	66.5	32.3
2.976	5.00	2.1	68.9	29.0
2.989	5.00	1.4	68.5	30.0
2.989	4.98	2.4	69.1	28.5
2.980	4.99	1.9	68.3	29.8
2.978	5.00	1.9	67.9	30.2
2.988	4.99	1.4	66.4	32.2
2.986	5.00	1.1	64.2	34.7
2.990	5.00	1.2	65.3	33.5
3.000	5.00	0.8	63.8	35.3
2.994	4.99	0.5	61.5	37.9
2.998	4.98	0.8	64.2	35.0
2.985	4.98	1.6	64.5	33.9
3.004	4.99	0.5	62.7	36.7
3.010	4.99	0.4	62.1	37.5
3.009	4.98	0.3	62.4	37.3
3.011	4.99	0.3	62.9	36.8
3.038	4.94	0.1	63.6	36.3
3.018	4.98	0.2	63.0	36.8
3.014	4.99	0.1	61.4	38.5
3.012	5.00	0.0	59.2	40.8
3.01	5.00	0.3	59.9	39.8
3.016	5.00	0.0	57.1	42.9
3.017	4.99	0.1	56.6	43.3
3.01	5.00	0.1	56.9	43.0
3.023	4.99	0.0	56.9	43.1
3.016	4.99	0.2	58.6	41.2
3.019	4.99	0.0	59.3	40.7
3.018	4.99	0.4	59.4	40.1
3.019	4.99	0.0	61.9	38.1
3.015	4.99	0.0	58.4	41.6
3.021	5.00	0.0	57.9	42.1
3.015	4.99	0.0	57.0	43.0
3.014	5.00	0.0	56.3	43.8
3.018	5.00	0.0	57.6	42.4
3.011	5.00	0.0	57.7	42.3
3.024	4.98	0.0	57.3	42.7
3.027	4.99	0.2	57.3	42.5
3.017	4.99	0.1	58.1	41.8
3.017	4.99	0.0	58.2	41.8
3.019	5.00	0.0	57.4	42.6
3.021	4.99	0.0	57.8	42.2
3.006	5.00	0.0	57.5	42.5

3.011	5.01	0.0	57.9	42.1
3.019	5.00	0.0	57.4	42.6
2.915	5.00	7.3	66.2	26.5
2.919	5.01	7.4	65.5	27.1
2.923	5.00	6.9	66.2	26.9
2.911	4.99	8.3	66.3	25.5
2.929	5.00	7.1	65.7	27.2
2.937	4.99	6.4	62.7	30.8
2.935	4.99	6.7	63.4	29.9
2.919	5.00	7.6	67.2	25.3
2.915	4.99	8.4	66.2	25.4
2.926	4.99	7.3	65.5	27.3
2.933	4.98	7.4	64.9	27.7
2.928	5.00	6.9	65.9	27.3
2.927	5.00	7.2	66.3	26.5
2.936	4.98	6.9	65.7	27.4
2.935	4.99	5.7	66.1	28.2
2.944	5.00	5.1	65.9	29.0
2.966	4.98	3.9	63.3	32.7
2.974	5.01	3.0	59.6	37.5
2.982	4.98	2.5	60.1	37.4
2.985	4.98	2.3	58.3	39.5
2.992	4.99	1.8	56.9	41.2
2.980	4.99	2.1	56.6	41.2
2.988	4.98	1.8	55.8	42.4
2.982	5.00	1.7	55.4	42.9
2.987	4.99	1.6	56.4	42.0
2.985	4.98	1.7	55.6	42.7
2.995	4.99	1.6	56.0	42.4
2.979	5.00	2.3	55.5	42.2
2.990	4.98	2.0	55.6	42.4
2.974	4.99	2.2	54.9	42.8
2.981	5.00	1.7	57.2	41.1
2.978	4.99	2.0	58.6	39.3
2.978	5.01	2.1	58.6	39.3
2.985	4.99	1.4	60.2	38.4
2.99	4.99	1.4	57.4	41.1
2.978	5.00	1.5	60.0	38.5
2.988	4.99	1.3	55.0	43.7
2.978	5.00	1.1	57.6	41.3
2.991	4.99	0.9	56.7	42.4
2.989	5.00	1.0	56.2	42.8
2.989	5.01	0.8	56.0	43.2
2.986	4.99	1.4	61.2	37.4
2.981	5.00	1.7	63.9	34.4
2.98	4.99	1.9	62.6	35.6
2.985	5.00	1.4	63.2	35.4
2.977	5.00	1.9	63.4	34.7

2.984	5.00	1.7	62.4	35.9
2.985	4.99	1.7	62.4	35.9
2.984	5.00	1.2	61.9	36.9
2.982	4.99	1.3	62.6	36.1
2.959	5.03	7.2	61.4	31.3
2.998	4.99	1.1	61.7	37.2
2.998	4.99	0.5	56.9	42.6
2.986	5.00	0.6	57.5	41.9
2.994	4.99	0.2	58.3	41.5
3.010	4.98	0.3	53.6	46.1
2.995	5.00	0.4	56.3	43.3
2.998	5.01	0.4	57.3	42.3
2.998	4.99	0.2	55.0	44.8
2.997	5.00	0.4	57.0	42.6
2.970	5.03	1.2	62.9	35.9
3.000	4.99	0.3	58.0	41.7
3.003	4.99	0.2	57.1	42.7
3.011	4.99	0.1	61.1	38.8
3.015	4.99	0.3	62.0	37.7
2.994	5.01	0.6	66.4	33.0
3.001	5.00	0.4	61.6	38.0
3.019	4.99	0.2	63.0	36.8
3.017	5.00	0.1	63.1	36.8
3.015	5.00	0.0	62.5	37.5
3.022	4.99	0.2	63.9	35.9
3.021	4.99	0.1	63.3	36.6
3.010	5.00	0.2	62.3	37.5
3.017	4.98	0.4	62.4	37.2
3.020	4.99	0.1	61.6	38.3
3.022	4.99	0.1	61.8	38.1
3.031	4.97	0.1	59.9	40.0
3.018	4.99	0.0	56.7	43.3
3.020	4.99	0.1	55.6	44.3
3.016	4.99	0.0	56.3	43.7
3.021	4.99	0.0	57.1	42.9
3.013	4.99	0.1	57.4	42.5
3.004	5.00	0.5	60.1	39.4
3.011	5.00	0.0	60.5	39.5
3.010	4.99	0.0	61.4	38.6
3.013	4.99	0.3	61.9	37.8
3.011	5.01	0.0	62.8	37.2
3.022	4.99	0.1	61.7	38.2
3.026	4.98	0.2	61.9	37.9
3.025	4.99	0.0	61.2	38.8
3.023	4.99	0.0	61.1	38.9
3.021	5.00	0.3	62.9	36.8
3.012	5.00	0.2	64.1	35.7
3.018	4.99	0.1	62.3	37.6
3.015	5.00	0.0	61.1	38.9

3.027	4.98	0.0	59.4	40.6
3.022	5.00	0.2	62.0	37.8
3.015	4.99	0.2	61.8	38.0
3.020	4.99	0.1	63.0	36.9
3.016	5.00	0.1	62.9	37.0
3.002	4.98	1.4	64.5	34.1
3.012	4.98	0.3	62.1	37.6
3.009	5.00	0.2	63.0	36.8
3.017	4.99	0.0	63.2	36.8
3.015	4.99	0.0	61.6	38.4
3.024	4.98	0.0	61.3	38.7
3.019	4.98	0.1	60.9	39.0
3.013	5.00	0.0	57.4	42.6
3.019	4.97	0.0	56.6	43.4
3.015	4.99	0.1	56.2	43.7
2.860	5.00	13.8	67.1	19.1
2.851	5.00	14.0	66.5	19.4
2.875	4.99	12.2	67.1	20.7
2.862	5.00	12.7	68.3	19.1
2.858	5.00	12.3	68.4	19.3
2.848	4.99	14.9	67.9	17.2
2.834	5.00	16.0	67.9	16.1
2.839	4.98	16.4	68.6	15.0
2.848	4.99	15.7	68.0	16.3
2.866	4.99	12.9	68.2	18.9
2.909	4.99	8.8	65.9	25.3
2.901	5.00	8.6	65.3	26.2
2.902	4.99	9.8	66.3	23.9
2.84	5.00	15.2	69.4	15.4
2.907	5.00	8.9	66.0	25.1
2.901	5.00	9.1	66.3	24.6
2.849	5.00	15.5	69.1	15.4
2.837	4.98	16.9	66.9	16.1
2.822	5.00	17.5	67.5	15.0
2.827	5.00	16.2	68.0	15.9
2.892	4.99	11.0	66.7	22.3
2.900	5.00	8.6	66.2	25.2
2.851	4.99	14.2	69.5	16.3
2.784	4.99	23.0	68.8	8.3
2.839	4.98	17.3	69.3	13.4
2.923	4.99	8.3	63.6	28.1
2.968	5.00	3.1	56.2	40.6
2.966	5.00	3.5	56.2	40.3
2.972	5.00	2.6	56.5	40.9
2.974	4.99	3.0	55.6	41.5
2.953	5.00	4.1	59.1	36.8
2.965	4.99	3.6	56.8	39.7
2.973	5.00	3.0	55.0	41.9
2.966	4.99	3.3	55.1	41.7

2.967	4.99	3.5	55.8	40.8
2.977	4.99	3.0	54.9	42.1
2.969	5.00	3.1	55.3	41.6
2.981	4.98	2.7	53.3	44.0
2.978	5.00	2.8	53.5	43.6
2.973	4.99	2.5	54.0	43.5
2.961	4.99	3.5	54.0	42.5
2.964	5.00	3.0	54.2	42.8
2.966	5.00	3.2	54.6	42.1
2.952	5.02	3.4	54.9	41.7
2.968	5.00	3.2	54.7	42.1
2.969	4.99	3.1	55.5	41.5
2.968	4.99	3.3	54.9	41.9
2.995	4.99	0.6	64.0	35.4
3.002	4.99	0.2	63.4	36.3
3.004	4.98	0.2	61.2	38.6
2.997	4.99	0.0	63.8	36.2
3.012	4.97	0.0	62.7	37.3

Supplementary Table 1b Compositions of feldspars in feldspar clusters

	SiO_2	Al_2O_3	FeO*	CaO	SrO	Na_2O	K_2O	BaO
Anal. No.	wt%							
1 / 3 .	66.46	20.57	0.20	2.01	0.24	7.30	3.96	0.32
1 / 4 .	65.06	21.48	0.20	3.29	0.24	6.89	2.58	0.25
1 / 5 .	66.18	20.30	0.15	1.81	0.29	7.09	4.48	0.28
1 / 6 .	66.18	20.58	0.21	1.95	0.33	7.05	4.34	0.33
1 / 7 .	66.24	20.89	0.30	2.22	0.27	7.25	3.88	0.28
1 / 8 .	65.57	21.06	0.22	2.61	0.28	7.41	3.41	0.33
1 / 9 .	65.73	20.41	0.14	2.21	0.24	7.27	4.11	0.34
1 / 10 .	63.66	22.24	0.26	3.85	0.29	7.66	2.20	0.39
1 / 11 .	65.07	22.45	0.24	3.83	0.31	7.27	2.21	0.39
1 / 12 .	63.62	22.14	0.24	3.99	0.30	7.40	1.98	0.43
1 / 13 .	64.28	21.81	0.27	3.51	0.30	7.27	2.49	0.48
1 / 14 .	63.74	22.05	0.27	3.72	0.30	7.42	2.25	0.47
1 / 15 .	63.74	22.41	0.20	4.16	0.33	7.38	2.10	0.56
1 / 16 .	64.13	22.04	0.25	3.34	0.31	7.24	2.92	0.75
1 / 17 .	63.10	22.25	0.24	3.96	0.30	7.52	2.11	0.38
1 / 18 .	64.73	21.46	0.18	2.90	0.28	7.32	3.19	0.35
1 / 19 .	64.58	22.07	0.24	3.44	0.27	7.48	2.48	0.33
1 / 20 .	62.98	22.24	0.28	4.32	0.21	7.69	1.75	0.28
1 / 21 .	65.44	20.81	0.18	2.32	0.29	7.13	3.81	0.42
1 / 22 .	66.17	20.77	0.23	2.15	0.24	7.32	3.83	0.27
1 / 23 .	63.16	22.44	0.22	4.15	0.26	7.57	1.86	0.30
1 / 24 .	64.02	21.65	0.20	3.33	0.27	7.63	2.47	0.52
2 / 1 .	64.30	21.77	0.23	3.51	0.32	7.24	2.84	0.39
2 / 2 .	64.69	22.00	0.27	3.62	0.29	7.26	2.58	0.49
2 / 3 .	63.84	22.23	0.27	3.86	0.28	7.22	2.35	0.40
2 / 4 .	63.83	21.83	0.24	3.75	0.34	7.16	2.49	0.55
2 / 5 .	63.72	22.31	0.23	3.85	0.30	7.46	2.28	0.43
2 / 6 .	64.88	21.71	0.22	3.34	0.31	7.20	3.06	0.49
2 / 7 .	65.10	21.23	0.30	2.76	0.28	7.03	3.57	0.43
2 / 8 .	64.08	21.90	0.23	3.74	0.25	7.22	2.60	0.40
2 / 9 .	66.48	20.63	0.20	2.12	0.31	7.05	4.31	0.36
2 / 10 .	63.90	22.34	0.26	3.76	0.30	7.31	2.56	0.47
2 / 11 .	62.63	21.80	0.26	3.81	0.31	6.60	2.56	0.52
2 / 12 .	63.58	22.20	0.25	3.74	0.34	7.19	2.53	0.52
2 / 13 .	62.74	22.58	0.22	4.26	0.30	7.10	2.03	0.49
2 / 14 .	65.35	21.23	0.24	2.75	0.31	7.23	3.43	0.34
2 / 16 .	64.96	21.11	0.17	2.69	0.30	7.07	3.52	0.33
2 / 17 .	62.95	23.29	0.25	4.94	0.25	7.21	1.42	0.22
2 / 18 .	62.13	23.12	0.19	5.02	0.26	7.42	1.38	0.29
2 / 19 .	62.11	23.51	0.27	5.24	0.28	7.16	1.30	0.39
2 / 20 .	64.74	21.13	0.19	2.65	0.37	7.34	3.10	0.58
2 / 21 .	67.22	19.30	0.19	0.85	0.18	6.18	6.13	0.31
2 / 22 .	67.10	19.29	0.18	0.70	0.23	6.09	6.62	0.23
2 / 23 .	67.53	19.06	0.19	0.58	0.23	5.90	6.81	0.22
2 / 24 .	67.24	18.76	0.20	0.46	0.16	5.63	7.31	0.18

2 / 25 .	67.02	18.94	0.19	0.61	0.24	5.86	6.90	0.24
3 / 1 .	65.49	20.75	0.20	2.41	0.28	7.33	3.69	0.29
3 / 2 .	66.03	20.46	0.19	1.90	0.29	7.20	4.16	0.34
3 / 3 .	65.83	20.80	0.24	2.26	0.27	7.28	3.80	0.36
3 / 4 .	65.02	21.32	0.20	2.99	0.29	7.29	2.92	0.34
3 / 5 .	65.79	20.60	0.26	2.17	0.29	7.20	3.97	0.33
3 / 6 .	63.83	22.16	0.28	3.89	0.34	7.48	2.12	0.41
3 / 7 .	63.64	22.15	0.26	3.72	0.29	7.62	2.31	0.48
3 / 8 .	64.00	21.99	0.26	3.55	0.33	7.46	2.37	0.58
3 / 9 .	63.74	22.39	0.28	4.00	0.36	7.37	2.20	0.57
3 / 10 .	63.72	21.63	0.17	3.35	0.31	7.27	2.75	0.60
3 / 11 .	64.75	21.11	0.19	2.89	0.32	7.24	3.34	0.36
3 / 12 .	64.96	21.42	0.22	3.14	0.25	7.03	2.99	0.38
3 / 13 .	64.91	21.38	0.26	2.84	0.28	7.37	3.16	0.27
3 / 15 .	62.71	22.77	0.30	4.86	0.20	7.40	1.54	0.18
3 / 16 .	65.83	20.71	0.23	2.25	0.29	7.32	3.81	0.53
3 / 17 .	62.87	22.88	0.30	4.59	0.26	7.38	1.54	0.42
3 / 18 .	64.34	21.92	0.24	3.36	0.27	7.47	2.47	0.63
3 / 19 .	66.96	19.71	0.18	1.22	0.25	6.28	5.12	0.42
3 / 20 .	67.10	19.32	0.25	0.92	0.20	6.40	5.98	0.23
3 / 21 .	67.74	18.87	0.31	0.49	0.19	5.87	7.41	0.19
3 / 22 .	67.40	18.92	0.24	0.52	0.25	5.82	7.10	0.20
3 / 23 .	67.67	19.16	0.18	0.75	0.22	6.24	6.58	0.29
3 / 24 .	67.57	19.16	0.17	0.53	0.22	5.90	7.22	0.25
3 / 25 .	67.52	18.95	0.21	0.48	0.22	5.72	7.34	0.20
4 / 1 .	63.89	21.98	0.28	3.81	0.30	7.03	2.15	0.40
4 / 2 .	64.52	21.96	0.26	3.70	0.31	7.21	2.34	0.53
4 / 3 .	63.11	22.31	0.24	4.16	0.31	7.46	1.92	0.47
4 / 5 .	65.31	21.10	0.20	2.69	0.27	7.15	3.46	0.39
4 / 6 .	64.30	22.05	0.18	3.54	0.27	7.50	2.42	0.28
4 / 7 .	68.35	21.74	0.25	2.38	0.29	7.10	3.70	0.30
4 / 9 .	62.00	21.84	0.23	3.89	0.35	6.99	2.32	0.55
4 / 10 .	63.00	22.35	0.24	4.24	0.29	7.55	1.90	0.45
4 / 11 .	65.82	21.48	0.23	2.77	0.30	7.35	3.36	0.37
4 / 13 .	62.76	21.53	0.25	3.53	0.34	6.91	2.65	0.57
4 / 14 .	63.84	21.84	0.23	3.70	0.32	7.27	2.44	0.48
4 / 15 .	63.68	21.89	0.25	3.72	0.25	7.12	2.38	0.49
4 / 16 .	63.30	22.24	0.21	3.92	0.28	7.39	2.17	0.46
4 / 17 .	63.15	22.35	0.30	4.12	0.34	7.48	2.01	0.49
4 / 18 .	64.88	21.24	0.19	2.66	0.27	7.11	3.61	0.32
4 / 19 .	64.99	21.48	0.21	2.82	0.30	7.18	3.32	0.34
4 / 20 .	65.77	20.95	0.26	2.31	0.25	7.04	3.89	0.42
4 / 21 .	63.19	22.47	0.28	4.14	0.26	7.36	1.98	0.37
4 / 22 .	65.78	20.78	0.15	2.46	0.30	7.13	3.54	0.39
4 / 23 .	63.72	22.11	0.23	3.75	0.29	7.53	2.24	0.44
4 / 24 .	65.62	21.12	0.21	2.52	0.27	7.13	3.47	0.38
4 / 25 .	66.96	20.36	0.21	1.88	0.20	7.21	4.11	0.24

5 / 1 .	63.53	22.23	0.24	3.98	0.29	7.51	2.00	0.40
5 / 2 .	63.86	22.02	0.23	3.67	0.30	7.35	2.17	0.47
5 / 3 .	63.49	22.22	0.22	3.88	0.32	7.44	2.19	0.44
5 / 4 .	63.94	22.08	0.26	3.72	0.24	7.51	2.25	0.49
5 / 5 .	64.01	22.15	0.23	3.76	0.28	7.43	2.27	0.35
5 / 6 .	65.20	20.99	0.22	2.72	0.31	7.22	3.36	0.39
5 / 8 .	65.02	21.20	0.22	2.62	0.33	7.46	3.34	0.49
5 / 9 .	65.98	20.77	0.25	2.34	0.28	7.18	3.50	0.35
5 / 10 .	64.70	20.45	1.23	2.57	0.26	7.11	3.63	0.31
5 / 11 .	64.11	21.98	0.28	3.60	0.28	7.58	2.41	0.31
5 / 12 .	63.53	22.66	0.23	4.36	0.30	7.42	1.77	0.41
5 / 13 .	64.46	21.81	0.61	3.46	0.25	7.01	1.66	0.23
5 / 14 .	62.73	22.76	0.29	4.57	0.29	7.40	1.63	0.26
5 / 15 .	64.17	21.98	0.24	3.45	0.33	7.47	2.53	0.52
5 / 16 .	63.31	22.54	0.26	4.31	0.26	7.59	1.85	0.40
5 / 17 .	63.89	22.07	0.21	3.47	0.33	7.48	2.50	0.56
5 / 18 .	63.68	22.22	0.24	3.88	0.34	7.33	2.12	0.54
5 / 19 .	66.27	20.82	0.23	2.13	0.34	7.09	3.82	0.30
5 / 20 .	65.64	21.00	0.23	2.37	0.24	7.32	3.53	0.33
5 / 21 .	65.06	20.87	0.23	2.56	0.30	7.37	3.42	0.32
5 / 22 .	66.67	20.52	0.17	1.97	0.20	7.22	3.94	0.30
5 / 23 .	66.71	20.51	0.24	2.10	0.24	7.49	3.84	0.22
5 / 24 .	66.60	20.05	0.20	1.61	0.23	7.17	4.54	0.33
5 / 25 .	66.63	19.99	0.15	1.69	0.19	7.03	4.47	0.33
6 / 1 .	65.60	21.19	0.20	2.72	0.28	7.38	3.27	0.44
6 / 2 .	65.71	20.92	0.21	2.53	0.27	7.20	3.73	0.32
6 / 3 .	65.54	21.07	0.23	2.48	0.30	6.98	3.66	0.34
6 / 4 .	65.75	20.89	0.27	2.37	0.24	7.20	3.82	0.33
6 / 5 .	66.00	22.61	0.23	3.70	0.33	7.08	2.45	0.56
6 / 6 .	64.40	20.92	0.21	3.33	0.30	5.91	2.32	0.55
6 / 7 .	63.86	22.06	0.19	3.71	0.32	7.28	2.53	0.58
6 / 8 .	63.65	22.52	0.21	4.04	0.32	7.25	2.16	0.62
6 / 9 .	63.79	22.71	0.27	4.24	0.29	7.24	1.96	0.44
6 / 10 .	63.94	22.69	0.29	4.07	0.31	7.39	1.98	0.47
6 / 11 .	65.03	21.34	0.27	2.81	0.31	7.08	3.31	0.44
6 / 12 .	65.45	20.80	0.27	2.35	0.29	7.11	3.84	0.44
6 / 13 .	64.55	22.11	0.27	3.45	0.30	7.23	2.69	0.42
6 / 14 .	66.07	21.04	0.24	2.46	0.29	7.22	3.55	0.31
6 / 15 .	64.19	22.07	0.29	3.79	0.30	6.91	2.53	0.40
6 / 16 .	63.53	22.24	0.22	3.73	0.29	7.36	2.33	0.48
6 / 17 .	66.27	20.59	0.23	2.15	0.29	7.11	4.13	0.44
6 / 19 .	63.93	22.09	0.23	3.82	0.28	7.49	2.31	0.46
6 / 21 .	63.56	22.36	0.26	3.96	0.23	7.53	2.18	0.45
6 / 22 .	63.97	22.04	0.27	3.74	0.24	7.41	2.24	0.39
6 / 23 .	63.82	22.08	0.26	3.70	0.35	7.45	2.36	0.49
6 / 24 .	64.89	21.51	0.23	3.04	0.31	7.36	2.90	0.51
6 / 25 .	66.00	20.88	0.21	2.34	0.29	7.42	3.45	0.25

Explanation: locations of profiles shown on Fig. 5

FeO*, all Fe as Fe^{2+}

Formulae on the basis of 8 oxygens							
Rb_2O	Total	Si	Al	Fe^{3+}	Ca	Sr	Na
0.10	101.18	2.928	1.068	0.007	0.095	0.006	0.624
0.13	100.11	2.884	1.123	0.007	0.156	0.006	0.592
0.09	100.67	2.935	1.061	0.005	0.086	0.008	0.610
0.13	101.12	2.924	1.072	0.008	0.092	0.009	0.604
0.10	101.42	2.912	1.082	0.011	0.105	0.007	0.618
0.06	100.96	2.896	1.096	0.008	0.123	0.007	0.635
0.13	100.58	2.920	1.069	0.005	0.105	0.006	0.626
0.13	100.68	2.825	1.163	0.010	0.183	0.007	0.659
0.11	101.88	2.843	1.157	0.009	0.179	0.008	0.616
0.09	100.22	2.831	1.161	0.009	0.190	0.008	0.639
0.12	100.52	2.853	1.141	0.010	0.167	0.008	0.625
0.11	100.36	2.836	1.156	0.010	0.177	0.008	0.640
0.12	101.04	2.821	1.169	0.008	0.197	0.008	0.633
0.12	101.13	2.842	1.151	0.009	0.159	0.008	0.622
0.14	100.01	2.819	1.171	0.009	0.189	0.008	0.651
0.12	100.56	2.874	1.123	0.007	0.138	0.007	0.630
0.14	101.06	2.849	1.148	0.009	0.163	0.007	0.640
0.08	99.84	2.813	1.171	0.010	0.207	0.005	0.666
0.12	100.52	2.907	1.090	0.007	0.110	0.007	0.614
0.13	101.13	2.917	1.079	0.009	0.101	0.006	0.626
0.09	100.04	2.814	1.179	0.008	0.198	0.007	0.654
0.09	100.18	2.853	1.137	0.008	0.159	0.007	0.659
0.09	100.69	2.853	1.138	0.008	0.167	0.008	0.623
0.10	101.31	2.850	1.143	0.010	0.171	0.007	0.620
0.12	100.56	2.833	1.163	0.010	0.183	0.007	0.621
0.09	100.33	2.844	1.147	0.009	0.179	0.009	0.618
0.13	100.72	2.826	1.166	0.008	0.183	0.008	0.642
0.11	101.31	2.862	1.129	0.008	0.158	0.008	0.616
0.11	100.86	2.885	1.109	0.011	0.131	0.007	0.604
0.08	100.52	2.845	1.146	0.009	0.178	0.006	0.621
0.11	101.58	2.924	1.070	0.007	0.100	0.008	0.601
0.08	101.00	2.828	1.165	0.010	0.178	0.008	0.627
0.16	98.65	2.836	1.163	0.010	0.185	0.008	0.580
0.13	100.47	2.830	1.164	0.009	0.179	0.009	0.620
0.09	99.86	2.807	1.191	0.008	0.204	0.008	0.616
0.13	101.01	2.888	1.106	0.009	0.130	0.008	0.620
0.13	100.28	2.891	1.107	0.006	0.128	0.008	0.610
0.11	100.63	2.785	1.214	0.009	0.234	0.006	0.618
0.12	99.91	2.775	1.217	0.007	0.240	0.007	0.643
0.12	100.38	2.762	1.232	0.010	0.250	0.007	0.617
0.11	100.29	2.886	1.110	0.007	0.126	0.010	0.634
0.11	100.50	2.990	1.012	0.007	0.041	0.005	0.533
0.15	100.61	2.987	1.012	0.007	0.033	0.006	0.525
0.11	100.64	3.002	0.999	0.007	0.028	0.006	0.508
0.11	100.10	3.010	0.990	0.007	0.022	0.004	0.489

0.15	100.15	2.999	0.999	0.007	0.029	0.006	0.509
0.10	100.54	2.907	1.086	0.007	0.114	0.007	0.631
0.12	100.70	2.927	1.069	0.007	0.090	0.007	0.619
0.13	100.98	2.910	1.084	0.009	0.107	0.007	0.624
0.12	100.50	2.883	1.114	0.007	0.142	0.007	0.626
0.10	100.70	2.916	1.076	0.010	0.103	0.008	0.619
0.13	100.66	2.831	1.158	0.010	0.185	0.009	0.643
0.11	100.58	2.828	1.161	0.009	0.177	0.008	0.656
0.09	100.65	2.841	1.151	0.010	0.169	0.008	0.642
0.08	101.00	2.822	1.168	0.011	0.190	0.009	0.632
0.07	99.87	2.852	1.141	0.006	0.160	0.008	0.631
0.10	100.31	2.883	1.108	0.007	0.138	0.008	0.625
0.13	100.51	2.879	1.119	0.008	0.149	0.006	0.604
0.13	100.63	2.878	1.117	0.010	0.135	0.007	0.633
0.13	100.10	2.793	1.195	0.011	0.232	0.005	0.639
0.10	101.10	2.911	1.079	0.009	0.107	0.008	0.628
0.12	100.37	2.795	1.199	0.011	0.219	0.007	0.636
0.11	100.81	2.850	1.145	0.009	0.159	0.007	0.641
0.10	100.25	2.976	1.033	0.007	0.058	0.006	0.541
0.12	100.51	2.984	1.012	0.009	0.044	0.005	0.552
0.09	101.20	3.004	0.986	0.011	0.023	0.005	0.505
0.15	100.61	3.003	0.994	0.009	0.025	0.006	0.503
0.15	101.24	2.994	0.999	0.007	0.036	0.006	0.535
0.16	101.20	2.996	1.001	0.006	0.025	0.006	0.508
0.13	100.77	3.004	0.994	0.008	0.023	0.006	0.494
0.08	99.92	2.846	1.154	0.010	0.182	0.008	0.607
0.10	100.95	2.851	1.144	0.010	0.175	0.008	0.618
0.10	100.09	2.816	1.174	0.009	0.199	0.008	0.646
0.11	100.71	2.894	1.102	0.008	0.128	0.007	0.615
0.10	100.66	2.847	1.151	0.007	0.168	0.007	0.644
0.04	104.19	2.916	1.093	0.009	0.109	0.007	0.587
0.13	98.29	2.822	1.172	0.009	0.190	0.009	0.616
0.11	100.13	2.811	1.176	0.009	0.203	0.008	0.653
0.10	101.79	2.885	1.110	0.008	0.130	0.008	0.625
0.12	98.65	2.844	1.150	0.009	0.171	0.009	0.607
0.11	100.22	2.845	1.147	0.008	0.177	0.008	0.628
0.14	99.92	2.843	1.152	0.009	0.178	0.006	0.616
0.10	100.07	2.824	1.169	0.008	0.187	0.007	0.639
0.10	100.34	2.813	1.174	0.011	0.196	0.009	0.646
0.08	100.36	2.885	1.113	0.007	0.127	0.007	0.613
0.12	100.76	2.878	1.121	0.008	0.134	0.008	0.617
0.11	101.01	2.907	1.091	0.009	0.109	0.006	0.603
0.12	100.19	2.814	1.180	0.010	0.198	0.007	0.635
0.11	100.65	2.913	1.085	0.006	0.117	0.008	0.612
0.16	100.49	2.833	1.158	0.009	0.179	0.008	0.649
0.13	100.89	2.900	1.100	0.008	0.119	0.007	0.611
0.12	101.28	2.943	1.055	0.008	0.088	0.005	0.614

0.12	100.31	2.826	1.166	0.009	0.190	0.007	0.648
0.13	100.19	2.842	1.155	0.008	0.175	0.008	0.634
0.14	100.33	2.826	1.166	0.008	0.185	0.008	0.642
0.08	100.58	2.837	1.155	0.009	0.177	0.006	0.646
0.10	100.58	2.837	1.157	0.008	0.179	0.007	0.638
0.09	100.54	2.894	1.098	0.008	0.129	0.008	0.621
0.12	100.80	2.883	1.108	0.008	0.125	0.009	0.641
0.08	100.73	2.916	1.082	0.009	0.111	0.007	0.615
0.12	100.42	2.886	1.075	0.046	0.123	0.007	0.615
0.11	100.66	2.842	1.148	0.010	0.171	0.007	0.651
0.10	100.80	2.811	1.182	0.009	0.207	0.008	0.637
0.11	99.61	2.864	1.142	0.023	0.165	0.006	0.604
0.12	100.04	2.796	1.196	0.011	0.218	0.007	0.640
0.10	100.81	2.844	1.148	0.009	0.164	0.008	0.642
0.10	100.66	2.809	1.179	0.009	0.205	0.007	0.653
0.12	100.63	2.838	1.156	0.008	0.165	0.009	0.644
0.11	100.48	2.830	1.164	0.009	0.185	0.009	0.632
0.14	101.16	2.920	1.081	0.009	0.100	0.009	0.606
0.10	100.76	2.903	1.095	0.008	0.112	0.006	0.628
0.10	100.22	2.896	1.095	0.009	0.122	0.008	0.636
0.10	101.09	2.935	1.065	0.006	0.093	0.005	0.616
0.13	101.49	2.929	1.061	0.009	0.099	0.006	0.638
0.13	100.85	2.947	1.046	0.007	0.076	0.006	0.615
0.14	100.61	2.952	1.044	0.006	0.080	0.005	0.604
0.10	101.20	2.892	1.101	0.007	0.128	0.007	0.631
0.09	100.99	2.903	1.090	0.008	0.120	0.007	0.617
0.11	100.71	2.901	1.099	0.009	0.118	0.008	0.599
0.07	100.98	2.906	1.088	0.010	0.112	0.006	0.617
0.12	103.08	2.852	1.152	0.008	0.171	0.008	0.593
0.11	98.08	2.907	1.113	0.008	0.161	0.008	0.517
0.12	100.65	2.837	1.155	0.007	0.176	0.008	0.627
0.10	100.86	2.820	1.176	0.008	0.192	0.008	0.623
0.10	101.03	2.816	1.182	0.010	0.201	0.007	0.619
0.13	101.28	2.817	1.179	0.011	0.192	0.008	0.631
0.10	100.70	2.882	1.115	0.010	0.133	0.008	0.608
0.09	100.65	2.905	1.088	0.010	0.112	0.007	0.612
0.14	101.18	2.848	1.150	0.010	0.163	0.008	0.618
0.10	101.30	2.906	1.091	0.009	0.116	0.007	0.616
0.12	100.60	2.845	1.153	0.011	0.180	0.008	0.593
0.12	100.31	2.829	1.167	0.008	0.178	0.008	0.636
0.04	101.26	2.922	1.070	0.008	0.102	0.007	0.608
0.14	100.81	2.835	1.155	0.008	0.181	0.007	0.644
0.13	100.67	2.821	1.170	0.010	0.188	0.006	0.648
0.13	100.44	2.840	1.153	0.010	0.178	0.006	0.638
0.07	100.65	2.835	1.156	0.010	0.176	0.009	0.641
0.12	100.90	2.872	1.122	0.009	0.144	0.008	0.631
0.12	100.95	2.911	1.085	0.008	0.111	0.007	0.635

K	Ba	Rb	Σ cations	An	Ab	Or
0.223	0.005	0.003	4.96	10.1	66.3	23.7
0.146	0.004	0.004	4.92	17.5	66.2	16.3
0.254	0.005	0.002	4.97	9.0	64.2	26.7
0.245	0.006	0.004	4.96	9.8	64.2	26.0
0.218	0.005	0.003	4.96	11.1	65.8	23.1
0.192	0.006	0.002	4.97	13.0	66.8	20.2
0.233	0.006	0.004	4.97	10.9	65.0	24.1
0.124	0.007	0.004	4.98	18.9	68.2	12.9
0.123	0.007	0.003	4.94	19.5	67.1	13.4
0.113	0.008	0.003	4.96	20.2	67.9	12.0
0.141	0.008	0.004	4.96	17.9	67.0	15.1
0.128	0.008	0.003	4.97	18.7	67.8	13.5
0.118	0.010	0.004	4.97	20.8	66.7	12.5
0.165	0.013	0.004	4.97	16.8	65.8	17.4
0.120	0.007	0.004	4.98	19.7	67.8	12.5
0.181	0.006	0.003	4.97	14.5	66.4	19.0
0.140	0.006	0.004	4.96	17.3	67.9	14.8
0.100	0.005	0.002	4.98	21.3	68.5	10.3
0.216	0.007	0.003	4.96	11.7	65.3	23.0
0.215	0.005	0.004	4.96	10.8	66.4	22.8
0.106	0.005	0.003	4.97	20.7	68.3	11.0
0.141	0.009	0.002	4.98	16.6	68.7	14.7
0.161	0.007	0.003	4.97	17.6	65.5	16.9
0.145	0.008	0.003	4.96	18.2	66.2	15.5
0.133	0.007	0.003	4.96	19.6	66.2	14.2
0.141	0.010	0.003	4.96	19.0	65.9	15.1
0.129	0.008	0.004	4.97	19.2	67.3	13.5
0.172	0.008	0.003	4.96	16.7	65.1	18.2
0.202	0.007	0.003	4.96	14.0	64.5	21.5
0.147	0.007	0.002	4.96	18.8	65.6	15.6
0.242	0.006	0.003	4.96	10.6	63.7	25.7
0.144	0.008	0.002	4.97	18.8	66.0	15.2
0.148	0.009	0.005	4.94	20.3	63.6	16.2
0.144	0.009	0.004	4.97	18.9	65.8	15.3
0.116	0.009	0.003	4.96	21.8	65.8	12.4
0.193	0.006	0.004	4.96	13.8	65.7	20.5
0.200	0.006	0.004	4.96	13.7	65.0	21.3
0.080	0.004	0.003	4.95	25.1	66.3	8.6
0.079	0.005	0.003	4.98	25.0	66.8	8.2
0.074	0.007	0.003	4.96	26.5	65.6	7.8
0.176	0.010	0.003	4.96	13.5	67.7	18.8
0.348	0.005	0.003	4.94	4.4	57.9	37.7
0.376	0.004	0.004	4.96	3.6	56.2	40.2
0.386	0.004	0.003	4.94	3.0	55.1	41.9
0.417	0.003	0.003	4.95	2.4	52.7	45.0

0.394	0.004	0.004	4.95	3.1	54.6	42.3
0.209	0.005	0.003	4.97	12.0	66.1	21.9
0.235	0.006	0.003	4.96	9.5	65.5	24.9
0.214	0.006	0.004	4.96	11.3	66.0	22.7
0.165	0.006	0.003	4.95	15.2	67.1	17.7
0.224	0.006	0.003	4.96	10.9	65.4	23.7
0.120	0.007	0.004	4.97	19.5	67.8	12.7
0.131	0.008	0.003	4.98	18.4	68.1	13.6
0.134	0.010	0.003	4.97	17.8	67.9	14.2
0.124	0.010	0.002	4.97	20.0	66.8	13.1
0.157	0.011	0.002	4.97	16.9	66.5	16.6
0.189	0.006	0.003	4.97	14.5	65.6	19.9
0.169	0.007	0.004	4.95	16.1	65.5	18.3
0.179	0.005	0.004	4.97	14.2	66.9	18.9
0.087	0.003	0.004	4.97	24.2	66.7	9.1
0.215	0.009	0.003	4.97	11.2	66.1	22.6
0.087	0.007	0.004	4.96	23.2	67.5	9.3
0.140	0.011	0.003	4.97	17.0	68.2	14.9
0.290	0.007	0.003	4.92	6.5	60.8	32.7
0.339	0.004	0.003	4.95	4.7	59.0	36.3
0.419	0.003	0.003	4.96	2.4	53.3	44.3
0.404	0.004	0.004	4.95	2.7	54.0	43.4
0.371	0.005	0.004	4.96	3.8	56.8	39.4
0.408	0.004	0.004	4.96	2.7	53.9	43.4
0.416	0.003	0.004	4.95	2.5	52.9	44.6
0.122	0.007	0.002	4.94	19.9	66.6	13.4
0.132	0.009	0.003	4.95	18.9	66.8	14.3
0.109	0.008	0.003	4.97	20.8	67.7	11.5
0.196	0.007	0.003	4.96	13.6	65.5	20.9
0.137	0.005	0.003	4.97	17.7	67.9	14.4
0.201	0.005	0.001	4.93	12.1	65.4	22.4
0.135	0.010	0.004	4.97	20.2	65.5	14.3
0.108	0.008	0.003	4.98	21.0	67.7	11.2
0.188	0.006	0.003	4.96	13.8	66.3	19.9
0.153	0.010	0.003	4.96	18.4	65.2	16.4
0.139	0.008	0.003	4.96	18.7	66.6	14.7
0.135	0.009	0.004	4.95	19.2	66.3	14.5
0.124	0.008	0.003	4.97	19.7	67.3	13.0
0.114	0.008	0.003	4.98	20.5	67.5	12.0
0.205	0.006	0.002	4.96	13.4	64.9	21.7
0.188	0.006	0.004	4.96	14.2	65.7	20.0
0.219	0.007	0.003	4.96	11.7	64.7	23.6
0.112	0.006	0.003	4.97	20.9	67.2	11.9
0.200	0.007	0.003	4.95	12.6	65.9	21.5
0.127	0.008	0.004	4.97	18.7	68.0	13.3
0.195	0.007	0.004	4.95	12.9	66.0	21.1
0.231	0.004	0.003	4.95	9.5	65.8	24.7

0.114	0.007	0.004	4.97	19.9	68.1	11.9
0.123	0.008	0.004	4.96	18.8	68.0	13.2
0.124	0.008	0.004	4.97	19.5	67.5	13.0
0.127	0.009	0.002	4.97	18.6	68.0	13.4
0.128	0.006	0.003	4.96	18.9	67.5	13.6
0.190	0.007	0.003	4.96	13.7	66.0	20.2
0.189	0.009	0.003	4.98	13.1	67.1	19.8
0.197	0.006	0.002	4.95	12.0	66.6	21.4
0.207	0.005	0.003	4.97	13.0	65.1	21.9
0.136	0.005	0.003	4.97	17.8	68.0	14.2
0.100	0.007	0.003	4.96	21.9	67.5	10.6
0.094	0.004	0.003	4.90	19.1	70.0	10.9
0.093	0.005	0.003	4.97	22.9	67.3	9.8
0.143	0.009	0.003	4.97	17.3	67.7	15.1
0.105	0.007	0.003	4.98	21.3	67.9	10.9
0.142	0.010	0.003	4.97	17.4	67.7	14.9
0.120	0.009	0.003	4.96	19.7	67.4	12.8
0.214	0.005	0.004	4.95	10.9	65.8	23.3
0.199	0.006	0.003	4.96	12.0	66.9	21.2
0.194	0.005	0.003	4.97	12.8	66.8	20.4
0.221	0.005	0.003	4.95	10.0	66.2	23.8
0.215	0.004	0.004	4.96	10.4	67.0	22.6
0.256	0.006	0.004	4.96	8.1	64.9	27.0
0.253	0.006	0.004	4.95	8.6	64.5	27.0
0.184	0.008	0.003	4.96	13.6	66.9	19.5
0.210	0.006	0.002	4.96	12.6	65.2	22.2
0.207	0.006	0.003	4.95	12.7	64.9	22.4
0.215	0.006	0.002	4.96	11.9	65.3	22.8
0.135	0.009	0.003	4.93	19.0	66.0	15.0
0.134	0.010	0.003	4.86	19.8	63.7	16.5
0.143	0.010	0.003	4.97	18.6	66.2	15.1
0.122	0.011	0.003	4.96	20.5	66.5	13.0
0.110	0.008	0.003	4.95	21.6	66.6	11.8
0.111	0.008	0.004	4.96	20.6	67.6	11.9
0.187	0.008	0.003	4.95	14.3	65.5	20.2
0.218	0.008	0.003	4.96	11.9	65.0	23.1
0.151	0.007	0.004	4.96	17.5	66.3	16.2
0.199	0.005	0.003	4.95	12.4	66.2	21.4
0.143	0.007	0.003	4.94	19.6	64.7	15.6
0.132	0.008	0.003	4.97	18.8	67.2	14.0
0.233	0.008	0.001	4.96	10.8	64.5	24.7
0.131	0.008	0.004	4.97	19.0	67.3	13.7
0.124	0.008	0.004	4.98	19.6	67.5	12.9
0.127	0.007	0.004	4.96	18.9	67.7	13.5
0.134	0.009	0.002	4.97	18.5	67.4	14.0
0.164	0.009	0.003	4.96	15.3	67.2	17.4
0.194	0.004	0.003	4.96	11.8	67.6	20.6

2.37666

Description

Tabular crystal. Profile 1.
Length of profile 0.18 cm

core to rim profile across
tabular crystal with one
irregular edge. Profle 2.
Length 0.24 cm

Core to rim profile 3, across
tabular crystal.
Length = 0.19 cm

Core to rim profile 4, across
hour-glass shaped crystal.
Length = 0.20 cm

Core to rim profile 5, across
platy crystal.
Length = 0.20 cm

Core to rim profile 6, across
anhedral plate. Length = 0.18 cm

Supplementary Table 1c Compositions of feldspars: phenocrysts and matrix grains in xenoliths and prob

Sample	**Ttg-hg#1**							
Image	10	10	10	10	10	8	8	12
Anal. no.	3	4	5	6	7	22	23	21/25
Occurrence	antecryst (Fig. 3a) ==========					heavily resorbed antecryst		triangular pl
Form	suhedral plate					originally rectangular		
wt%								
SiO_2	56.37	56.68	58.07	56.94	61.45	62.10	61.82	57.15
Al_2O_3	26.88	26.42	25.64	26.61	23.83	22.92	23.61	26.05
Fe_2O_3*	0.59	0.47	0.60	0.60	0.50	0.37	0.40	0.70
CaO	9.62	8.93	8.17	8.94	5.60	4.63	5.53	9.04
SrO	0.14	0.19	0.21	0.17	0.09	0.07	0.07	0.19
Na_2O	5.50	5.52	6.13	5.74	7.87	8.26	8.10	5.52
K_2O	0.70	0.86	1.06	0.84	0.45	0.75	0.70	0.94
BaO	0.17	0.15	b.d.l.	0.22	0.37	b.d.l.	0.10	0.18
Total	99.97	99.22	99.88	100.06	100.16	99.10	100.33	99.77
Formulae on basis of 8 oxygens								
Si	2.540	2.568	2.609	2.561	2.731	2.777	2.742	2.577
Al	1.428	1.411	1.358	1.411	1.248	1.208	1.234	1.385
Fe^{3+}	0.031	0.025	0.032	0.032	0.026	0.020	0.021	0.037
Ca	0.464	0.434	0.393	0.431	0.267	0.222	0.263	0.437
Sr	0.004	0.005	0.005	0.004	0.002	0.002	0.002	0.005
Na	0.481	0.485	0.534	0.501	0.678	0.716	0.697	0.483
K	0.040	0.050	0.061	0.048	0.026	0.043	0.040	0.054
Ba	0.003	0.003	0.000	0.004	0.006	0.000	0.002	0.003
Σ cations	4.99	4.98	4.99	4.99	4.98	4.99	5.00	4.98
An	47.1	44.8	39.8	44.0	27.5	22.6	26.3	44.9
Ab	48.8	50.1	54.0	51.1	69.9	73.0	69.7	49.6
Or	4.1	5.1	6.1	4.9	2.6	4.4	4.0	5.6

Fe_2O_3*, all Fe as Fe^{3+}

b.d.l., below detection limit

ɔable antecrysts

12	12	13	13	13	13	13	13	13
22/26	23/27	24	25	26	27	32	33	34
ıenocryst in xenolith		phenocryst in xenolith			phen in xen	phen in xen	phen in xen; core + rim	
56.63	56.47	53.68	55.45	55.69	56.50	60.39	56.37	57.22
26.14	26.50	28.22	27.02	26.77	26.09	24.08	26.96	25.86
0.64	0.66	0.59	0.64	0.74	0.67	0.63	0.68	0.72
9.20	9.79	11.60	10.39	10.07	9.32	5.99	9.74	8.62
0.12	0.14	0.24	0.16	0.26	0.19	0.09	0.11	0.28
5.46	5.48	4.29	5.14	5.19	5.66	6.85	5.30	5.90
0.88	0.87	0.57	0.73	0.76	0.88	1.75	0.76	1.05
b.d.l.	0.21	0.12	0.18	b.d.l.	b.d.l.	0.35	0.24	0.22
99.07	100.12	99.31	99.71	99.48	99.31	100.13	100.16	99.87
2.568	2.545	2.448	2.513	2.525	2.561	2.701	2.536	2.582
1.397	1.408	1.517	1.443	1.430	1.394	1.270	1.430	1.375
0.034	0.035	0.032	0.034	0.039	0.036	0.033	0.036	0.039
0.447	0.473	0.567	0.504	0.489	0.453	0.287	0.470	0.417
0.003	0.004	0.006	0.004	0.007	0.005	0.002	0.003	0.007
0.480	0.479	0.379	0.452	0.456	0.498	0.594	0.462	0.516
0.051	0.050	0.033	0.042	0.044	0.051	0.100	0.044	0.060
0.000	0.004	0.002	0.003	0.000	0.000	0.006	0.004	0.004
4.98	5.00	4.98	5.00	4.99	5.00	4.99	4.98	5.00
45.7	47.2	57.9	50.5	49.4	45.2	29.3	48.1	42.0
49.1	47.8	38.7	45.2	46.1	49.7	60.6	47.4	52.0
5.2	5.0	3.4	4.2	4.4	5.1	10.2	4.5	6.1

							GF1A
13	13		quench enclave				11
29	30		2	3	5	6	35
matrix crystal in xeno.			long thin rod		prismatic: titanite borders		phen in xen
			133 x 5 µm		43 x 12 µm		
63.28	63.18		61.13	66.78	58.19	68.80	65.51
18.73	18.40		23.95	20.88	25.50	18.98	19.51
bd	0.19		0.97	0.53	1.14	0.65	0.33
bd	0.38		6.34	2.17	8.29	0.31	0.97
bd	bd		0.28	0.29	0.25	0.31	b.d.l.
1.60	1.52		6.61	9.72	6.09	10.69	5.41
13.16	13.54		0.68	0.38	0.95	0.60	7.51
2.02	1.05		0.28	0.16	0.14	b.d.l.	0.69
98.79	98.26		100.24	100.91	100.55	100.34	99.93
2.971	2.970		2.713	2.909	2.599	2.998	2.954
1.036	1.020		1.253	1.072	1.343	0.975	1.037
0.000	0.011		0.051	0.027	0.060	0.033	0.017
0.000	0.019		0.302	0.101	0.397	0.014	0.047
0.000	0.000		0.007	0.007	0.006	0.008	0.000
0.146	0.139		0.569	0.821	0.528	0.903	0.473
0.788	0.812		0.039	0.021	0.054	0.033	0.432
0.037	0.019		0.005	0.003	0.002	0.000	0.012
4.98	4.99		4.94	4.96	4.99	4.97	4.97
0.0	2.0		33.2	10.7	40.6	1.5	4.9
15.6	14.3		62.6	87.0	53.9	95.0	49.7
84.4	83.7		4.2	2.2	5.5	3.5	45.4

							anals 30
	27	27	27	27	19	23	23
	7	8	9	10	15	29	30
	all are matrix crystals in xenolith				in xenol mx	phen in xen	microphen
	57.01	60.87	61.44	58.46	67.57	60.34	59.96
	25.59	22.54	22.48	25.28	14.71	24.30	25.09
	1.06	0.56	0.42	1.01	5.69	0.28	0.14
	8.49	4.97	4.35	8.18	b.d.l.	5.78	6.68
	0.18	0.06	bd	0.08	bd	0.22	0.17
	6.27	6.42	6.91	6.47	7.19	7.72	7.43
	0.53	1.08	2.18	0.41	6.01	0.85	0.52
	0.16	0.30	0.15	0.25	b.d.l.	b.d.l.	b.d.l.
	99.29	96.80	97.93	100.14	101.17	99.49	99.99
	2.579	2.783	2.790	2.615	2.970	2.705	2.675
	1.365	1.215	1.203	1.333	0.762	1.284	1.319
	0.057	0.030	0.023	0.053	0.295	0.015	0.008
	0.412	0.243	0.212	0.392	0.000	0.278	0.319
	0.005	0.002	0.000	0.002	0.000	0.006	0.004
	0.550	0.569	0.608	0.561	0.613	0.671	0.643
	0.031	0.063	0.126	0.023	0.337	0.049	0.030
	0.003	0.005	0.003	0.004	0.000	0.000	0.000
	5.00	4.91	4.96	4.98	4.98	5.01	5.00
	41.5	27.8	22.4	40.1	0.0	27.8	32.2
	55.4	65.0	64.3	57.5	64.5	67.3	64.8
	3.1	7.2	13.3	2.4	35.5	4.9	3.0

ı-41 of uncertain paragenesis					**GF3**	
23	24	24	25	25	GF3-1	GF3-1
31	37	41	51	52	4	5
microphen	microphen	microphen	fragment of m'phen		matrix plate core & rim	
					308 x 123 µm	
50.37	57.05	47.85	50.90	50.04	52.92	58.34
30.70	26.66	32.72	30.30	30.71	29.05	25.19
0.69	0.32	0.57	0.93	0.97	0.67	0.78
13.87	8.86	15.96	14.34	14.27	12.43	8.07
0.16	0.17	0.15	0.35	0.29	0.34	0.22
3.34	6.09	2.43	3.38	3.11	4.02	5.82
0.16	0.58	0.07	0.25	0.19	0.44	0.99
b.d.l.	b.d.l.	b.d.l.	b.d.l.	b.d.l.	0.12	0.42
99.29	99.73	99.75	100.45	99.58	99.99	99.83
2.309	2.569	2.198	2.313	2.292	2.404	2.625
1.659	1.415	1.772	1.623	1.658	1.555	1.336
0.037	0.017	0.031	0.050	0.052	0.036	0.041
0.681	0.427	0.786	0.698	0.700	0.605	0.389
0.004	0.004	0.004	0.009	0.008	0.009	0.006
0.297	0.532	0.216	0.298	0.276	0.354	0.508
0.009	0.033	0.004	0.014	0.011	0.025	0.057
0.000	0.000	0.000	0.000	0.000	0.002	0.007
5.00	5.00	5.01	5.01	5.00	4.99	4.97
69.0	43.1	78.1	69.1	70.9	61.4	40.8
30.1	53.6	21.5	29.5	28.0	36.0	53.2
0.9	3.4	0.4	1.4	1.1	2.6	6.0

				FC		
GF-3	GF3-2	GF3-3	GF3-3	3(FC)	3 (FC)	
6	14	18	19	10	11	2
interstitial	mtx plate	matrix laths		intergrown w. oliv.		
67.05	55.63	52.76	55.16	65.66	65.91	61.13
17.91	27.62	29.17	27.80	20.60	20.67	23.95
0.96	0.74	0.68	0.74	0.60	0.68	0.97
0.18	10.51	12.41	10.91	2.03	2.03	6.34
0.16	0.32	0.34	0.28	0.31	0.27	0.28
4.91	4.86	3.98	4.58	7.53	7.58	6.61
9.27	0.62	0.53	0.70	3.66	3.76	0.68
b.d.l.	0.17	0.12	0.12	0.21	0.28	0.28
100.44	100.47	99.99	100.29	100.60	101.18	100.24
3.006	2.500	2.398	2.486	2.904	2.901	2.713
0.947	1.463	1.562	1.477	1.074	1.072	1.253
0.051	0.039	0.037	0.039	0.031	0.035	0.051
0.009	0.506	0.604	0.527	0.096	0.096	0.302
0.004	0.008	0.009	0.007	0.008	0.007	0.007
0.427	0.423	0.351	0.400	0.646	0.647	0.569
0.530	0.036	0.031	0.040	0.207	0.211	0.039
0.000	0.003	0.002	0.000	0.004	0.005	0.005
4.97	4.98	4.99	4.98	4.97	4.97	4.94
0.9	52.4	61.3	54.5	10.1	10.0	33.2
44.2	43.9	35.6	41.4	68.1	67.8	62.6
54.9	3.7	3.1	4.2	21.8	22.1	4.2

3	5	6
66.78	58.19	68.80
20.88	25.50	18.98
0.53	1.14	0.65
2.17	8.29	0.31
0.29	0.25	0.31
9.72	6.09	10.69
0.38	0.95	0.60
0.16	0.14	b.d.l.
100.91	100.55	100.34
2.909	2.599	2.998
1.072	1.343	0.975
0.027	0.060	0.033
0.101	0.397	0.014
0.007	0.006	0.008
0.821	0.528	0.903
0.021	0.054	0.033
0.003	0.002	0.000
4.96	4.99	4.97
10.7	40.6	1.5
87.0	53.9	95.0
2.2	5.5	3.5

Supplementary Table 2a Compositions of olivine

Sample	**Ttg-hg#1**							
Image	2	3	4	4	1 (FE)	1(FE)	1 (FE)	2 (FE)
Anal. no.	5	22	1	3	2	3	4	10
Occurrence	phenocryst	phenocryst	phenocryst	phenocryst	phenocryst	phen core & intermed		m'phen co
Form	resorb prism	euh hexagon	euh X-sectior	subh plate	anh plate	partly resorb plate		rounded
Size	292x175 µm	250x190 µm	625x625µm	313x313 µm	437x397 µm	833 x 516 µm		103 x 6
wt%								
SiO_2	29.91	29.85	29.71	30.21	30.00	29.81	29.69	29.61
TiO_2	0.03	b.d.l.	0.04	0.03	0.04	0.04	0.05	0.05
FeO*	65.87	66.36	65.51	64.68	63.12	62.91	63.59	63.26
MnO	3.57	3.54	3.56	3.59	3.40	3.45	3.41	3.45
NiO	-	-	-	-	-	-	-	-
ZnO	0.14	0.25	0.12	0.14	0.19	0.13	0.14	bd
MgO	1.02	0.97	0.96	2.14	2.97	3.18	2.97	2.71
CaO	0.18	0.20	0.26	0.18	0.34	0.33	0.33	0.42
Total	100.72	101.17	100.16	100.97	100.06	99.85	100.18	99.50
Formulae on the basis of 4 oxygens								
Si	0.999	0.995	0.998	0.998	0.995	0.990	0.986	0.990
Ti	0.001	0.000	0.001	0.001	0.001	0.001	0.001	0.001
Fe^{2+}	1.840	1.849	1.840	1.787	1.750	1.748	1.767	1.769
Mn	0.101	0.100	0.101	0.100	0.095	0.097	0.096	0.098
Ni								
Zn	0.003	0.006	0.003	0.003	0.005	0.003	0.003	0.000
Mg	0.051	0.048	0.048	0.105	0.147	0.157	0.147	0.135
Ca	0.006	0.007	0.009	0.006	0.012	0.012	0.012	0.015
Σ cations	3.00	3.01	3.00	3.00	3.00	3.01	3.01	3.01
Fo	2.5	2.4	2.4	5.3	7.4	7.9	7.3	6.7
Fa	92.4	92.6	92.5	89.7	87.8	87.3	87.9	88.4
Tp	5.1	5.0	5.1	5.0	4.8	4.8	4.8	4.9

FeO*, all Fe as Fe^{2+}

b.d.l., below detection limit

Dash, not reported

			GF1A				
2 (FE)	5 (FE)	5 (FE)	1	1	1	1	5
11	17	18	1	2	3	4	21
re & rim	phenocryst		phenocryst				phenoc
plate	partly resorb X-sect		partly resorbed. Rounded; 1, core, 2-4, rim				partly resorbe
3 µm	685 x 410 µm		543 x 457 µm				336 x 226 µm
29.47	29.13	29.32	35.75	35.59	35.76	35.68	35.28
0.04	b.d.l.	0.03	0.11	0.04	0.03	0.05	b.d.l.
63.51	65.67	65.56	37.30	36.95	36.97	37.50	37.37
3.24	3.52	3.35	1.69	1.64	1.70	1.70	2.35
-	-	-	-	-	-	-	-
0.15	0.16	0.29	0.06	0.05	b.d.l.	b.d.l.	b.d.l.
2.78	0.92	0.86	26.02	25.96	26.05	26.06	25.34
0.43	0.15	0.19	0.19	0.16	0.19	0.20	0.20
99.62	99.55	99.60	101.12	100.39	100.70	101.19	100.54
0.986	0.989	0.993	0.998	1.000	1.001	0.996	0.995
0.001	0.000	0.001	0.002	0.001	0.001	0.001	0.000
1.777	1.865	1.858	0.871	0.868	0.865	0.875	0.882
0.092	0.101	0.096	0.040	0.039	0.040	0.040	0.056
0.004	0.004	0.007	0.001	0.001	0.000	0.000	0.000
0.139	0.047	0.043	1.082	1.087	1.086	1.084	1.065
0.015	0.005	0.007	0.006	0.005	0.006	0.006	0.006
3.01	3.01	3.01	3.00	3.00	3.00	3.00	3.00
6.9	2.3	2.2	54.3	54.5	54.5	54.2	53.2
88.5	92.7	93.0	43.7	43.5	43.4	43.8	44.0
4.6	5.0	4.8	2.0	2.0	2.0	2.0	2.8

				FC			
5	18	18	18	2 (FC)	2 (FC)	2 (FC)	2 (FC)
22	8	9	10	6	7	8	9
:ryst	phenocryst			anh grain in ol-cpx cluster		in ol-cpx cluster	
ed plate	partly resorbed basal section			quasi-square		squashed elongate	
core and rim	200 x 180 µm			412 x 324 µm		1250 x 440 µm	
35.50	29.68	29.21	29.91	31.64	31.41	32.80	32.67
b.d.l.	b.d.l.	b.d.l.	b.d.l.	0.03	b.d.l.	b.d.l.	b.d.l.
36.63	66.23	66.21	66.21	53.13	53.53	47.59	46.52
2.20	3.65	3.68	3.40	2.92	2.79	2.25	2.24
-	-	-	-	-	-	-	-
0.09	0.22	b.d.l.	0.24	b.d.l.	b.d.l.	0.13	b.d.l.
25.43	0.76	0.81	0.80	11.16	11.16	16.34	17.03
0.19	0.17	0.18	0.17	0.30	0.35	0.19	0.26
100.04	100.71	100.09	100.73	99.18	99.24	99.30	98.72
1.002	0.995	0.988	1.000	0.995	0.990	0.994	0.991
0.000	0.000	0.000	0.000	0.001	0.000	0.000	0.000
0.865	1.857	1.872	1.852	1.397	1.410	1.206	1.181
0.053	0.104	0.105	0.096	0.078	0.074	0.058	0.058
0.002	0.005	0.000	0.006	0.000	0.000	0.003	0.000
1.070	0.038	0.041	0.040	0.523	0.524	0.738	0.770
0.006	0.006	0.007	0.006	0.010	0.012	0.006	0.008
3.00	3.01	3.01	3.00	3.00	3.01	3.01	3.01
53.8	1.9	2.0	2.0	26.2	26.1	36.9	38.3
43.5	92.9	92.8	93.2	69.9	70.2	60.3	58.8
2.6	5.2	5.2	4.8	3.9	3.7	2.9	2.9

GF3					
GF3-1	GF3-1	GF3-2	GF3-2	GF3-3	GF3-3
1	2	8	9	15	16
phenocryst w. opx mantle		phenocryst w. opx mantle		ol phenocryst cluster	
hexagonal plate		hexag'l plate: rim & core		hex plt rim	hex plt core
277 x 154 µm		167 x 83 µm		455x265 µm	492x303 µm
38.64	38.43	38.07	38.23	38.32	38.19
0.03	0.04	0.03	0.05	0.04	0.03
19.90	19.93	21.10	21.40	19.81	20.49
0.37	0.38	0.31	0.41	0.29	0.35
0.12	0.18	0.19	0.22	0.22	0.11
b.d.l.	b.d.l.	b.d.l.	0.09	0.11	0.09
41.02	40.89	39.60	39.77	41.24	40.22
0.16	0.18	0.18	0.17	0.17	0.17
100.24	100.03	99.48	100.34	100.20	99.65
0.993	0.991	0.992	0.990	0.986	0.991
0.001	0.001	0.001	0.001	0.001	0.001
0.428	0.430	0.460	0.463	0.426	0.445
0.008	0.008	0.007	0.009	0.006	0.008
0.002	0.004	0.004	0.005	0.005	0.002
0.000	0.000	0.000	0.002	0.002	0.002
1.571	1.571	1.538	1.535	1.582	1.556
0.004	0.005	0.005	0.005	0.005	0.005
3.01	3.01	3.01	3.01	3.01	3.01
78.3	78.2	76.7	76.5	78.5	77.5
21.3	21.4	22.9	23.1	21.2	22.1
0.4	0.4	0.3	0.4	0.3	0.4

Supplementary Table 2b Compositions of pyroxenes

Sample	**Ttg-hg#1**							
Image	2	5	2 (FE)	2 (FE)	2 (FE)	2 (FE)	2 (FE)	2.16
Anal. no.	6	16	12	13	14	15	16	9
Occurrence	inclus. in oliv	incl in ab ph	rim (12) to core (16) through zoned phenocryst					in felds phen cor
Form	round; grey	rounded	partly resorbed stubby prism					round, mantled l
Size	10 x 10 µm	<10 µm	873 x 397 µm					
wt%								
SiO_2	49.94	49.29	48.38	48.34	48.63	49.03	48.80	48.43
TiO_2	0.34	0.24	0.30	0.26	0.32	0.29	0.32	0.28
Al_2O_3	0.59	0.13	0.25	0.22	0.31	0.37	0.35	0.22
Cr_2O_3	0.11	b.d.l.	b.d.l.	b.d.l.	b.d.l.	b.d.l.	b.d.l.	b.d.l.
FeO*	21.85	27.69	25.58	26.14	25.25	22.76	22.81	25.55
MnO	1.21	1.31	1.15	1.21	1.16	1.23	1.23	1.27
ZnO	b.d.l	b.d.l.	-	-	-	-	-	-
MgO	6.02	2.26	3.28	2.70	3.56	5.30	5.19	3.55
CaO	19.62	18.27	19.39	19.18	19.47	20.02	19.76	19.24
Na_2O	0.80	0.94	0.79	0.90	0.81	0.73	0.62	0.81
K_2O	b.d.l.	0.02	-	-	-	-	-	-
Total	100.48	100.15	99.12	98.95	99.51	99.73	99.08	99.35
Formulae on basis of 6 oxygens								
Si	1.976	2.008	1.982	1.989	1.980	1.971	1.974	1.979
Ti	0.010	0.007	0.009	0.008	0.010	0.009	0.010	0.009
Al	0.028	0.006	0.012	0.011	0.015	0.018	0.017	0.011
Cr	0.003	0.000	0.000	0.000	0.000	0.000	0.000	0.000
Fe^{2+}	0.723	0.943	0.876	0.900	0.860	0.765	0.772	0.873
Mn	0.041	0.045	0.040	0.042	0.040	0.042	0.042	0.044
Zn	0.000	0.000	0.000	0.000	0.000	0.000	0.000	-
Mg	0.355	0.137	0.200	0.166	0.216	0.317	0.313	0.216
Ca	0.832	0.797	0.851	0.846	0.850	0.862	0.856	0.843
Na	0.061	0.074	0.063	0.072	0.064	0.057	0.049	0.064
K	0.000	0.001	0.000	0.000	0.000	0.000	0.000	-
Σ cations	4.03	4.02	4.03	4.03	4.03	4.04	4.03	4.04
Ca	43.55	42.46	44.15	44.26	44.12	44.34	44.12	43.61
Mg	18.59	7.31	10.39	8.67	11.22	16.32	16.12	11.19
Fe	37.86	50.23	45.46	47.08	44.66	39.34	39.76	45.20

FeO*, all Fe as Fe^{2+}

b.d.l., below detection limit

Dash, not reported

	GF1A						
2.16	11	27t	27t	27t	2	2	2
10	36	11	12	13	7	8	9
e & rim	m'phen in xen	matrix crystals in xen		mx Xal in xen	phenocryst; core & rim		phenocryst
by a'bole	euhed plate	rounded plate		prismatic	slightly rounded plate		round plate
	39 x 29 μm	16 x 11 μm	rim & core	13 x 5 μm	179 x 126 μm		147x126 μm
48.38	51.14	50.50	51.20	51.44	49.16	51.94	50.39
0.34	0.37	1.02	0.83	0.66	0.32	b.d.l.	1.04
0.56	0.85	1.39	1.15	0.79	0.31	0.18	3.65
b.d.l.	0.10	b.d.l.	b.d.l.	0.12	b.d.l.	b.d.l.	b.d.l.
27.88	17.51	13.32	14.48	24.97	23.79	31.38	8.21
1.16	1.64	0.39	0.43	0.65	1.22	1.50	0.14
-	b.d.l.	b.d.l.	b.d.l.	b.d.l.	b.d.l.	b.d.l.	b.d.l.
2.85	12.46	13.57	14.14	16.72	4.55	0.03	14.70
17.02	15.67	17.96	16.23	4.30	19.66	0.42	21.63
1.69	0.27	0.28	0.22	0.06	0.69	11.95	0.40
-	0.03	0.03	0.04	b.d.l.	b.d.l.	b.d.l.	b.d.l.
99.88	100.04	98.46	98.72	99.71	99.70	97.40	100.16
1.979	1.965	1.940	1.958	1.973	1.982	2.167	1.875
0.010	0.011	0.029	0.024	0.019	0.010	0.000	0.029
0.027	0.039	0.063	0.052	0.036	0.015	0.009	0.160
0.000	0.003	0.000	0.000	0.004	0.000	0.000	0.000
0.954	0.563	0.428	0.463	0.801	0.802	1.095	0.255
0.040	0.053	0.013	0.014	0.021	0.042	0.053	0.004
-	0.000	0.000	0.000	0.000	0.000	0.000	0.000
0.174	0.714	0.777	0.806	0.956	0.273	0.002	0.815
0.746	0.645	0.739	0.665	0.177	0.849	0.019	0.862
0.134	0.020	0.021	0.016	0.004	0.054	0.967	0.029
-	0.001	0.001	0.002	0.000	0.000	0.000	0.000
4.06	4.01	4.01	4.00	3.99	4.03	4.31	4.03
39.82	33.58	38.03	34.39	9.14	44.12	1.68	44.61
9.27	37.14	39.96	41.67	49.43	14.20	0.17	42.17
50.91	29.29	22.01	23.95	41.43	41.67	98.15	13.22

13	13	13	3	3	3	19	19	20/22
40	41	42	12	13	14	17	18	19
phenocryst: core to rim			phen; core (13), mid (14), rim (12)			mx crystals in xenolith		m'phen core
partly resorbed euhedral plate			subhedral prism			anhedral plates		stubby pr
200 x 175 µm			678 x 153 µm					91 x 41
51.26	51.14	51.13	48.29	48.15	47.78	59.06	52.15	49.77
0.53	0.52	0.52	0.21	0.22	0.26	0.56	1.36	0.41
3.23	3.16	2.85	0.26	0.27	0.29	8.35	0.67	1.01
b.d.l.	b.d.l.	b.d.l.	b.d.l.	b.d.l.	b.d.l.	b.d.l.	b.d.l.	b.d.l.
8.81	8.65	8.68	29.96	29.97	29.93	14.56	27.78	18.69
0.22	0.21	0.22	1.90	1.91	1.84	0.48	1.11	0.44
b.d.l.	b.d.l.	b.d.l.	0.09	b.d.l.	b.d.l.	b.d.l.	0.28	b.d.l.
14.48	14.61	14.68	0.45	0.49	0.41	0.30	0.38	22.48
20.88	21.09	21.06	19.02	18.97	19.08	0.10	0.16	1.76
0.38	0.37	0.32	0.48	0.49	0.54	8.33	12.83	b.d.l.
-	-	-	b.d.l.	b.d.l.	b.d.l.	4.32	0.10	b.d.l.
99.79	99.75	99.46	100.66	100.47	100.13	96.37*	97.62**	94.56
1.911	1.908	1.914	1.990	1.988	1.982	2.247	2.156	1.948
0.015	0.015	0.015	0.007	0.007	0.008	0.016	0.042	0.012
0.142	0.139	0.126	0.013	0.013	0.014	0.374	0.033	0.047
0.000	0.000	0.000	0.000	0.000	0.000	0.000	0.000	0.000
0.275	0.270	0.272	1.033	1.035	1.038	0.463	0.960	0.612
0.007	0.007	0.007	0.066	0.067	0.065	0.015	0.039	0.015
0.000	0.000	0.000	0.003	0.000	0.000	0.000	0.009	0.000
0.805	0.812	0.819	0.028	0.030	0.025	0.017	0.023	1.311
0.834	0.843	0.845	0.840	0.839	0.848	0.004	0.007	0.074
0.027	0.027	0.023	0.038	0.039	0.043	0.615	1.028	0.000
			0.000	0.000	0.000	0.210	0.005	0.000
4.02	4.02	4.02	4.02	4.02	4.02	3.96	4.30	4.02
43.59	43.79	43.65	44.20	44.07	44.36	0.84	0.72	3.70
42.05	42.19	42.31	1.45	1.58	1.33	3.51	2.36	65.67
14.36	14.02	14.04	54.34	54.35	54.31	95.65	96.92	30.64

						FC	
20/22	24	24	25	25	25	2 (FC)	2 (FC)
20	36	39	43	44	48	4	5
and rim	frag of m'ph	microphen	m'phen core and rim		m'phenocryst	in cluster w olivine	
rism	prismatic	rounded	subhedral prism		round plate	fat anhedral sausage	
µm	121x30 µm	121x91 µm	229 x 71 µm		170x130 µm	970 x 440 µm	
52.46	52.99	50.73	48.16	48.42	52.69	50.16	49.60
0.38	0.12	0.37	0.32	0.29	0.42	0.33	0.35
0.96	0.41	0.87	0.22	0.24	1.02	0.87	0.92
b.d.l.	b.d.l.	b.d.l.	0.26	0.16	b.d.l.	b.d.l.	b.d.l.
18.67	23.66	17.01	27.93	27.12	8.71	14.92	16.31
0.42	1.63	1.70	2.04	2.07	0.82	0.96	1.07
b.d.l.	b.d.l.	b.d.l.	b.d.l.	b.d.l.	b.d.l.	-	-
23.67	21.68	9.81	1.45	2.19	15.29	10.29	9.07
1.66	0.64	18.90	18.99	19.23	20.20	20.29	19.98
0.05	b.d.l.	0.42	0.77	0.71	0.39	0.57	0.58
b.d.l.	b.d.l.	b.d.l.	b.d.l.	b.d.l.	b.d.l.	-	-
98.27	101.13	99.81	100.14	100.43	99.54	98.39	97.88
1.964	1.974	1.970	1.981	1.978	1.968	1.964	1.966
0.011	0.003	0.011	0.010	0.009	0.012	0.010	0.010
0.042	0.018	0.040	0.011	0.012	0.045	0.040	0.043
0.000	0.000	0.000	0.008	0.005	0.000	0.000	0.000
0.585	0.737	0.552	0.961	0.927	0.272	0.488	0.541
0.013	0.051	0.056	0.071	0.072	0.026	0.032	0.036
0.000	0.000	0.000	0.000	0.000	0.000	0.000	0.000
1.321	1.204	0.568	0.089	0.133	0.851	0.600	0.536
0.067	0.026	0.786	0.837	0.842	0.809	0.851	0.848
0.004	0.000	0.032	0.061	0.056	0.028	0.043	0.045
0.000	0.000	0.000	0.000	0.000	0.000	0.000	0.000
4.01	4.01	4.01	4.03	4.03	4.01	4.03	4.02
3.38	1.30	41.25	44.36	44.26	41.85	43.87	44.08
66.98	61.21	29.78	4.71	7.01	44.06	30.95	27.83
29.65	37.49	28.97	50.93	48.72	14.09	25.18	28.09

				GF3			
3 (FC)	3 (FC)	5 (FC)	5 (FC)	GF3-1	GF3-1	GF3-2	GF3-3
14	15	17	18	3	7	10	17
intergrn w mica & feld		large, at triple junction		mantle on ol	microphen	mantle on ol	mantle on ol
rectangular plate		mushroom + short stalk		ol is hexag		ol is hexag	ol is hexag
65 x 42 μm: core & rim		757 x 408 μm					
50.82	51.12	50.19	49.95	35.35	35.36	36.04	35.39
0.15	0.07	0.34	0.30	0.09	0.07	0.08	0.09
0.77	0.58	0.95	0.87	0.50	0.52	0.16	0.70
b.d.l.	b.d.l.	b.d.l.	b.d.l.	b.d.l.	b.d.l.	b.d.l.	b.d.l.
13.07	14.19	16.27	16.54	30.87	32.99	31.28	31.27
0.97	1.03	1.13	1.12	0.56	0.51	0.60	0.54
-	-	-	-	-	-	-	-
11.53	11.43	9.91	9.44	26.08	24.65	29.02	26.29
20.16	20.08	19.86	19.66	0.66	0.66	0.42	0.74
0.49	0.48	0.58	0.57	b.d.l.	b.d.l.	b.d.l.	b.d.l.
-	-	-	-	-	-	-	-
97.96	98.98	99.23	98.45	94.11	94.76	97.60	95.02
1.977	1.977	1.980	1.987	1.542	1.546	1.514	1.531
0.004	0.002	0.010	0.009	0.003	0.002	0.003	0.003
0.035	0.026	0.000	0.000	0.026	0.027	0.008	0.036
0.000	0.000	0.000	0.000	0.000	0.000	0.000	0.000
0.425	0.459	0.537	0.550	1.126	1.206	1.099	1.131
0.032	0.034	0.038	0.038	0.021	0.019	0.021	0.020
0.000	0.000	0.000	0.000	-	-	-	-
0.668	0.659	0.583	0.560	1.695	1.606	1.817	1.694
0.840	0.832	0.840	0.838	0.031	0.031	0.019	0.034
0.037	0.036	0.044	0.044	0.000	0.000	0.000	0.000
0.000	0.000	0.000	0.000	-	-	-	-
4.02	4.03	4.03	4.03	4.44	4.44	4.48	4.45
43.45	42.68	42.85	43.02	1.08	1.09	0.64	1.20
34.56	33.79	29.74	28.73	59.44	56.49	61.91	59.25
21.99	23.54	27.40	28.25	39.48	42.42	37.45	39.55

Supplementary Table 2c Compositions of amphibole phenocrysts

Sample	**Ttg-hg#1**					
Image	1	1	1	3	3	3
Session	11.1.18					
Anal. no.	1	2	3	27	32	33
Occurrence	phenocryst	phenocryst	phenocryst	phenocryst	phenocryst	phenocryst
Form	prism	spade-shape	rectang. pl.	euh plate	euh plate	????
Size	645x160 µm	258x160 µm	234x218 µm	162 x147 µm	74 x 74 µm	????
SiO2	48.84	48.72	46.76	48.92	47.06	46.32
TiO2	0.78	0.98	1.49	0.95	1.24	1.54
Al2O3	0.75	0.78	2.24	0.80	2.25	2.25
FeO*	36.58	35.54	31.10	36.28	31.7	30.91
MnO	1.24	1.04	0.93	0.99	0.96	0.85
ZnO	0.16	0.20	bd	0.27	0.26	0.23
MgO	0.35	0.40	3.22	0.48	3.12	3.07
CaO	1.32	1.29	6.86	1.36	6.67	6.60
Na2O	6.96	6.98	4.03	7.02	3.93	3.96
K2O	1.05	1.05	0.98	1.07	0.99	0.99
Cl	0.05	0.03	0.09	0.05	0.09	0.08
F	bd	bd	bd	bd	bd	bd
Sum	98.08	97.01	97.70	98.19	98.27	96.80
O ≡ F, Cl	0.01	0.01	0.02	0.01	0.02	0.02
Total	98.07	97.00	97.68	98.18	98.25	96.78

Co, Ni, Zn, Cr all bd
** altered strip (10 µm) at edge of crystal

Si	0.813	0.811	0.778	0.814	0.783	0.771
Ti	0.010	0.012	0.019	0.012	0.016	0.019
Al	0.015	0.015	0.044	0.016	0.044	0.044
Fe	0.509	0.495	0.433	0.505	0.441	0.430
Mn	0.017	0.015	0.013	0.014	0.014	0.012
Zn	0.002	0.002	0.000	0.003	0.003	0.003
Mg	0.009	0.010	0.080	0.012	0.077	0.076
Ca	0.024	0.023	0.122	0.024	0.119	0.118
Na	0.225	0.225	0.130	0.227	0.127	0.128
K	0.022	0.022	0.021	0.023	0.021	0.021
Cl	0.001	0.001	0.003	0.001	0.003	0.002
F	0.000	0.000	0.000	0.000	0.000	0.000
Mg/Mg+Fe	0.02	0.02	0.16	0.02	0.15	0.15

4	4	5		5 (FE)	5 (FE)		2.16 20.2.18
2	4	15		19	20		11
microphen	incl in ol phen	phenocryst		rim & core of phenocryst			mantles cpx
euh X-sect	anh plate	subh plate		slightly resorb prism			irregular
188x125 µm	55x47 µm	190x138 µm		600 x 210 µm			>60 µm
46.12	48.17	47.38		46.68	46.23		45.48
1.55	0.46	1.31		1.21	1.45		1.45
2.86	2.49	1.97		2.02	2.21		2.91
31.02	27.53	31.46		31.31	31.08		29.73
0.92	1.00	1.07		0.98	0.98		0.95
0.18	0.14	0.14		-	-		-
3.28	6.61	3.33		3.30	3.01		4.20
7.52	7.27	6.63		6.51	6.61		7.29
3.68	4.04	4.06		4.13	3.87		3.84
0.99	0.98	0.98		1.13	1.21		1.16
0.10	0.09	0.08		0.08	0.08		0.10
-	-	bd		0.80	0.76		0.69
98.22	98.78	98.41		98.15	97.49		97.80
0.02	0.02	0.02		0.36	0.34		0.31
98.20	98.76	98.39		97.79	97.15		97.49
0.768	0.802	0.788	0.000	0.777	0.769	0.000	0.757
0.019	0.006	0.016	0.000	0.015	0.018	0.000	0.018
0.056	0.049	0.039	0.000	0.040	0.043	0.000	0.057
0.432	0.383	0.438	0.000	0.436	0.433	0.000	0.414
0.013	0.014	0.015	0.000	0.014	0.014	0.000	0.013
0.002	0.002	0.002	0.000				
0.081	0.164	0.083	0.000	0.082	0.075	0.000	0.104
0.134	0.130	0.118	0.000	0.116	0.118	0.000	0.130
0.119	0.130	0.131	0.000	0.133	0.125	0.000	0.124
0.021	0.021	0.021	0.000	0.024	0.026	0.000	0.025
0.003	0.003	0.002	0.000	0.002	0.002	0.000	0.003
		0.000		0.042	0.040		0.036
0.16	0.30	0.16		0.16	0.15		0.20

			GF1A	
9	9	9	2	4
21.2.18			17.1.18	
			10	17
phenocryst with many MI			fragment	phenocryst: 20,
euhedral basal section			triangular	
585 x 535 µm			22x16 µm	
47.44	46.43	46.10	46.61	43.83
1.17	1.34	1.48	0.76	1.39
1.39	1.99	2.21	8.12	10.14
34.26	31.26	31.46	15.01	16.86
1.15	1.03	0.97	0.42	0.55
-	-	-	bd	bd
1.93	3.16	3.15	12.22	11.09
3.97	6.69	6.78	11.84	11.27
5.05	3.99	3.94	0.85	1.50
1.02	1.13	1.14	0.49	0.95
0.05	0.08	0.09	0.04	0.10
bd	bd	bd	bd	bd
97.43	97.10	97.32	96.36	97.68
0.01	0.02	0.02	0.01	0.02
97.42	97.08	97.30	96.35	97.66
0.789	0.773	0.767	0.776	0.729
0.015	0.017	0.019	0.010	0.017
0.027	0.039	0.043	0.159	0.199
0.477	0.435	0.438	0.209	0.235
0.016	0.015	0.014	0.006	0.008
			0.000	0.000
0.048	0.078	0.078	0.303	0.275
0.071	0.119	0.121	0.211	0.201
0.163	0.129	0.127	0.027	0.048
0.022	0.024	0.024	0.010	0.020
0.001	0.002	0.003	0.001	0.003
0.000	0.000	0.000	0.000	0.000
0.09	0.15	0.15	0.59	0.54

4	4	4	12	15	26
					22.1.18
18	19	20	37	50	16
core, 19, mid; 17, 18, rim			inclus in feld	phen: core	m'ph in xen
partly resorbed prism			rounded	resorb prism	wedge
383 x 117 µm			47x35 µm	116 x 63 µm	18 x 7 µm
43.30	44.31	43.44	47.29	50.76	42.35
1.52	1.55	1.30	1.02	0.87	1.76
10.25	9.30	9.83	1.59	2.44	12.85
17.17	17.03	17.61	37.72	11.42	13.04
0.57	0.69	0.72	1.38	0.57	0.28
bd	bd	bd	bd	bd	bd
10.77	11.19	10.63	0.92	12.13	12.65
11.29	11.19	11.31	1.94	20.77	11.04
1.55	1.44	1.47	6.36	0.71	2.30
1.01	0.95	1.12	0.31	bd	0.43
0.08	0.08	0.09	0.05	bd	0.04
bd	bd	bd	bd	bd	bd
97.51	97.73	97.52	98.58	99.67	96.74
0.02	0.02	0.02	0.01	0.00	0.01
97.49	97.71	97.50	98.57	99.67	96.73
0.721	0.737	0.723	0.787	0.845	0.705
0.019	0.019	0.016	0.013	0.011	0.022
0.201	0.182	0.193	0.031	0.048	0.252
0.239	0.237	0.245	0.525	0.159	0.181
0.008	0.010	0.010	0.019	0.008	0.004
0.000	0.000	0.000	0.000	0.000	0.000
0.267	0.278	0.264	0.023	0.301	0.314
0.201	0.200	0.202	0.035	0.370	0.197
0.050	0.046	0.047	0.205	0.023	0.074
0.021	0.020	0.024	0.007	0.000	0.009
0.002	0.002	0.003	0.001	0.000	0.001
0.000	0.000	0.000	0.000	0.000	0.000
0.53	0.54	0.52	0.04	0.65	0.63

24	24	24	24	25	25
19.1.18					
35	38	40	42	45	46
all are anhedral fragments of microphens from prismatic to platy small!				phenocryst wedge-shaped 243 x 100 µm	
43.30	43.08	47.96	42.57	42.68	46.22
2.03	2.25	1.49	1.90	3.06	1.16
11.16	10.59	6.25	12.02	9.90	8.95
13.37	14.70	15.46	12.98	17.56	14.51
0.33	0.41	0.73	0.28	0.35	0.54
bd	bd	0.17	bd	bd	bd
13.85	12.36	13.07	13.73	10.70	13.76
11.08	11.65	11.01	11.12	10.90	10.74
2.16	2.11	1.50	2.34	2.09	1.35
0.48	0.86	0.54	0.43	0.67	0.40
0.05	0.05	0.04	0.04	0.04	0.09
bd	bd	bd	bd	bd	bd
97.81	98.06	98.22	97.41	97.95	97.72
0.01	0.01	0.01	0.01	0.01	0.02
97.80	98.05	98.21	97.40	97.94	97.70
0.721	0.717	0.798	0.708	0.710	0.769
0.025	0.028	0.019	0.024	0.038	0.015
0.219	0.208	0.123	0.236	0.194	0.176
0.186	0.205	0.215	0.181	0.244	0.202
0.005	0.006	0.010	0.004	0.005	0.008
0.000	0.000	0.002	0.000	0.000	0.000
0.344	0.307	0.324	0.341	0.265	0.341
0.198	0.208	0.196	0.198	0.194	0.192
0.070	0.068	0.048	0.076	0.067	0.044
0.010	0.018	0.011	0.009	0.014	0.008
0.001	0.001	0.001	0.001	0.001	0.003
0.000	0.000	0.000	0.000	0.000	0.000
0.65	0.60	0.60	0.65	0.52	0.63

25	25
49	50
phenocryst core & rim	
rounded plate	
250 x 70 µm	
45.29	44.83
1.27	1.35
5.02	5.05
26.59	27.37
1.07	1.08
0.13	bd
5.41	5.13
8.81	8.32
3.36	3.05
0.88	0.92
0.21	0.24
0.35	0.45
98.39	97.79
0.20	0.24
98.19	97.55
0.754	0.746
0.016	0.017
0.098	0.099
0.370	0.381
0.015	0.015
0.002	0.000
0.134	0.127
0.157	0.148
0.108	0.098
0.019	0.020
0.006	0.007
0.018	0.024
0.27	0.25

Supplementary Table 3a Composition of ilmenite and magnetite phenocrysts

Mineral	Ilmenite						
Sample	**Ttg-hg#1**						**GF1A**
Image	9	2(FE)	2	2.14	2.14	2.14	1
Anal. no.	18	9	7	5	12	13	5
Occurrence	microphen	microphen	assocd w olv	inclus in oliv	partly resorbed plate		stellate gp
Form	euhed prism	platy, w. Cpx	anhedr plate	round blob	arcuate, mantled by mica		elongate
Size	220 x 37 µm	48 x 42 µm	75 x 50 µm	~65 µm	max dimensions234 x 169 µm		171x40 µm
wt%							
SiO_2	0.04	0.08	b.d.l.	0.04	0.09	b.d.l.	b.d.l.
TiO_2	50.52	50.28	50.15	50.22	48.76	50.99	49.30
Nb_2O_5	0.73	0.62	0.44	0.77	0.84	0.18	b.d.l.
Al_2O_3	b.d.l.	b.d.l.	b.d.l.	b.d.l.	b.d.l.	b.d.l.	0.27
V_2O_3	0.13	0.26	0.13	0.22	0.22	0.29	0.17
Cr_2O_3	b.d.l.	b.d.l.	b.d.l.	b.d.l.	b.d.l.	b.d.l.	b.d.l.
FeO*	46.34	46.86	46.66	46.84	46.89	45.37	44.51
MnO	1.79	1.69	2.03	1.74	1.76	1.85	1.34
MgO	0.05	0.15	0.05	0.10	0.10	0.17	3.61
ZnO	b.d.l.	b.d.l.	b.d.l.	b.d.l.	b.d.l.	b.d.l.	b.d.l.
CaO	b.d.l.	0.03	b.d.l.	b.d.l.	0.22	b.d.l.	0.03
Fe_2O_3	3.1	3.9	4.1	4.7	5.7	2.2	8.9
FeO	43.6	43.3	43	43.3	41.7	43.4	36.5
Total	100	100.4	99.9	100.3	99.5	99.3	100.1
Formulae on basis of 3 oxygens							
Si	0.001	0.002	0.000	0.001	0.002	0.000	0.000
Ti	0.964	0.954	0.957	0.954	0.935	0.975	0.912
Al	0.000	0.000	0.000	0.000	0.000	0.000	0.008
Fe3+	0.058	0.075	0.078	0.075	0.110	0.042	0.164
Cr	0.000	0.000	0.000	0.000	0.000	0.000	0.000
Fe2+	0.924	0.913	0.911	0.914	0.889	0.923	0.751
Mn	0.038	0.036	0.044	0.037	0.038	0.040	0.028
Mg	0.002	0.006	0.002	0.004	0.004	0.006	0.132
Ca	0.000	0.001	0.000	0.000	0.006	0.006	0.001
Zn	0.000	0.000	0.000				0.000
V	0.003	0.005	0.003	0.005	0.005	0.006	0.003
Nb	0.010	0.008	0.006	0.010	0.011	0.002	0.000
X_{ilm}/X_{usp}	96.9	96.0	95.9	96.0	94.4	98.1	90.2

FeO*, all Fe as Fe^{2+}

b.d.l., below detection limit

		Magnetite			
		Ttg-hg#1	**GF1A**		
1	23	2	14	14	8
6	34	8	44	45	28
in ol phen	m'phen	incl in oliv	phenocryst, core & rim		phenocryst
fat rays	round plate	hexag plate	slightly resorbed hexagon		with zircon
141x69 µm	56 x 52 µm	31 x 28 µm	160 x 137 µm		64x50 µm
0.03	0.03	0.10	0.07	0.10	0.05
49.76	42.69	18.56	24.07	24.02	5.28
b.d.l.	0.16	b.d.l.	b.d.l.	b.d.l.	b.d.l.
0.20	0.09	0.13	1.01	0.98	1.31
0.14	0.21	0.28	b.d.l.	b.d.l.	0.29
b.d.l.	b.d.l.	b.d.l.	b.d.l.	b.d.l.	b.d.l.
44.29	50.80	72.49	69.56	70.60	85.96
1.20	3.49	1.03	2.11	2.08	0.82
3.63	1.49	0.03	0.79	0.82	1.01
b.d.l.	0.19	0.78	0.15	0.21	0.08
b.d.l.	b.d.l.	b.d.l.	0.07	b.d.l.	b.d.l.
8.0	20.8	29.9	21.6	22.4	57.8
37.1	32.1	45.5	50.1	50.5	34
100	101.2	96.4	100	101.1	100.6
		Formulae on basis of 4 oxygens			
0.001	0.001	0.004	0.003	0.004	0.002
0.921	0.800	0.547	0.673	0.665	0.149
0.006	0.003	0.006	0.044	0.043	0.058
0.148	0.390	0.883	0.604	0.62	1.631
0.000	0.000	0.000	0.000	0.000	0.000
0.764	0.668	1.493	1.559	1.553	1.066
0.025	0.074	0.034	0.066	0.065	0.026
0.133	0.055	0.002	0.044	0.045	0.057
0.000	0.000	0	0.003	0.000	0.000
0.000	0.004	0.023	0.004	0.006	0.002
0.003	0.004	0.009	0.000	0.000	0.009
0.000	0.002	0.000	0.000	0.000	0.000
91.2	77.6	54.6	67.9	67.1	14.3

		GF3	
13	21	GF3-2	
43	27	11	13
inclus in abole	phenocryst	platy incl in ol (11) and cpx (13)	
anh plate	subh plate	anhedral	square
38x20 µm	80x80 µm	29x21 µm	10 x 10 µm
0.07	0.07	0.09	0.07
6.98	4.93	17.00	14.32
b.d.l.	b.d.l.	b.d.l.	b.d.l.
0.17	0.50	3.39	4.76
0.62	b.d.l.	1.04	0.98
0.34	b.d.l.	6.04	7.62
78.31	80.16	65.07	62.76
0.27	7.69	0.57	0.50
2.91	0.22	3.18	3.69
0.07	0.63	0.14	0.18
0.29	b.d.l.	b.d.l.	0.05
52.5	58.9	25.9	27.2
31	27.2	41.8	38.3
95.3	100.1	99.1	97.7
0.003	0.003	0.003	0.003
0.205	0.141	0.467	0.395
0.008	0.023	0.146	0.206
1.546	1.69	0.710	0.750
0.011	0.000	0.174	0.221
1.015	0.866	1.276	1.173
0.009	0.248	0.018	0.016
0.17	0.013	0.173	0.202
0.012	0.000	0.000	0.002
0.002	0.018	0.004	0.005
0.019	0.000	0.030	0.029
0.000	0.000	0.000	0.000
20.6	2.0	56.3	50.8

Supplementary Table 3b Compositions of apatite (micro)phenocrysts

Sample	Ttg-hg#1					GF1A
Anal. no.	1	2	6	7	8	16
Occurrence	partly resorbed m'phen		inclusion in felds phen: rim to core			inclus in ab
Form	subhedral basal section		euhedral prism: oscill zoned			rounded
Size	21 x 19 µm		73 x 23 µm			<10 µm
wt%						
P_2O_5	39.11	40.10	40.33	37.72	40.84	39.53
SiO_2	1.92	1.55	0.91	2.40	1.04	0.96
Y_2O_3	0.37	0.26	0.16	0.50	0.14	b.d.l.
La_2O_3	1.15	1.18	0.84	1.48	0.74	0.09
Ce_2O_3	3.02	2.57	1.99	3.61	1.71	0.14
Nd_2O_3	1.25	1.12	1.04	1.75	0.67	b.d.l.
MgO	b.d.l.	b.d.l.	b.d.l.	b.d.l.	b.d.l.	0.20
CaO	51.99	53.54	53.66	51.23	53.99	54.52
MnO	0.12	0.08	0.17	0.19	0.15	0.17
FeO*	0.26	0.21	1.88	1.48	1.30	0.84
SrO	b.d.l.	b.d.l.	b.d.l.	b.d.l.	b.d.l.	b.d.l.
Na_2O	0.39	0.26	0.34	0.27	0.21	0.17
F	1.87	1.94	2.94	2.72	3.07	1.72
Cl	b.d.l.	b.d.l.	b.d.l.	b.d.l.	b.d.l.	0.70
SO_3	b.d.l.	b.d.l.	b.d.l.	b.d.l.	b.d.l.	0.53
Sum	101.45	102.81	104.26	103.35	103.86	99.57
0 ≡ F, Cl	0.79	0.82	1.24	1.15	1.29	0.92
Total	100.66	101.99	103.02	102.20	102.57	98.65
Si+REE	0.32	0.26	0.17	0.39	0.17	0.09
Formulae on the basis of 13 oxygens						
La	0.037	0.037	0.026	0.047	0.023	0.003
Ce	0.096	0.081	0.062	0.115	0.053	0.004
Y	0.017	0.012	0.007	0.023	0.006	0.000
Ca	4.853	4.915	4.867	4.770	4.870	5.065
Sr	0.000	0.000	0.000	0.000	0.000	0.000
Na	0.066	0.043	0.056	0.045	0.034	0.029
Mg	0.000	0.000	0.000	0.000	0.000	0.026
Fe^{2+}	0.019	0.015	0.133	0.108	0.092	0.061
Mn	0.009	0.006	0.012	0.014	0.011	0.012
Sum M	5.098	5.108	5.163	5.123	5.088	5.200
P	2.884	2.907	2.889	2.774	2.910	2.901
Si	0.167	0.133	0.077	0.209	0.088	0.083
S	0.000	0.000	0.000	0.000	0.000	0.035
Sum T	3.051	3.040	2.966	2.983	2.997	3.019
F	0.515	0.526	0.787	0.748	0.817	0.472
Cl	0.000	0.000	0.000	0.000	0.000	0.104

OH	0.485	0.474		0.213	0.252	0.183	0.424
Σ cations	8.15	8.15		8.13	8.11	8.09	8.22

FeO*, all Fe as Fe^{2+}

OH = (1-(F+Cl))

b.d.l., below detection limit

ab, amphibole; ilm, ilmenite; rut, rutile

31	32
in ilm-rut-	cluster
slim prism	X-section
56 x 10 µm	13 x 12 µm
40.56	40.57
0.85	0.74
b.d.l.	b.d.l.
0.40	0.29
0.90	0.66
b.d.l.	b.d.l.
0.06	0.07
53.64	54.37
0.14	0.14
0.31	0.85
0.10	0.12
0.09	0.27
2.29	2.38
0.38	0.45
0.04	0.62
99.76	101.53
1.07	1.13
98.69	100.40
0.11	0.09
0.013	0.009
0.028	0.021
0.000	0.000
4.969	4.953
0.005	0.006
0.015	0.045
0.008	0.009
0.022	0.060
0.010	0.010
5.071	5.112
2.968	2.919
0.073	0.063
0.003	0.040
3.044	3.022
0.626	0.640
0.056	0.066

0.317	0.294
8.12	8.13

Supplementary Table 3c Composition of micas

Sample	**Ttg-hg#1**				**FC**		
Image	4	4	2.15	2.15	1 (FC)	1 (FC)	1 (FC)
Anal. no.			14	15	1	2	3
Occurrence	replacing ilmen phen		in oliv-ilm cluster		in dark string		in feldsp
Form	irregular mantle		replacing ilmenite		rect plate	hexagon	elongate plt
Size					304x101 µm	145x130 µm	290x116 µm
wt%							
SiO_2	37.21	36.51	36.56	36.82	36.45	36.41	35.59
TiO_2	3.66	4.11	2.85	3.53	5.09	4.76	4.65
Al_2O_3	10.56	11.24	9.16	9.25	12.53	12.46	11.91
V_2O_3	b.d.l.	b.d.l.	0.15	0.12	0.14	0.12	0.12
FeO*	28.48	29.78	29.02	29.07	20.23	19.90	19.70
MnO	0.43	0.37	0.47	0.45	0.36	0.38	0.31
MgO	6.06	5.72	6.85	7.13	11.70	11.46	12.51
SrO	b.d.l.	b.d.l.	0.09	0.10	0.08	0.14	0.06
Na_2O	0.61	0.61	0.70	0.67	0.88	0.66	0.66
K_2O	8.60	8.56	9.57	9.69	9.58	9.53	9.63
BaO	b.d.l.	b.d.l.	b.d.l.	b.d.l.	0.24	0.34	0.32
F	b.d.l.	b.d.l.	1.36	1.55	1.17	1.15	1.33
Cl	0.13	0.12	0.13	0.13	0.13	0.14	0.18
Sum	95.74	97.02	96.91	98.51	98.58	97.45	96.97
0 ≡ F, Cl	0.04	0.03	0.61	0.69	0.52	0.51	0.60
Total	95.70	96.09	96.30	97.82	98.06	96.94	96.37
Formulae on the basis of 11 oxygens							
Si	2.966	2.890	2.919	2.888	2.735	2.761	2.719
Al	0.992	1.049	0.862	0.855	1.108	1.114	1.073
Sum T	3.958	3.938	3.781	3.744	3.843	3.874	3.792
Ti	0.219	0.245	0.171	0.208	0.287	0.271	0.267
V	0.000	0.000	0.010	0.008	0.008	0.007	0.007
Fe	1.899	1.971	1.938	1.907	1.269	1.262	1.259
Mn	0.029	0.025	0.032	0.030	0.023	0.024	0.020
Mg	0.720	0.675	0.815	0.834	1.308	1.295	1.425
Sum M	2.867	2.916	2.966	2.987	2.896	2.860	2.978
Sr	0.000	0.000	0.004	0.005	0.003	0.006	0.003
Na	0.094	0.094	0.108	0.102	0.128	0.097	0.098
K	0.875	0.864	0.975	0.970	0.917	0.922	0.939
Ba	0.000	0.000	0.000	0.000	0.007	0.010	0.010
Sum A	0.969	0.958	1.087	1.076	1.056	1.035	1.049
F	0.000	0.000	0.343	0.385	0.278	0.276	0.321
Cl	0.000	0.000	0.000	0.000	0.000	0.000	0.000
OH	2.000	2.000	1.656	1.615	1.722	1.724	1.678
Sum X	2.000	2.000	2.000	2.000	2.000	2.000	2.000

Σ cations	7.79	7.81	7.83	7.81	7.79	7.77	7.82
Mg/(Mg+Fe)	0.27	0.25	0.30	0.30	0.51	0.51	0.53

FeO*, all Fe as Fe^{2+}

b.d.l., below detection limit

OH = (2-(F+Cl))

3 (FC)	3 (FC)	2 (FC)
12	13	16
in cluster w felds and cpx		in mafic "arc"
fat pound note sign		long plate
85 x 47 µm		797x217 µm
39.70	38.72	35.45
1.75	1.50	5.81
11.95	11.90	12.50
b.d.l.	b.d.l.	0.15
15.55	13.89	20.11
0.26	0.25	0.30
17.63	18.35	10.88
0.09	0.12	0.14
0.74	0.72	0.78
9.86	9.95	9.61
0.17	0.18	0.28
1.68	1.75	1.18
0.09	0.08	0.13
99.47	97.41	97.32
0.73	0.75	0.53
98.74	96.66	96.79
2.863	2.841	2.703
1.016	1.029	1.123
3.879	3.870	3.827
0.095	0.083	0.333
0.000	0.000	0.009
0.938	0.852	1.282
0.016	0.016	0.019
1.895	2.006	1.236
2.944	2.957	2.881
0.004	0.005	0.006
0.103	0.102	0.115
0.907	0.931	0.935
0.005	0.005	0.008
1.019	1.044	1.065
0.383	0.406	0.285
0.000	0.000	0.000
1.617	1.594	1.715
2.000	2.000	2.000

7.84	7.87	7.77
0.67	0.70	0.49

Supplementary Table 4a Compositions of fluorite phenocrysts

Sample	**Ttg-hg#1**						
Image	9	9	9	9	7	19	19
Anal. no.	13	14	15	16	9	10	11
Occurrence	partly enclosed in ab phen		partly enclosed in ab phen		phenocryst	phenocryst	phenocryst
Form	rounded		rounded		part alt'd phen	euh square	euh square
Size	107 x 71 µm		171 x 129 µm		150x100 µm	195x152m	163x130m
wt%							
Ca	52.76	52.94	52.87	53.08	47.50	53.74	53.38
La	-	-	-	-	0.64	b.d.l.	b.d.l.
Ce	-	-	-	-	1.76	b.d.l.	b.d.l.
Y	0.20	0.16	0.17	0.13	1.74	0.19	0.12
F	46.99	48.02	47.61	47.20	46.76	46.61	47.46
Cl	-	-	-	-	b.d.l.	b.d.l.	b.d.l.
Total	99.95	101.12	100.65	100.41	98.40	100.54	100.96

b.d.l., below detection limit

Dash, not determined

* Total includes 0.44 wt% Nd

5	5	5	3	6 (FE)	6 (FE)	6 (FE)	2.11
12	13	14	3	1	2	3	4
phenocryst			microphen	phenocryst		incl in oliv	incl in abole
euhedral plate; core to rim			hexagonal	slightly rounded hexagon			ovoidal
207 x 155 µm			162 x 88 µm	262 x 167 µm		71 x 48 µm	50 x 25 µm
53.43	52.68	53.02	51.36	51.30	50.27	50.77	48.95
b.d.l.	b.d.l.	b.d.l.	b.d.l.	-	-	-	b.d.l.
b.d.l.	b.d.l.	b.d.l.	b.d.l.	-	-	-	0.63
0.17	b.d.l.	b.d.l.	0.14	0.23	0.24	0.11	1.02
46.67	47.84	47.66	49.29	48.72	49.31	48.99	48.86
b.d.l.	b.d.l.	b.d.l.	b.d.l.	b.d.l.	b.d.l.	b.d.l.	b.d.l.
100.27	100.52	100.68	100.79	100.25	99.82	99.87	99.90*

Supplementary Table 4b Compositions of zircon phenocrysts

Sample	**GF1A**						
Image	5	7	7	7	8	14	14
Anal. no.	23	25	26	27	29	46	47
Occurrence	inclus in oliv	m'phen assoc'd with ilmenite			w. mag phen	inclusions (46, 47 partial) in o	
Form		prism; 26, core, 25, 27 rims			resorb hexagon	subh hexag	core & rim
Size		38 x 22 µm			43x32 µm	60x39 µm	
wt%							
P_2O_5	b.d.l.	0.22	0.08	0.17	0.15	0.07	b.d.l.
SiO_2	32.44	32.73	32.78	32.66	32.57	32.76	32.82
TiO_2	b.d.l.	b.d.l.	b.d.l.	b.d.l.	0.10	0.06	b.d.l.
ZrO_2	65.80	64.63	64.33	63.20	63.24	64.26	63.84
HfO_2	0.79	1.34	0.94	1.30	0.92	1.09	0.80
ThO_2	b.d.l.	b.d.l.	b.d.l.	0.11	0.83	b.d.l.	b.d.l.
UO_2	b.d.l.	b.d.l.	b.d.l.	0.16	0.30	b.d.l.	b.d.l.
Y_2O_3	b.d.l.	b.d.l.	b.d.l.	b.d.l.	0.12	b.d.l.	b.d.l.
Ce_2O_3	b.d.l.	b.d.l.	b.d.l.	b.d.l.	b.d.l.	b.d.l.	b.d.l.
Yb_2O_3	b.d.l.	b.d.l.	b.d.l.	b.d.l.	b.d.l.	b.d.l.	b.d.l.
CaO	0.05	0.05	b.d.l.	b.d.l.	b.d.l.	b.d.l.	b.d.l.
FeO*	0.51	0.68	0.77	1.19	2.51	0.36	0.32
Total	99.59	99.65	98.90	98.79	100.74	98.60	97.78
Formulae on basis of 4 oxygens							
P	0.000	0.006	0.002	0.004	0.004	0.002	0.000
Si	0.998	1.004	1.011	1.011	0.998	1.013	1.021
Ti	0.000	0.000	0.000	0.000	0.002	0.001	0.000
Zr	0.988	0.967	0.968	0.954	0.945	0.969	0.968
Hf	0.007	0.012	0.008	0.011	0.008	0.010	0.007
Th	0.000	0.000	0.000	0.001	0.006	0.000	0.000
U	0.000	0.000	0.000	0.001	0.002	0.000	0.000
Y	0.000	0.000	0.000	0.000	0.002	0.000	0.000
Ce	0.000	0.000	0.000	0.000	0.000	0.000	0.000
Yb	0.000	0.000	0.000	0.000	0.000	0.000	0.000
Ca	0.002	0.002	0.000	0.000	0.000	0.000	0.000
Fe^{2+}	0.013	0.017	0.020	0.031	0.064	0.009	0.008
Σ cations	2.01	2.01	2.01	2.01	2.03	2.00	2.00

FeO*, all Fe as Fe^{2+}

b.d.l., below detection limit

14	14	16	16	19	19	19	19
48	49	51	52	11	12	13	14
xide phenocryst		phenocryst		unusual, fragmented grain in xenolith			
subh plate	flat plate	partly resorb prism		forms three parts of a hollow arcuate chain			
29x18 µm	24 x 8 µm	156 x 81 µm: core & rim		largest fragment is 50 x 23 µm			
b.d.l.	b.d.l.	b.d.l.	0.12	0.30	0.42	0.66	0.79
32.85	32.27	32.29	32.55	31.87	31.21	30.48	32.45
0.37	0.75	b.d.l.	b.d.l.	b.d.l.	0.11	0.14	0.33
63.84	64.72	64.33	63.85	59.19	59.04	59.16	50.88
0.83	0.78	0.60	0.52	1.22	0.97	0.53	0.76
b.d.l.	b.d.l.	0.11	0.12	0.26	0.44	0.38	0.37
b.d.l.	b.d.l.	b.d.l.	b.d.l.	b.d.l.	b.d.l.	b.d.l.	b.d.l.
b.d.l.	b.d.l.	0.59	0.31	0.49	1.20	1.32	1.12
b.d.l.	b.d.l.	b.d.l.	b.d.l.	4.67	3.39	2.95	4.12
b.d.l.	b.d.l.	b.d.l.	b.d.l.	0.35	0.40	0.47	0.55
b.d.l.	b.d.l.	b.d.l.	b.d.l.	b.d.l.	b.d.l.	b.d.l.	0.04
1.78	2.47	0.12	bd	0.32	0.14	0.25	3.30
99.67	100.99	98.04	97.47	98.67	97.32	96.34	94.71
0.000	0.000	0.000	0.003	0.008	0.011	0.018	0.022
1.007	0.983	1.007	1.015	1.009	0.999	0.984	1.051
0.009	0.017	0.000	0.000	0.000	0.003	0.003	0.008
0.954	0.962	0.978	0.971	0.914	0.922	0.932	0.804
0.007	0.007	0.005	0.005	0.011	0.009	0.005	0.007
0.000	0.000	0.001	0.001	0.002	0.003	0.003	0.003
0.000	0.000	0.000	0.000	0.000	0.000	0.000	0.000
0.000	0.000	0.010	0.005	0.008	0.020	0.023	0.019
0.000	0.000	0.000	0.000	0.055	0.040	0.035	0.049
0.000	0.000	0.000	0.000	0.003	0.004	0.005	0.005
0.000	0.000	0.000	0.000	0.000	0.000	0.000	0.001
0.046	0.063	0.003	0.000	0.008	0.004	0.007	0.089
2.02	2.03	2.00	2.00	2.02	2.02	2.01	2.06

21	21
25	26
phenocryst	incl in mag
euh prism	round plate
70 x 10 µm	15 x 12 µm
0.09	0.17
32.64	32.27
b.d.l.	0.13
65.37	64.44
1.50	1.46
b.d.l.	b.d.l.
b.d.l.	b.d.l.
b.d.l.	b.d.l.
b.d.l.	b.d.l.
b.d.l.	b.d.l.
b.d.l.	b.d.l.
0.55	3.04
100.15	101.51
0.002	0.004
1.000	0.983
0.000	0.003
0.977	0.957
0.013	0.013
0.000	0.000
0.000	0.000
0.000	0.000
0.000	0.000
0.000	0.000
0.000	0.000
0.014	0.077
2.01	2.04

Supplementary Table 4c Compositions of chevkinite-(Ce) phenocrysts

Sample	**Ttg-hg#1**						
Image	16	16	16	18/20	18/20	18/20	18/20
Anal. no.	1	2	3	1	2	3	4
Occurrence	phenocryst			phenocryst			
Form	partly resorb prism		fragmented	partly resorbed, fragmented. Zoned in greys, v			
Size	38 x 11 μm			68 x 41 μm			
wt%							
Nb_2O_5	1.21	1.05	1.02	1.06	1.13	0.96	0.97
Ta_2O_5	0.08	0.14	0.10	0.09	0.12	0.12	0.16
SiO_2	19.47	19.52	19.91	19.28	19.10	19.39	19.29
TiO_2	17.28	17.27	16.75	17.56	17.28	17.72	17.58
ZrO_2	0.33	0.32	0.24	0.52	0.36	0.44	0.40
HfO_2	0.10	0.12	b.d.l.	b.d.l.	0.12	0.10	0.12
ThO_2	0.76	0.52	0.43	0.42	1.17	1.07	1.07
Al_2O_3	0.02	0.06	0.09	0.03	0.04	0.05	0.03
Y_2O_3	0.23	0.24	0.24	0.24	0.28	0.23	0.28
La_2O_3	12.79	13.12	12.83	12.83	12.44	12.71	12.44
Ce_2O_3	23.14	23.44	22.78	23.38	23.59	22.98	23.47
Pr_2O_3	3.00	3.10	2.91	3.15	2.94	3.12	2.96
Nd_2O_3	6.20	5.95	5.85	5.98	6.49	5.68	6.24
Sm_2O_3	0.53	0.47	0.49	0.47	0.41	0.45	0.50
Gd_2O_3	0.35	0.34	0.30	0.34	0.35	0.27	0.28
MgO	0.04	0.04	0.03	0.04	0.03	0.05	0.04
CaO	1.77	1.77	1.72	2.16	1.82	2.25	1.94
MnO	b.d.l.	b.d.l.	0.11	b.d.l.	b.d.l.	0.07	b.d.l.
FeO*	11.93	12.01	11.80	11.72	11.97	11.74	11.83
Total	99.23	99.48	97.60	99.27	99.64	99.40	99.60

FeO*, all Fe as Fe^{2+}

b.d.l., below detection limit

Dash, not reported

18/20 5	18/20 6	18/20 7	1 (FE) 7	1/3 (FE) 8
vith one dark patch		tch (7)	incl in oliv anh plate 79 x 48 µm	encl by ilm hexagonal 19 x 13 µm
0.96	0.99	1.05	1.27	1.26
0.14	0.11	0.11	b.d.l.	b.d.l.
19.07	19.23	19.73	19.65	19.85
17.04	17.31	18.45	18.16	18.87
0.32	0.37	1.36	1.02	1.47
0.11	0.07	0.06	-	-
1.28	1.15	0.63	0.86	0.78
0.04	0.05	0.14	0.23	0.27
0.36	0.32	0.45	0.28	0.38
12.34	12.40	11.87	12.85	11.94
23.73	23.22	20.95	21.91	21.13
3.10	3.00	2.79	1.90	1.94
6.46	6.57	5.10	5.43	5.47
0.58	0.52	0.35	0.38	0.54
0.32	0.30	0.25	0.45	0.32
0.02	0.05	0.10	0.16	0.19
1.52	1.85	3.81	3.36	4.12
0.13	b.d.l.	0.14	0.22	0.17
11.94	12.24	11.86	11.07	11.31
99.46	99.75	99.20	99.20	100.01

Supplementary Table 5a. Compositions of matrix glass and melt inclusions

Sample	Pantelleritic - Ttg-hg#1							
	1	2	3	4	5	6	7	8
wt%								
SiO_2	72.45	72.60	73.08	73.10	71.72	72.20	71.14	72.89
TiO_2	0.29	0.22	0.24	0.28	0.21	0.27	0.25	0.31
ZrO_2	0.85	0.89	0.97	0.91	0.83	1.01	0.81	0.91
Al_2O_3	9.34	9.47	9.21	9.35	9.46	9.27	9.21	9.35
FeO*	5.67	5.88	5.98	5.98	6.31	6.11	7.18	5.78
MnO	0.21	0.08	0.20	0.25	0.26	0.21	0.12	0.11
MgO	0.02	0.02	bd	bd	bd	0.02	bd	bd
CaO	0.09	0.10	0.09	0.10	0.12	0.06	0.06	0.06
Na_2O	5.74	6.12	6.08	5.84	6.81	6.45	7.98	6.24
K_2O	5.03	5.00	5.17	5.18	3.83	4.82	2.59	3.98
SO_3	0.03	bd	bd	0.03	0.07	0.03	bd	0.03
F	1.69	1.62	1.13	0.96	1.12	2.03	1.37	0.23
Cl	0.70	0.80	0.73	0.72	0.40	0.73	0.32	0.76
Sum	102.11	102.80	102.88	102.70	101.14	103.21	101.03	100.65
O ≡ F, Cl	0.87	0.86	0.64	0.57	0.56	1.02	0.65	0.27
Total	101.24	101.94	102.24	102.13	100.58	102.19	100.38	100.38
PI	1.59	1.63	1.69	1.63	1.62	1.71	1.73	1.56
F + Cl	2.39	2.42	1.86	1.68	1.52	2.76	1.69	0.99

Explanation: analyses 40, 41, 46-48 and 49 are from melt inclusions in alkali feldspar, olivine, amphibole and clinop

Samples numbered 33, 34, 40 and 41 are partly devitrified

FeO*, all Fe as Fe^{2+}

PI, Peralkalinity Index (mol. $(Na_2O+K_2O)/A_{l2}O_3$).

9	10	11	12	13	14	15	16	17
70.98	72.01	71.45	70.84	72.04	72.30	71.80	72.28	72.24
0.26	0.33	0.30	0.31	0.29	0.29	0.28	0.25	0.27
0.83	0.92	1.04	0.91	0.95	0.89	0.89	0.84	0.85
9.17	9.10	9.17	9.03	9.18	9.23	9.29	9.32	9.29
5.85	5.76	5.78	6.96	5.84	5.86	5.65	6.06	6.03
0.21	0.18	0.14	0.15	0.25	0.21	0.24	0.18	0.15
bd	bd	bd	bd	bd	bd	0.02	bd	bd
0.12	0.12	0.24	0.06	0.06	0.07	0.08	0.05	0.08
4.60	4.91	5.07	5.74	5.72	5.68	5.76	6.85	6.05
4.98	4.79	5.17	4.60	4.15	4.50	4.22	5.31	5.15
0.03	0.05	bd	bd	0.03	0.11	0.05	0.06	0.07
1.08	0.74	1.42	1.50	0.85	1.19	1.08	1.24	0.85
0.82	0.73	0.80	0.53	0.78	0.35	0.56	0.52	0.94
98.93	99.64	100.58	100.63	100.14	100.68	99.92	102.96	101.97
0.64	0.48	0.78	0.75	0.53	0.58	0.58	0.64	0.56
98.29	99.16	99.80	99.88	99.61	100.10	99.34	102.32	101.41
1.41	1.46	1.52	1.60	1.51	1.54	1.51	1.83	1.67
1.90	1.47	2.22	2.03	1.63	1.54	1.64	1.76	1.79

ɔyroxene, respectively.

18	19	20	21	22	23	24	25	26
73.10	72.86	73.24	72.53	73.44	73.11	72.40	72.77	72.76
0.25	0.26	0.20	0.27	0.31	0.25	0.29	0.26	0.22
0.95	1.03	0.86	0.88	0.83	0.89	0.86	0.97	0.91
9.32	9.20	9.43	9.25	9.31	9.25	9.28	9.35	9.18
5.62	6.08	6.13	5.95	6.00	6.06	5.99	5.91	6.39
0.18	0.12	0.16	0.22	0.21	0.16	0.24	0.21	0.23
bd	bd	bd	0.02	bd	bd	bd	bd	0.02
0.06	0.08	0.06	0.07	0.05	bd	0.06	0.08	0.06
5.92	5.90	6.24	5.97	6.22	5.68	5.95	6.36	5.60
4.92	5.13	5.07	5.02	4.91	5.03	4.94	4.48	5.40
0.03	bd	0.06	bd	bd	bd	bd	0.09	bd
1.02	1.24	1.18	1.30	1.18	1.35	0.85	1.24	1.74
0.72	0.78	0.68	0.69	0.66	0.62	0.60	0.70	0.70
102.09	102.68	103.31	102.17	103.12	102.4	101.46	102.42	103.21
0.59	0.70	0.65	0.70	0.65	0.71	0.49	0.68	0.89
101.50	101.98	102.66	101.47	102.47	101.69	100.97	101.74	102.32
1.62	1.66	1.67	1.65	1.67	1.60	1.63	1.64	1.64
1.74	2.02	1.86	1.99	1.84	1.97	1.45	1.94	2.44

						Comenditic - Ttg-hg#1	
27	28	29	30	31	32	33	34
71.67	72.06	71.21	71.69	72.15	71.05	73.18	74.27
0.30	0.28	0.23	0.26	0.25	0.25	0.23	0.20
0.92	0.87	0.77	0.84	0.73	0.75	0.63	0.52
9.24	9.07	8.92	9.06	9.29	8.95	10.07	10.23
6.57	5.73	6.02	6.04	6.11	6.10	5.07	4.31
0.26	0.10	0.23	0.18	0.17	0.22	0.09	0.19
0.02	0.03	bd	bd	bd	bd	0.02	bd
0.08	0.09	0.05	0.09	0.10	0.06	0.15	0.08
6.46	5.40	5.96	5.99	5.40	5.94	6.06	4.58
5.02	4.81	5.01	4.95	5.85	5.96	4.82	4.85
bd	0.03	bd	bd	0.08	bd	bd	0.03
2.23	0.96	1.23	0.92	0.85	0.92	0.91	0.59
0.67	0.81	0.79	0.77	0.37	0.82	0.24	0.27
103.44	100.24	100.42	100.79	101.35	101.02	101.47	100.12
1.09	0.59	0.74	0.60	0.46	0.62	0.44	0.31
102.35	99.65	99.68	100.19	100.89	100.40	101.03	99.81
1.74	1.55	1.71	1.68	1.64	1.81	1.51	1.25
2.90	1.77	2.02	1.69	1.22	1.74	1.15	0.86

35	36	37	38	39	40	41	42	43
73.64	74.83	74.58	74.52	74.09	73.21	74.03	74.14	73.55
0.20	0.24	0.15	0.19	0.14	0.21	0.25	0.16	0.23
0.56	0.36	0.42	0.42	0.32	0.40	0.32	0.18	0.24
10.28	10.62	10.50	10.67	10.70	10.46	10.59	10.44	10.29
4.20	3.89	3.93	3.72	3.58	3.67	3.97	3.83	3.76
0.08	0.09	0.06	0.14	0.13	0.02	0.13	0.15	bd
bd	bd	bd	0.02	0.02	0.04	0.02	bd	0.03
0.13	0.11	0.17	0.14	0.18	0.21	0.23	0.19	0.19
5.33	5.11	5.37	5.15	4.74	4.32	4.41	4.50	4.82
4.74	4.68	4.60	4.67	5.13	5.01	5.01	5.18	4.52
bd	bd	0.10	bd	0.04	bd	0.04	bd	bd
0.35	0.41	0.58	0.81	0.65	0.76	0.81	0.47	1.16
0.43	0.28	0.47	0.24	0.47	0.47	0.46	0.49	0.30
99.94	100.62	100.93	100.69	100.19	98.78	100.27	99.73	99.09
0.24	0.24	0.35	0.40	0.38	0.43	0.45	0.34	0.57
99.70	100.38	100.58	100.29	99.81	98.35	99.82	99.39	98.52
1.35	1.27	1.32	1.27	1.25	1.20	1.20	1.25	1.25
0.78	0.69	1.05	1.05	1.12	1.23	1.27	0.96	1.46

					FC
44	45	46	47	48	49
74.12	74.40	73.64	73.70	74.50	67.04
0.23	0.18	0.22	0.22	0.22	0.30
0.42	0.23	0.38	0.32	0.29	0.43
10.39	10.40	10.32	10.46	10.57	16.47
3.99	3.59	3.98	3.69	4.01	2.49
bd	0.12	0.05	0.13	0.12	0.13
bd	bd	bd	bd	bd	0.04
0.15	0.25	0.19	0.20	0.18	0.45
5.01	4.86	4.98	4.51	4.62	6.05
4.84	4.85	5.23	5.62	5.13	6.21
bd	bd	bd	0.03	0.04	0.04
0.56	0.59	0.93	0.53	0.56	0.46
0.57	0.41	0.49	0.48	0.50	0.49
100.28	99.88	100.41	99.89	100.74	100.60
0.40	0.36	0.53	0.36	0.38	0.33
99.88	99.52	99.88	99.53	100.36	100.27
1.30	1.27	1.34	1.29	1.24	1.01
1.13	1.00	1.42	1.01	1.06	0.95

Supplementary Table 5b. Major element analyses of various Gold Flat Tuff samples

	1	2	2	4	5	6
Sample	TP-9	N-121	TP-20B	TP-12	avge welded	D110872W
Reference	1	1	1	1	2	2
wt%						
SiO_2	68.4	69.3	69.1	67.1	69.5	67.1
TiO_2	0.25	0.33	0.26	0.28	0.3	0.28
ZrO_2	-	-	-	-	0.6	-
Al_2O_3	11.3	11.9	12.1	10.7	11.5	10.4
Fe_2O_3	4.7	3.6	3.8	4.2	4.0	4.2
FeO	0.58	1.6	1.3	1.5	1.2	1.5
FeO*	4.81	4.8	4.7	5.4	4.8	5.3
MnO	0.17	0.16	0.16	0.18	0.16	0.18
MgO	0.43	0.16	0.31	0.36	0.3	0.36
CaO	1.0	0.57	0.45	0.39	0.5	0.39
Na_2O	4.8	5.1	5.4	4.8	5.2	4.8
K_2O	4.9	4.8	4.8	4.9	4.8	4.7
P_2O_5	0.7	0.1	0.05	0.07	0.07	0.07
Cl	0.02	0.18	0.31	0.51	0.2	0.51
F	0.44	0.47	0.62	0.88	0.5	0.88
H_2O+	0.53	0.63	0.63	2.6	0.6	2.6
H_2O-	0.35	0.28	0.25	0.46	0.3	0.46
CO_2	0.7	-	-	-	0.05	-
Sum	99.27	99.18	99.54	98.93	99.78	98.43
PI	1.17	1.14	1.16	1.23	1.20	1.25

References: 1, previously unpublished data, compiled by DCN; 2, Noble, 1965.

FeO*, all Fe as Fe^{2+}

Dash, not reported

PI, Peralkalinity Index (mol. $(Na_2O+K_2O)/Al_2O_3$)